THE APPLICATION OF OPTICAL INTERFEROMETRY TO TIME DEPENDENT UNBONDING

(Parts 1, 2 and 3)

Thesis by

Kenneth Macdougall Liechti

In Partial Fulfillment of the Requirements

For the Degree of

Doctor of Philosophy

California Institute of Technology

Pasadena, California

(1980)

Submitted April 21, 1980

ACKNOWLEDGEMENTS

I would like to thank all those faculty who have contributed to my education by their teaching example. In particular, I wish to thank my advisor, Professor W. G. Knauss, who suggested the thesis topic and provided much encouragement and understanding, not only in academic matters. I also greatly appreciate the teaching and support of Professor C. D. Babcock.

The support of the Air Force Office of Scientific Research, where this work was initiated under Mr. W. J. Walker and assisted with understanding and interest by Lt. Col. J. D. Morgan, is gratefully acknowledged.

In a thesis with such emphasis on experiment special thanks must go to all members of the Aeronautics Machine and Electronics Shops whose help and advice were so willingly given. I much appreciate the help of Mrs. B. Wood and Mr. H. Hamaguchi in the preparation of figures and pictures for the thesis. I am greatly indebted to Mrs. M. Matteson for typing the manuscript so efficiently and at such short notice. My thanks in this regard also go to Ms. M. Clark for her last-minute help.

In recognition of their endless care and support, I dedicate this thesis to my parents.

ABSTRACT

Improved methods of adhesive joining for constructing structural elements have led to an increase in the use of bonding. Bonding is already widely used in the aerospace industry. It allows potential for greater weight and manufacturing cost savings when compared to mechanical fastening as well as providing better fatigue resistant capabilities. More accurate design or life prediction based on a better understanding of adhesive joint failure will allow far more extensive and safer use of adhesively bonded structures. The possibility of time dependent failure is introduced in bonding by the fact that many adhesives are polymers and measurably viscoelastic under many circumstances. Failure can occur by unbonding at the adherend-adhesive interface or totally within the adhesive. Here the time dependent failure by unbonding at the interface is addressed as one initial investigation of the whole problem.

In many engineering problems the modelling of failure has been based on linear fracture mechanics. The extent to which the use of the linear theory can be justified is often questionable in view of the nonlinearity of the local crack front deformation field. One aspect of the current investigation is therefore the measurement of the local crack front deformation to examine the limits of the validity for the linear theory and to provide a basis for future modelling.

Within this framework, particular attention is paid to the aspects of local failure mode interaction and the time dependence of the unbonding process.

The small displacements in the crack front region require a resolution on the order of a wavelength of light. The experimental techniques used are therefore based on optical interferometry. The displacements applied to the adherends are controlled to the same order by a novel, thermally actuated servoloading device.

The thesis is divided into three distinct parts. The first part deals with the development of the experimental techniques used to measure the unbound profiles as well as to measure and control the displacements applied to the adherends. For stationary cracks, the second part describes experiments which examine the extent of the nonlinearity in the crack front deformation field while fracture criteria are developed and compared for unbonding rates in steadily propagating cracks. Finally, proposals for improvement of the experimental techniques and further experiments are discussed in the third part.

TABLE OF CONTENTS

PART 1

An Experimental Technique for Determining the Profile of Unbonds at Material Interfaces

ABSTRACT

Current analyses of adhesive joint failure average out the effects of the adhesive layer. The pitfalls of this averaging approach are outlined in order to demonstrate the need to observe and measure the local fracture processes directly. In allowing for realistically sized bond thicknesses, optical interferometry is shown to be suitable for such measurements. The method of crack opening interferometry, previously applied to the measurement of crack profiles in cracked monolithic bodies, is therefore developed to determine the interfacial unbound profiles in an adhesive joint. A consequence of using crack opening interferometry and the fact that we wish to address the time dependent failure of adhesive joints is that the relative displacements of the adherends must also be measured to the resolution of optical interferometry. The development of a system to measure and control the adherend displacements both normal and tangential to the bondline to the order of 0.16 μm is described. The displacements are provided by the thermal dilation of actuator tubes in a specially constructed loading device, measured by two Michelson interferometers and controlled by a microprocessor in a feedback loop. Some initial results are presented to illustrate the capabilities of the experimental techniques developed.

TABLE OF CONTENTS

LIST OF FIGURES

1.1 INTRODUCTION

The increased use of adhesives to achieve structural joints promises several advantages over mechanical fasteners. Substantial savings are possible through weight reduction and in manufacturing costs when adhesive joints are used. Thin and contoured sheets can be more effectively joined. Stress concentrations and galvanic corrosion also tend to be reduced, promising structures that are less fatigue-critical. These advantages attract interest in both the aerospace and automotive industries. Sealants are finding increased use in these as well as the building industry and in a variety of encapsulation applications, solar cell encapsulation being potentially important.

These advantages have, however, been sometimes outweighed in the past because of an apparent low reliability and durability. Yet, on closer examination, it seems that this seemingly low reliability and durability can be accounted for by environmental effects and time dependent processes not previously considered. More thorough structural mechanics considerations, including these effects, are therefore called for. Better adhesive materials and improved methods of metal surface preparation (phospheric anodizing of aluminum) makes this closer look feasible now.

Usually, analyses of bonded joint failure are approached through peel testing or "thickness-averaged" fracture mechanics. Peel testing approaches the adhesion problem by

specifying relatively thin adherends which undergo large (often elastoplastic) deformations. Test results or analyses are concerned with net forces acting on the adhesive system and the resulting deformations[1,2,3]. "Thickness-averaged" fracture mechanics[4,5,6,7,8], deals primarily with (2 dimensional) plate or beam-like geometries, two plates being joined along a line by an adhesive layer. Since the adhesive layer is usually thin compared to the thickness of the plates, the thickness of the adhesive layer is deemed negligible, thus reducing the plate problem to the fracture of a homogeneous plate containing a weak material plane. The problem is then usually further analyzed by applying fracture mechanics concepts developed for homogeneous bodies. As a result, certain fracture parameters which are normally considered material constants must then be made functions of the bondline thickness. Peel and thickness averaged fracture mechanics neglect the local fracture processes in the adhesive itself. They therefore provide an indirect interpretation of the fracture processes. The peel mode involves very different deformations than those in thickness-averaged fracture mechanics, yet no attempt is made to unify these two approaches. Joints which may not involve conditions commensurate with peel or thickness-averaged fracture mechanics are nonetheless designed on the basis of either approach. Another indirect interpretation of fracture processes comes from post fracture surface analysis. Reconstruction of the

fracture processes can be ambiguous and open to potentially non-unique interpretations. It would seem mandatory, therefore, to examine the conditions that lead to joint failure in more detail than either peel mode and thickness-averaged fracture or the second guessing from past fracture surface examination can portray.

Many structural adhesives are polymers and possess viscoelastic and time dependent properties, thus involving the total load history of a structural element in its life prediction. Adhesives are also sensitive to the thermal history (from both thermal dilatational and thermorheological considerations) as well as the moisture history of their service environment. Design procedures, based on experience obtained from designing with metals which are generally rate, thermorheologically and moisture insensitive, led to the concept of apparent random failure of adhesive joints. The apparent randomness in the failure process is not inherent, but rather is a result of failure to consider time, temperature and moisture as factors contributing to joint failure. The local intensified stresses and deformations at the tip of an unbond are more affected by these parameters than are the global or net forces considered in peel and thickness-averaged fracture mechanics approaches.

In the characterization of the effects of cracks on structural bond behavior we are particularly interested in the interactions of the applied loadings normal and

tangential (shear) to the bondline as well as in the local crack tip deformations. When referring to local normal and tangential crack tip deformations (as opposed to the global or applied displacements), we will employ the terms mode I and mode II deformations respectively. This distinction must be made here because we are dealing with fracture at a bimaterial interface. The local normal and tangential crack front displacements are each coupled to both applied normal and tangential displacements. This is not the case for fracture in monolithic materials, where displacements applied normal to and tangential to the plane of the crack produce only normal and tangential crack tip displacements respectively. It is interesting to note in this context that early results in the analysis of large deformations at the tip of a crack reveal a small amount of mode I deformations for a purely tangential loading even for cracks in homogeneous materials.

Stone et al [9] attempted to design a specimen to study the fracture of a joint under a purely tangential loading as well as including thickness effects in analysis. However, a finite element analysis and experiments showed that normal loading was introduced along the bondline, making it a mixed mode specimen. Nonetheless, they found that the shear load required to grow the crack to a given length was much higher for this mixed mode specimen than for a purely normal loaded specimen. If a small amount of normal load was added in the mixed mode specimen, a marked instability (through rapid

failure) in the crack growth occurred.

Another source of mode interaction is the mismatch in the material properties between the adherend and adhesive. Any "far field" loading gives rise to both mode I and mode II deformation. If mode I deformation does indeed dominate the failure criterion, then small amounts of mode I introduced, for example, by secondary or nonlinear effects under a shear loading could have a disproportionate effect.

These interactions will probably be strongest for interface cracks. We define an interface crack to be one in which no adhesive itself is left optically visible on the adherend. This leaves open the possibility of a molecular layer being left on the adherend but the size scale is then well below the minimum resolution of continuum mechanics. There have been claims that interfacial cracks do not occur in practice but Romanko [10] as well as Sykes et al [11] have observed interfacial cracks in joints under low frequency cyclic loading in a dry environment and in double cantilever beam specimens, respectively.

With regard to time dependent unbonding, we note that in fracture of monolithic viscoelastic materials the time dependence is introduced only through the time dependent material properties and loading history. The energy necessary to create new surface was found to be a constant, intrinsic property of the material [12]. Similarly, we expect the time dependence in unbonding to be introduced through the

viscoelastic adhesive material properties and the loading history and the adhesive energy to be a constant (if one discounts variations resulting from specimen preparation).

The present investigation, through careful experimentation, provides direct observation and measurement of the actual fracture processes at the crack tip on which more careful modelling and analysis may be based. Moreover, the results provide information on the limits to which current linear stress anaylses are valid and/or useful.

The stresses in a realistically dimensioned adhesive layer are not easily or directly accessible without assuming some constitutive law, linearly elastic behavior being the most common one. For example, if one were to use three dimensional frozen photoelasticity, the joint size would have to be scaled up on the order of 100 times and the resolution of time would be lost. The validity of any scaling up is questionable in view of the possibility that nonlinear aspects are present. We have therefore chosen to work with the deformation fields in the crack tip region and the displacements across the bondline in a nearly realistically configured geometry. Since stresses and strains involve the displacement gradients, precise measurements are called for.

Sommer [16] measured the crack profiles in cracked monolithic bodies using crack opening interferometry. The full three dimensional shape of the crack front is determined from an interference pattern giving a displacement resolution of

a half wavelength of the monochromatic light source (1.25×10^{-5} inches for helium neon laser light). The potential of crack opening interferometry for accurately measuring unbond profiles in adhesive joints was recognized and its feasibility was successfully determined in an initial study. An additional outcome of this study was the need for careful measurement and control of the relative displacements of the adherends.

The resolution of mechanical displacement measurement devices (linearly varying differential transformers, photonic sensors or eddy current devices) is such that unrealistically thick bonds would have to be used. On the other hand, optical interference techniques when used in conjunction with optically clear materials allow for realistically sized joints and direct observation of the unbonding processes.

To delineate the resolution required in this connection we note that, for example, the displacement across a 0.020 inch bond thickness of a butt joint subjected to a 1% strain is 2×10^{-4} inches. If one requires at least a 10% resolution of such displacement one has then to consider a displacement of 2×10^{-5} inches. By comparison, the wavelength (λ) of helium neon (laser) light is 2.5×10^{-5} inches. Optical interference techniques provide a resolution of at least 1.25×10^{-5} inches ($\lambda/2$). In addition to measuring such small displacements, one has to be able to control or prescribe displacements (at any time) to the same order.

The fine, relative displacements of the adherends normal to and tangential to the bondline are provided by a specially constructed loading frame which utilizes thermal dilatation of actuators. The displacements are measured by Michelson interferometers and microprocessor controlled in a feedback loop. The development of this displacement measurement and control system is described in Section 1.2. The development and manufacture of optically clear, stable and flawless specimens is outlined in Section 1.3. Section 1.4 describes the application of the crack opening interference method to cracked adhesive joints. Some initial results are also presented by way of an illustration of the method and the capabilities of the total system.

1.2 MEASUREMENT AND CONTROL OF APPLIED DISPLACEMENTS

Ultimately, we are interested in determining the effects of different combinations of displacements applied normal to and tangential to the bondline on the crack profile and crack propagation rate in an adhesive joint. There are many possible joint geometries to choose from. The butt joint was chosen because relative movements of the adherends can be carefully and independently controlled. However, the results should not necessarily and in general be restricted to the butt joint. Here, we attempt to relate the relative movements of adherends to local crack tip deformations and propagation rates in order to develop a criterion for unbonding under combined loading.

The development and operation of the loading device is described in Section 1.2.1. Specimen gripping is discussed in Section 1.2.2. Section 1.2.3 covers the measurement of the applied displacements and their control is described in Section 1.2.4.

1.2.1 Loading Device

A suitable loading device must then

a) permit independently controlled relative displacements of the adherends normal and tangential to the bondline to within one quarter wavelength of light;

b) be sufficiently stiff so as not to release energy during the fracture process, i.e. to prevent unstable crack

growth;

c) allow for observation of a crack at the adherend adhesive interface;

d) allow for control of the specimen's environment.

Considerations (a) and (b) provide the most critical constraints on a loading device. For example, in a load screw device 1/4 μm displacement resolution might be feasible but only at expense of stiffness and backlash. The relatively low stiffness and controllability of the fluid in hydraulic devices makes them unacceptable. On the other hand, thermal dilatation of rods provides suitably fine and controllable displacements and the stiffness requirements are easily met with zero backlash. A possible disadvantage is the restriction which the rate of heat transfer places on straining rates. However, since we are dealing with such small displacements, heat transfer rates do not unduly restrict the strain rates. Another possibility, brought to the author's attention following construction of the loading device, is that of magnetostriction. The attraction of using the magnetostriction effect is the instantaneous response rate. A cursory glance at the sizing indicates good feasibility although arrangement of the electromagnets could be cumbersome.

Heating of the actuator tubes is provided by band heaters clamped to their outside; vaporized liquid nitrogen is sprayed on the inside to provide cooling. Induction heat-

ing and resistive heating were also considered. Induction heating would provide high displacement rates but was too costly and cumbersome to apply. Resistive heating required unrealistically high currents because of the size of the actuator tubes (already determined by stiffness requirements). Water cooling provided unacceptably low displacement rates because of the relatively low temperature differences between cold water and projected maximum tube temperatures after heating. The lower limit of the displacement range is essentially limited to the resolution of the displacement measurement system and the sampling and decision times in any control loop. The device was designed for a displacement upper limit of 0.010 inches.

Figure 1 shows a schematic of the device and the mounting of the model joint. Displacement normal to and tangential to the bondline are independently controlled in the following way. Each normal displacement actuator tube is connected to a tangential actuator tube by connecting plates which also serve as specimen grips. The heating or cooling can be independently applied to the normal actuator tubes and the tangential actuator tubes. The symmetry of the arrangement is maintained by equal heating or cooling of each pair of normal and tangential actuator tubes. When the tubes are heated or cooled they will bend slightly due to the fact that they are connected. The connection will, in general, rotate resulting in a rotation of the adherends.

However, the symmetry of the arrangement and the equal heating or cooling within each normal and tangential actuator tube pair ensures that the adherends rotate to the same degree. Thus the adherend edges defining the bond thickness remain parallel. This bending of the tubes gives rise to small secondary normal and tangential displacements in addition to the primary thermal dilatation displacements. These are two orders of magnitude less and are easily corrected for in the feedback loop. The tubes are three inch stainless steel tubes having a half-inch wall thickness. These provide sufficient stiffness to counteract the lack of symmetry in the arrangement due to the bending movement produced by an unbond.

1.2.2 Specimen Gripping

The details of specimen mounting are shown in figure 2. The edges of the adherends are glued to the machine grips using a plastic steel epoxy. A 0.010 inch clearance between the adherends and the grips is filled by this epoxy. This ensures that the grips do not displace the adherends in any way during the mounting of the specimen. This method of load transfer was chosen in preference to direct clamping and bolting of the adherends to the grips. It was found that even careful shimming in the latter method did not prevent displacement during final tightening of the bolts. The small displacements induced in the final tightening were

often enough to cause the crack to run uncontrolled along the entire width of the specimen. The shimming procedure was very time consuming. Also, since the adherends are glass, load transfer to the specimen is better achieved through bonding in view of the brittle nature of glass.

1.2.3 Displacement Measurement

The small displacements applied to the adherends are measured by two Michelson interferometers, mounted on the specimen. The pickup locations are 0.075 inches from the adherend edges defining the bondline (figure 2). The components and optical paths of the system are identified in figure 3. They are arranged such that one interferometer measures displacements normal to the bondline while the other measures tangential displacements. (The possibility of relative rotation of the adherend faces is prevented by the symmetry of the arrangement of the loading device.) The photograph in Figure 4 shows the interferometers arranged as they would be on a specimen.

The Michelson interferometer produces a fringe pattern of concentric light and dark circles. As the path difference between the split beams changes (beams A and B in figure 3, for example), these circular fringes expand or contract as the path difference increases or decreases. If the circles are expanding, a new circle appears at the center each time the path difference changes by a half wave-

length of the monochromatic light source. For a contracting pattern circles disappear at the center. A stationary, centrally placed photodiode converts this varying light intensity (as the path difference changes) into a sinusoidally varying voltage signal when suitably amplified. A second photodiode placed within a quarter of the fringe spacing produces a similar voltage signal which is out of phase with the centrally located photodiode signal by less than 90 degrees. The sign of the phase difference is used to determine the direction of the path difference change and therefore whether to count up or down (separating adherends or moving them together).

The magnitude of the phase difference remains the same as long as the fringe pattern does not translate in addition to the contracting or expanding circles. This translation of the fringe pattern is caused by very small out of plane bending of the actuator tubes or unequal rotation of the adherends. Conversely, the fact that this fringe translation does not occur indicates that the adherend faces defining the bonding planes remain parallel in both planes. Such phenomena did occur initially due to hot spots in the band heaters and liquid nitrogen collecting on the bottom of the tubes. Decreasing the heating rate of the heaters and ensuring that only vaporized liquid nitrogen entered the actuator tubes eliminated the nonuniform temperature fields causing the problems.

It should be noted here that tracing causes of nonuniform or spurious displacements is difficult when dealing with such small displacements. For instance, the lines supplying the vaporized liquid nitrogen to the actuator had to be made very flexible so that their own contraction would not influence the displacements at the bondline. The optical table on which the loading device is mounted (to eliminate ground vibration) is made up of a thick steel plate resting on inner tubes. Pressing down on one corner of this plate is enough to cause observable displacements at the bondline.

Prior to using the Michelson interferometers a Mach Zehnder arrangement was extensively explored. It was found, however, that the contracting and expanding circles of the fringe pattern also translated. The movements causing the path difference changes are not normal to the mirrors, resulting in an effective translation of the light source and, therefore, the fringe pattern. An additional photodiode could be used to subtract out the translation but would greatly complicate data reduction. In a feedback control application this complication (through added programming steps) could adversely affect sampling rates, so the Mach Zehnder interferometer was abandoned. The resolution of L.V.D.T.'s or photonic sensors is barely sufficient for the bond thickness considered and they also suffer from drift in the electronic signal processing. This drift could be significant in long-time studies aimed at exploring viscoelastic

effects.

1.2.4 Displacement Control

Each normal and tangential interferometer then has a pair of photodiodes whose signal is amplified and sampled by the analog-to-digital converter module in an 8-bit microprocessor. Data sampling, and conversion, phase comparison and fringe counting, displacement history prescription and control decisions in a closed loop feedback are all software controlled. The control program is arranged such that most of the time is spent sampling the photodiode signals, awaiting the occurrence of a fringe. As soon as a fringe is registered, the sign of the phase difference between them is checked, and accordingly counted up or down. This current count (or displacement) is then compared with the prescribed displacement (set point) for that instant. The difference between the current and prescribed displacement is then used to decide to activate or deactivate the heaters or coolers. Thereafter the system returns to the data sampling. The time spent in phase comparison, set point comparison and signalling the heaters or coolers is so much smaller than that spent in photodiode signal sampling that the chances of missing a fringe are very small.

The fringe counting required some development. The main difficulty arose due to the fringe rates varying from essentially d.c. (say 10^{-4} Hz) to 2 Hz. We originally

counted fringes by counting maxima using slope changes in the sinusoidally varying photodiode signals. The advantage of this was that the signal amplitude could be allowed to vary as much as 3 volts over 10 volts full scale from one run to another. The main cause of this amplitude variation from one run to another is that the interferometers cannot be located exactly the same each time. (This affects the initial path difference between the interferometer elements, which, in turn, determines the fringe intensities and spacing.) However, slope detection, particularly for the 10^{-4} to 2 Hz fringe rates, is very noise sensitive. We also found that we were having to adjust the photodiode signal amplitudes quite carefully anyway as well as the phase difference between the central and off central photodiodes. This led us to develop a zero crossing, amplitude based algorithm. The zeros are automatically set after the first full fringe has passed each photodiode. Signal adjustment for amplitude and phase difference is the same as before but noise sensitivity is eliminated (up to about 40% noise to signal ratio). Counting maxima gave a displacement resolution of one fringe (or $\lambda/2$), whereas zero crossings give a one half fringe resolution ($\lambda/4$). Fewer programming steps are required thus increasing the sampling rate.

A real time module in the microprocessor allows us to prescribe time-varying applied displacement histories. Any prescribed displacement history can be preprogrammed into

the computer, limited only by the thermal response of the actuator tubes, sampling rate and measurement and control resolution.

The heaters are proportionally controlled by outputing a 0 to 10 volt signal (corresponding to 0 to 100% power) through a digital to analog module in the microprocessor to TRIAC solid state relays. The coolers are controlled in an on-off mode by solenoids activated by the control program. Proportional control allows minimization of set point overshoot and resultant possible stability problems. Some development was necessary to determine optimum heating rates in order to minimize overshoot but the flexibility of software control was really emphasized here. The set point can be controlled to within 6.25×10^{-6} inches (.16μm), the resolution limit imposed by counting every half fringe. All factors combined to produce a maximum displacement rate of 0.001 inch in 40 seconds.

1.3 SPECIMEN DEVELOPMENT AND MANUFACTURE

This chapter outlines the steps involved in the development and manufacture of suitable specimens. The specimens should allow complete experimental determination of the relative displacements of the adherends and be optically clear, stable and flawless. Factors contributing to the choice of the materials making up the specimen are illuminated in Section 1.3.1. Specimen preparation is discussed in Section 1.3.2. Finally, Section 1.3.3 describes the specimen mounting and crack initiation procedures.

1.3.1 Material Choice

The reasons for the choice of joint geometry were discussed in the previous section, with particular emphasis being placed on the ability to prescribe the relative displacements of the adherends. The measurement of these displacements is made at the pickup locations of the Michelson interferometers, 0.093 inches from the bondline. These displacements are assumed to be those actually occurring along the whole bondline. The basis for this assumption is that the adherends are rigid compared to the adhesive. The relative displacements can therefore be completely determined experimentally without recourse to analysis to correct for any relative displacement between the bondline and pickup location. In view of the nonlinear effects under study, such recourse to (linear) analysis would weaken the inde-

pendence of the experiment. Nevertheless, a finite element analysis was conducted to determine the extend of bondline deformation (apart from the rigid body displacement) of the adherends for different adherend to adhesive modulus ratios. The analysis provides order of magnitude criteria for a suitable material choice and does not therefore compromise the independence of the experiment. The effect of the extent of gripping along the specimen boundary was also examined.

The TEXGAP finite element code [13] was used. It uses a hybrid bimaterial crack element developed by Hong and Stern [14], making it very suitable for our purposes. The specimen geometry and loading analyzed are shown in figure 5. Figure 6 shows the results of the analysis for different adherend to adhesive modulus ratios. The adherend displacement (normalized by the applied displacement) normal to and 0.1 inches from the bondline is plotted vs. location across the specimen width. If the adherends were rigid this normalized displacement would be unity. It can be seen that, for a ratio of adherend to adhesive modulus of 10^4, a 4% error is introduced at the specimen center by assuming a constant displacement along the bondline as indicated by the interferometers. If the specimen is gripped along its entire width the error is reduced to about 0.5% (figure 7).

The use of interferometry in measuring the crack profile also affects the specimen material choice, particularly the adherend. We wish to observe and measure the

local three dimensional crack shape in the region of the crack front. This requires observation of the adherend adhesive interface plane rather than just the edge. The adherends should therefore be optically clear and stable. The adherend interfacing the adhesive should be optically flat (within $\lambda/4$ per inch).

After considerable development work, glass (BK-7) and Solithane were chosen as adherend and adhesive materials respectively. The modulus of the glass is 10^7 psi. Solithane has a rubbery modulus of 500 psi resulting in an adherend to adhesive modulus ratio of 2×10^4. Plexiglass was extensively considered as an adherend material before choosing glass. It promised easier fabrication to provide casting jig holes and interferometer mounting locations and also cheaper specimens. However, obtaining sufficiently flat adherend faces was almost impossible. The polishing and grinding caused plastic flow in the plexiglass, thus changing the refractive index. This in turn gave rise to considerable distortion of the beams reflected back from a crack, through the plexiglass. Polishing the glass is much easier and certainly offsets the difficulties in hole drilling.

Solithane was chosen as the adhesive in order to provide a sufficiently high adherend adhesive modulus ratio. It is a well characterized polyurethane elastomer previously used in fracture studies of monolithic, viscoelastic materials.

This potentially allows comparisons to be made between unbonding rates in joints and crack velocities in monolithic materials. It makes a relatively weak bond with glass, thus ensuring interfacial, as opposed to cohesive, failure. It can be cured at room temperature, eliminating residual stresses induced at high cure temperatures and different thermal expansion properties of glass and Solithane. However, residual stresses are introduced in the adhesive layer due to cure shrinkage of the Solithane.

1.3.2 Specimen Preparation

The specimen shown in figure 5 is cast as follows. The two adherends are clamped across the specimen thickness by two flat plates with the gap between them set by spacers defining the bond thickness. Once the adherends are clamped, the spacers are removed and injector nozzles attached to the jig plates, the nozzles being aligned with the bond thickness gap. A mixture of 60% Solithane prepolymer and 40% catalyst by weight is thoroughly mixed and degassed. The bubble-free mixture is then pressure injected into the gap, sealed and cured at room temperature for one week. Up to four specimens can be cast simultaneously from the same mixture, thus decreasing the possibility of material property and adhesive strength variations between specimens. Pressurized injection was found to be far superior to pouring or sucking the Solithane into the gap, particularly

with respect to lack of bubble generation.

1.3.3 Specimen Mounting and Crack Initiation

Once the specimen has cured it is glued (still in the casting jig) to the loading device grips using a plastic steel epoxy. Since the specimen is held fixed by the casting jig, the cure shrinkage of the plastic steel cannot introduce any initial loading. Mold release is applied to the sides of the adherends and grips to facilitate specimen removal following a test. The glass adherends can then be reused.

The casting jig is removed following a minimum 8 hour cure (at room temperature) of the plastic steel epoxy. Teflon tape is attached to one of the adherends on the face defining the adhesive adherend interface prior to casting. To initiate a crack, a 0.003 inch diameter wire is pulled along the Solithane-teflon tape interface like a cheese cutter until the end of the tape is reached. The wire is removed. The teflon tape serves to protect the glass adherend surface from scratching by the wire and also to indicate the initial crack length. (Figure 9)

Cracks are initiated in this way from both edges of the specimen along the glass-Solithane interface closest to the profile measurement device. The crack profile measurement is based on the first crack surface being that of the flat adherend face. Two cracks provide initial symmetry and also

ensure that the cracks run along the interface closest to the profile measurement device. It was sometimes found that, when a crack was initiated from only one side, another crack started anyway from the opposite edge of the specimen but always on the opposite interface. Worse still, it grew in preference to the wire-initiated crack, causing the loss of a specimen.

1.4 CRACK PROFILE MEASUREMENT

Crack opening interferometry has been used to measure directly the normal deformations in the crack front regions of cracked monolithic bodies [16]. These measurements quantify features of fracture processes occurring over very small dimensions. The crack face separation can be resolved to within half a wavelength of the viewing light at any point in the field of view (for sufficiently small gradients). In linearly elastic monolithic fracture studies, the relationship between the opening mode displacement and the stress intensity factors has been proposed to determine critical stress intensity factors of complex fracture problems where analysis is not tractable [18, 19]. However, the technique can also be applied to fundamental fracture studies to relate loading effects, crack propagation effects and time dependent aspects to changes in the crack profile. A practical problem with the method is that the crack faces need to be quite planar for interference to occur, a situation which does not always arise in the fracture of monolithic materials. The method is, however, particularly suited to the study of interfacial cracks because the adherend surface forming one of the crack faces can be carefully controlled for flatness.

The optical setup for the crack opening interference method is described in Section 1.4.1. The resolution limits of the method are discussed in Section 1.4.2, while Section 1.4.3 deals with possible methods to increase resolution.

Finally, initial results for a joint under normal applied displacements are presented in Section 1.4.4.

1.4.1 Experiment Setup

The decision to pursue the unbonding study followed the successful application of crack opening interferometry to an unbond in a prototype specimen (figure 9) whose geometry is different from that of the final specimen (figure 5). The final specimen geometry was determined by sizing considerations of the loading device and standard glass stock sizes. A schematic of the optical setup used in the crack opening interference method is shown in figure 10. When the coherent and monochromatic beams reflected by each face are combined, an interface pattern is formed. This pattern consists of light and dark fringes corresponding to loci of constructive and destructive interference respectively. In general, for normal incidence and an airfilled crack, each consecutive line of extinction corresponds to a change in the crack face separation of a half wavelength of the incident light. At a given fringe, m say, counted from the crack tip, the crack separation distance along that fringe is given by

$$h = m\,\lambda/2 \qquad m = 0, 1, 2, 3, \ldots\ldots$$

The fringes are contours of equal crack face separation from which the full three dimensional crack shape can be generated. For sufficiently small angles between the crack

faces fringes can be observed with the naked eye. A microscope is necessary to resolve the higher fringe densities produced by larger angles. The changing fringe patterns due to the applied loading are recorded through a closed circuit television camera on video tape for later data reduction. Figure 12 shows a schematic of the crack profile measurement system.

It was found that the "first surfaces" of the adherends (figure 11) had to be slightly inclined to those defining the bondline. If they are not sufficiently inclined, then fringes due to the adherend length are superimposed on those generated by the crack faces when viewed under the highly coherent laser illumination. The degree of coherence of sodium vapour lamps used in earlier work [16], [18] is much smaller and would not be capable of generating the adherend-length fringes. In the prototype specimen, the adherend faces had to be inclined at an angle of 5 degrees to avoid a superposition of fringe patterns, whereas in the finalized specimen a 42 minute wedge angle was sufficient. The reason for this difference is that the working distance of the microscope used in the development work was much shorter.

1.4.2 Resolution Limits

In the final setup (figure 12), the microscope provides a spatial resolution of 2.56×10^{-4} inches. This defines the resolution of the fringe and crack tip location. The

minimum resolvable fringe spacing between a light and a dark fringe is 6.4×10^{-4} inches. Fringes which are closer than 6.4×10^{-4} inches cannot be distinguished from one another. The crack profile cannot therefore be determined in such cases. The change in profile height between a light and dark fringe is 6.25×10^{-6} inches ($\lambda/4$). The minimum fringe spacing therefore determines the maximum profile gradient that can be measured (λc say). In this case $\lambda c = 33.5$ minutes $\left(\lambda c = \tan^{-1}(6.25 \times 10^{-6} \div 6.4 \times 10^{-4})\right)$. Note that it is not just the spatial resolution of the microscope which determines the critical crack profile angle but also the microscope working distance.

The determination of crack front location requires some explanation. Figure 13 depicts two possible cases for the location of the crack front. The shaded areas correspond to the area ahead of the crack front which is still bonded and also to fringes of extinction. The fringe spacing, fs, is the distance between a light and dark fringe. Assume the fringe thickness is the same as the fringe spacing. This is a limiting assumption. In figure 12a, where the crack front lies in an area of a forming but not yet fully formed bright fringe (i.e. the crack front is less than 1.5 fs away from the first fringe of extinction) there is no ambiguity in the determination of the crack front location. If the crack front lies in an area of the forming zero order fringe of extinction (figure 12b) it cannot be seen because destructive

interference is occurring and its location is therefore uncertain. The crack front could be as much as 2.5 fs away from the first order fringe of extinction. (Assuming the worst case of a linear crack profile; the crack front would be closer for a power law profile.) In taking the crack front to be at the boundary of the zero and half order fringe, the error in crack front location could be as much as one fringe spacing. In cases where the fringe spacing is the critical fringe spacing (or minimum resolvable fringe spacing) the error is on the same order as the fringe location resolution. For lower gradients either at low load levels or for stiff adhesives this could be considerable. In order to avoid this uncertainty determination of the crack front location is only made under the conditions of the case illustrated in figure 13a.

The gradient of a parabolic crack profile, predicted by linear elastic fracture mechanics close to the crack front, approaches infinity or angles of 90 degrees. The crack profile measurement system is limited to angles of 33.5 minutes, making its applicability, at first sight, questionable. However, it must be remembered that the crack face separation is very small (on the order of a few wavelengths of light). Thus, if a parabola does indeed describe the crack profile, then it is very long and thin with the large changes in profile gradients occurring within a very small distance from the crack front. In fact,

this large change in profile gradient must occur between the first order fringe of extinction, corresponding to a crack face separation of 1.25×10^{-5} inches, and the crack tip (the zero order fringe of extinction).

The question needs to be raised whether the first order fringe of extinction corresponds to a crack face separation of $\lambda/2$. The assumption is that the crack profile does not have the profile shown in figure 13c. In that case there could be a very steep front effectively providing a step discontinuity in the crack face separation, h_o say. To check this, observations of crack closure under a normal compressive applied displacement were made. Crack closure occurred through a decrease in length rather than through a simultaneous total contact of the two crack faces. The fringes were easily resolved right up to the crack front. It is unlikely that the profile depicted in figure 12c could be supported under a compressive load and this type of closure. Thus the first observable fringe does correspond to the first order fringe and a crack face separation of $\lambda/2$.

We make a distinction here between the "first observable fringe" and the "first resolvable fringe." The first observable fringe is taken to be the first order fringe of extinction. Under crack closure, sufficiently low loads or a stiff adhesive, the first observable fringe and the first resolvable fringe are the same. However, under higher loads the fringe density can become so high that fringes near the

crack front cannot be resolved by the microscope. Thus, while the crack front can be clearly discerned, there is an area of brightness behind the crack front where many fringes are superimposed on one another. The first fringe behind this bright area is taken to be the first resolvable fringe and is not the first order fringe. The question then arises of how to determine the order of the first resolvable fringe for these high fringe density cases. Loading is always commenced from a situation in which a first observable fringe is identified. The changing fringe patterns under loading are continuously recorded on the video system. The order of the first resolvable fringe at any time can then be determined by counting the number of fringes that pass a given location, well removed from the crack front, during that time.

1.4.3 Recommendations for Increasing Resolution

The first, and most expedient, method of increasing the resolution of the crack profile measurement is to shorten the working distance and increase the magnification of the microscope. When the layout of the optical elements used in the crack opening displacement method was first designed, the adherend length being considered was five inches. As a result, a microscope working distance of thirteen inches was necessary. The finalized adherend length is one inch, which would allow a considerable rearrangement of the elements to

produce a working distance of 4 inches. Included in this rearrangement, however, is the loss of capability to provide an environmental chamber. The restriction is not too severe because a compact method of heating the specimens using heating pads has been successfully developed. On the basis of our earlier experience with the prototype specimen, a four inch working distance should allow measurements of profile gradients on the order of three degrees. Some corrections may have to be made to the simple expression relating the wavelength of the light to the crack face separation to account for the larger angles.

The microscope was always focused on the adherend face describing one face of the unbond. However, different fringe patterns could be obtained by slight changes in the focal plane. A second approach to increasing the present resolution would be to understand the meaning and interrelationships of these different fringe patterns.

Finally, we consider the possibility of obtaining the unbond profile gradients directly (rather than differentiating the crack face separation distribution) using an optical shearing technique. Hung and Durelli [19] measured three surface displacement derivatives in a diffuse body simultaneously using a multiple image shearing camera. The sheared images of the body in its undeformed and deformed state were stored on the same photographic plate. The two images produce an interference pattern of a frequency variation type

whose intensity variations, captured by the film, are represented by the sum of a d.c. term and a high spatial frequency carrier amplitude modulated by a low frequency factor. The fringes are identified by areas of nulling carriers. The frequencies are, however, too high for the eye to resolve and the fringe pattern is invisible. Note that standard, visible interference patterns represent loci of points at which intensity is a minimum. Following double exposure, the photographic film was placed in an optical Fourier filtering arrangement to convert the fringes of frequency variation to those of intensity variation whose loci are isoparagogics. The derivative directions are obtained by correlating the direction of shift produced by the multiple image shearing camera to the orientation of the slit in the filtering plane of the Fourier filter.

The technique cannot be applied to following a sequence of events in real time because of the need for a double exposure (dictated by the use of diffuse surfaces). However, we can adapt the method to measure the crack profile gradients directly and in real time because we are using transparent materials with reflective surfaces. The reference state, which was provided by an exposure of the undeformed body, is now provided, at all times, by the undeforming, flat surface of the adherend face defining one face of an unbond. The deformed state is provided by the adhesive face defining the unbond. When the two faces are illuminated by

coherent light the image produced in the image plane of the shearing device can be Fourier filtered to produce fringes of constant profile gradient in real time. The fringe patterns could again be recorded by a video system. Unless an automatic system of filtering changing or two separate filtering systems can be provided, only one profile gradient can be obtained. In considering the resolution of the method, we use the results obtained in [19] for the particular case of the profile gradient in the direction of crack propagation, x say. The adhesive surface deformation is denoted by w. The profile gradient $(\frac{\partial w}{\partial x})$ in the direction of crack propagation is given by

$$\frac{\partial w}{\partial x} = -\frac{(2n+1)}{4} \frac{\lambda}{\delta x} \; ; \; n = 0, 1, 2 \ldots\ldots$$

where λ is the light source wavelength and δx is the shear produced by the image shearing device. The shear depends on the focal length of the device and wedge angle and index of refraction of the wedge making up the device. The change in gradient between two successive fringes,

$$\Delta\frac{\partial w}{\partial x} = \frac{\lambda}{2\delta x}$$

in [19], $\delta x \simeq 0.050$ inches, $\lambda = 2.5 \times 10^{-5}$ inches $\Rightarrow \Delta\frac{\partial w}{\partial x} = 0.86$ minutes. Thus each fringe corresponds to a gradient change of 0.86 minutes. In the crack opening displacement measurements, a total gradient change of 33 minutes was measured. In the same crack, the image shearing technique of the sensi-

tivity used in [19] would provide 40 fringes, which is rather high. However, if we use a wedge in front of a microscope to reduce the shear, δx, by a factor of ten, say, then the method may be feasible.

The time involved in further determination of the feasibility of the technique may be worth the reward of a direct determination of the profile gradient.

1.4.4 Initial Illustrative Results

Figure 14 shows a series of photographs of a stationary crack in a glass-Solithane joint taken at different normal load levels. The width of the picture covers one half of the specimen thickness. The crack, having the finger-like outline, is centered on the specimen midthickness. The dark area surrounding this finger indicates regions which are still bonded. Thus the crack does not extend all the way through the thickness but rather displays a fringe or tunnelling mode of fracture. The interference pattern used to generate the profile is the series of fringes contained within the crack outline. The fringe density increases as the applied normal displacement is increased to the extent that fringes are no longer distinguishable immediately behind the crack front.

A single central scan behind the crack front produces the profile along that line. A series of such scans for different normal loads is shown in figure 15. The crack

profile data are very consistent and allow precise measurement and evaluation. The distance from the crack front to the first resolvable fringe varies from 0.003 inches at zero load (its order was determined by scanning further behind the crack front than one field of view allows) to 0.00625 inches for an applied normal load of 2.375×10^{-4} inches. The crack face separation reaches a maximum approximately 0.012 inches from the crack tip.

The finger mode of fracture and the peak in the crack face separation are basically due to the low compressibility of the Solithane adhesive ($\nu=1/2$) and the constraint applied by the stiff adherends on the adhesive layer. The unresolvable fringes were not encountered in the prototype specimen (figure 9). The greater magnification and smaller working distance of the microscope used in the development stage increase the critical profile angle to about 2 degrees. Interface cracks were generated in the prototype specimen by wedging apart the thicker edges of the specimen. The thin, plexiglass adherends exeprienced considerable bending which would tend to reduce the angle between the crack faces. It should be noted that bending in a tapered cantilever beam (T.C.B.) specimens commonly used in adhesive fracture testing (which the prototype resembles) could similarly affect the crack profile near the crack front and subsequent crack initiation and propagation. Errors may be introduced by not accounting for this adherend distortion in the T.C.B.

specimen. The finger phenomenon was also observed in the prototype specimen. In this case there were a number of fingers defining the crack front (figure 10b). The fingers had a rather regular spacing between them.

The applicability of the crack profile measurement system to stiffer adhesives was confirmed using an Araldite epoxy system (modulus $\approx 2 \times 10^5$ psi). As expected, the profile gradients were much lower and fringes fully resolvable even for propagating cracks. Although there was some curvature to the crack front it was small and the crack front extended through the specimen thickness. The distortion in the adherends caused a rotation of the Michelson interferometers and a change in photodiode phase difference. In some cases this was severe enough to invalidate the data.

CONCLUSION

Let us summarize the findings on the applicability of the crack opening interference method to the measurement of the unbond profiles in adhesive joints and the requirements it places on the measurement and control of the displacements applied to the joint. The crack opening interference method has been successfully developed for the measurement of unbond profiles in carefully prepared adhesive joints. The resolution of the method is insufficient to fully resolve the high deformation gradients in joints where the adhesive layer has a low modulus and is hardly compressible. Although this restriction is not severe, modifications are proposed to further increase the resolution. The loading device constructed to independently apply displacements normal to and tangential to the bondline does so to within 0.16 μm making it completely compatible with the displacements measured by the crack opening interference method. Due to the high precision of the measurements that are made, a sound basis for modelling the behavior of adhesive joints for their subsequent design and life prediction is provided.

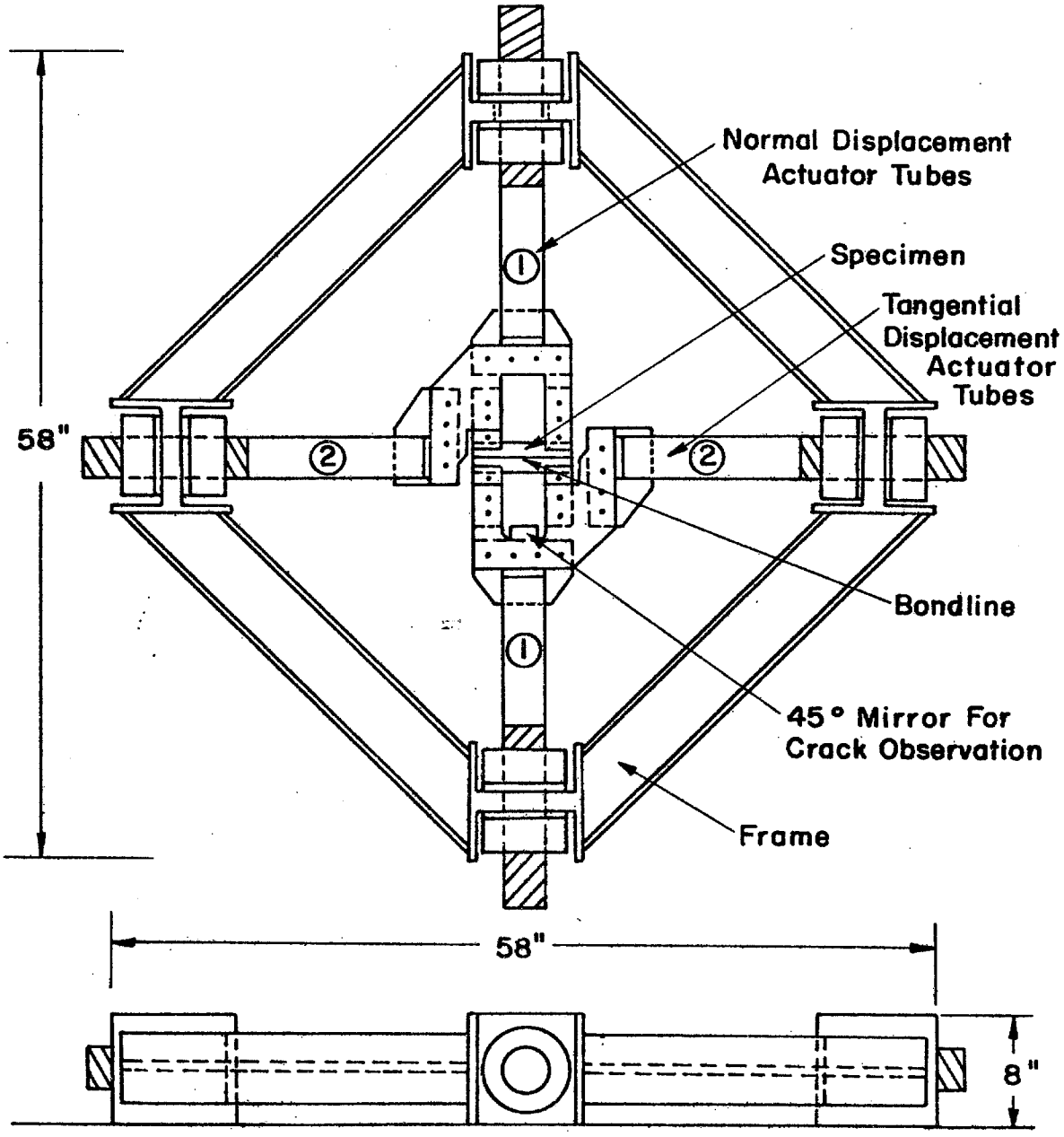

FIG. I THERMALLY ACTUATED SERVO LOADING DEVICE

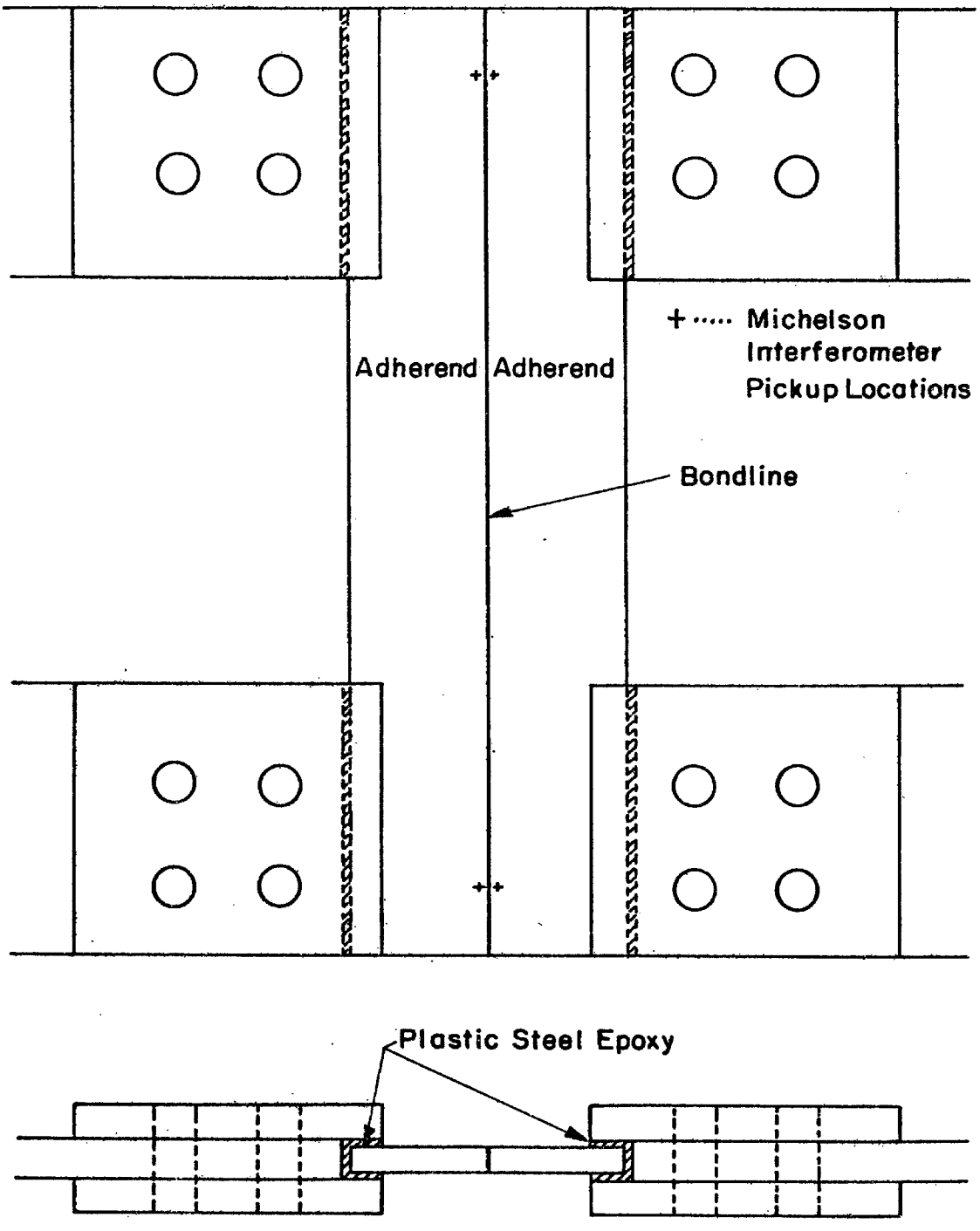

FIG. 2 SPECIMEN MOUNTING

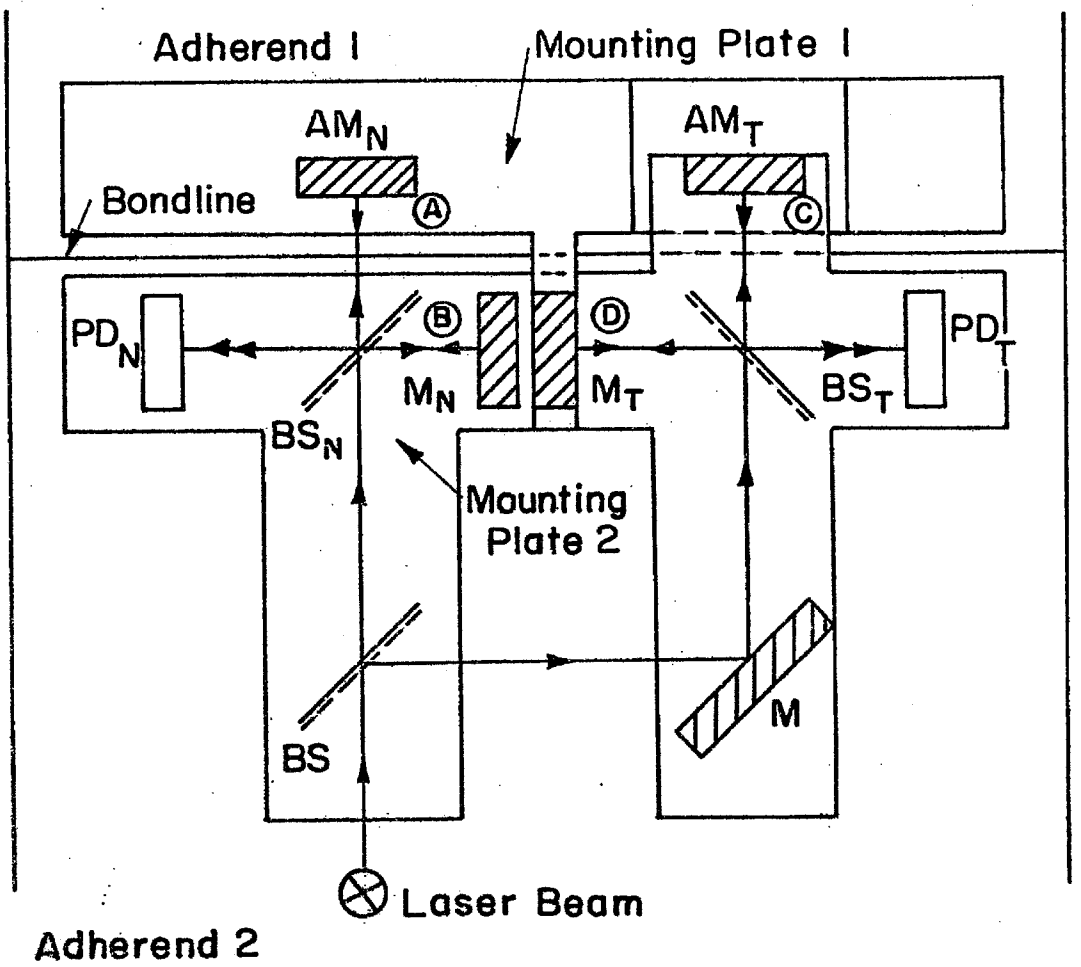

FIG.3 MICHELSON INTERFEROMETER ARRANGEMENT

Abbreviations: M = Mirror, AM = Adjustable Mirror, BS = Beam Splitter, PD = Photodiode Pair. Subscripts "N" and "T" refer to elements of the interferometers measuring displacements normal to and tangential to the bondline, respectively. Elements AM_N and M_T are attached to adherend 1 through mounting plate 1. Mounting plate 2 connects all other elements to adherend 2. Any displacement is resolved into its components normal to and tangential to the bondline by changes in path difference occurring between beams (A) and (B) and beams (C) and (D), respectively.

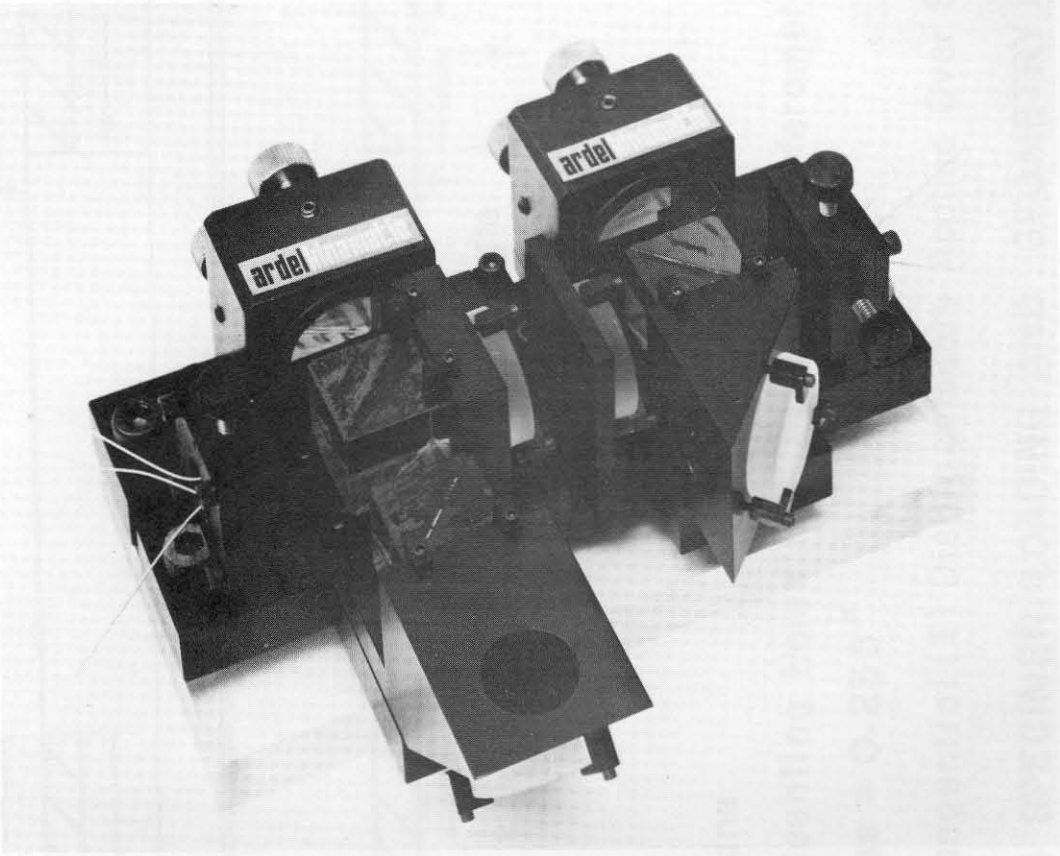

FIG. 4. MICHELSON INTERFEROMETERS

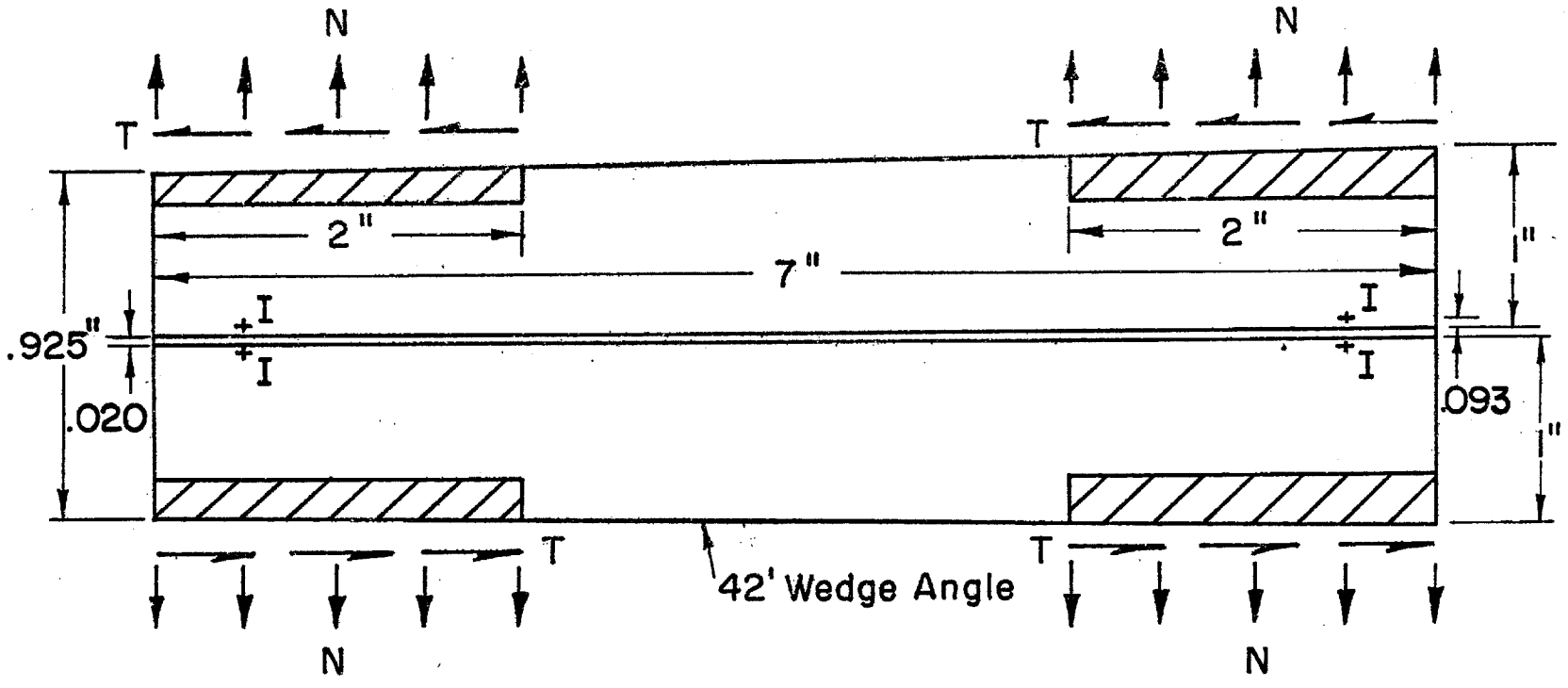

Adherends Glass

Adhesive Solithane

Locations I Are Mounting Holes For Michelson Interferometers

Specimen Thickness = 0.235"

Normal (N) And Tangential (T) Displacements Applied Over Shaded Areas

FIG. 5 SPECIMEN LOADING AND GEOMETRY

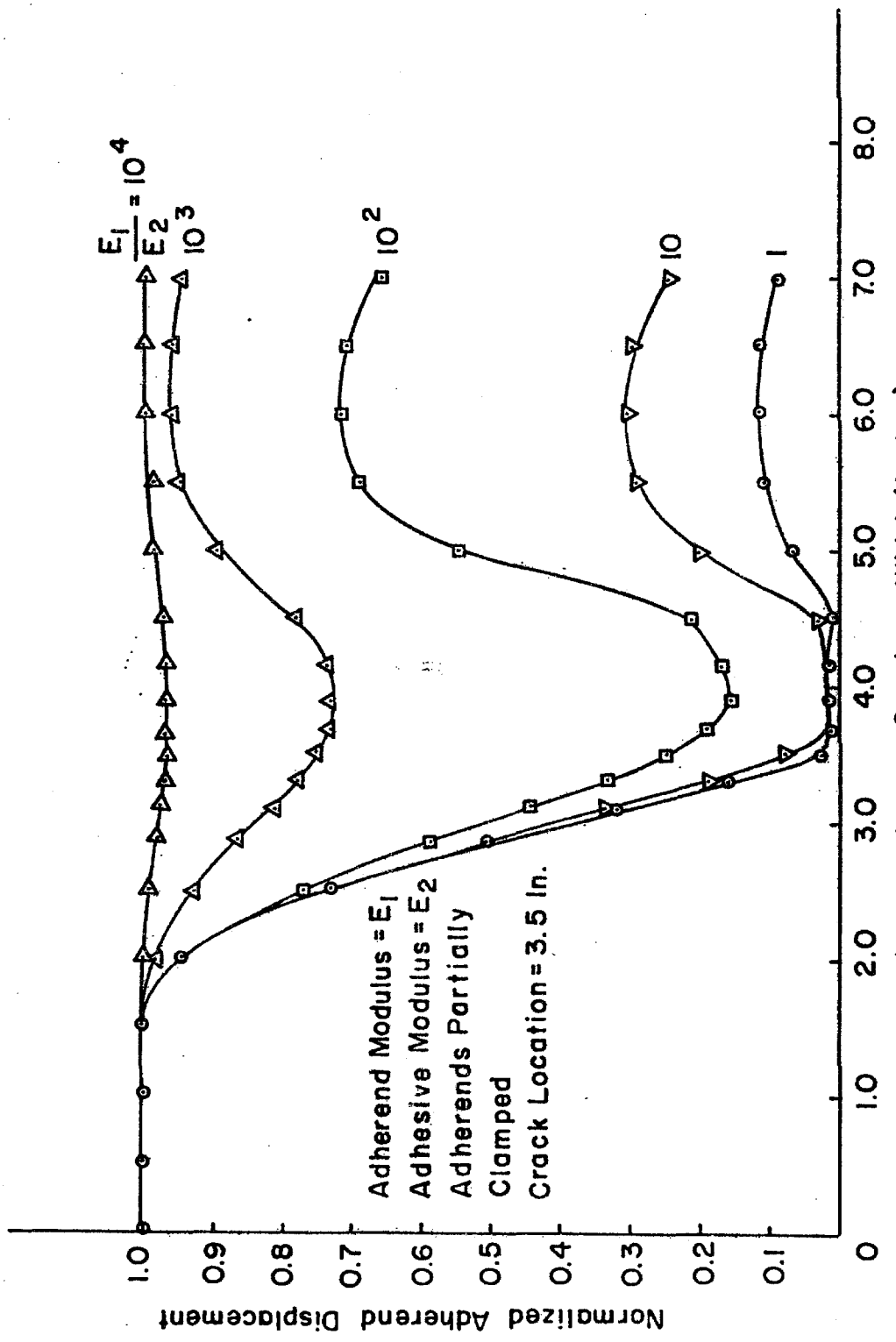

FIG. 6 EFFECT OF THE RATIO OF ADHEREND TO ADHESIVE MODULI ON THE ADHEREND DEFORMATION 0.1 INCHES FROM THE BONDLINE

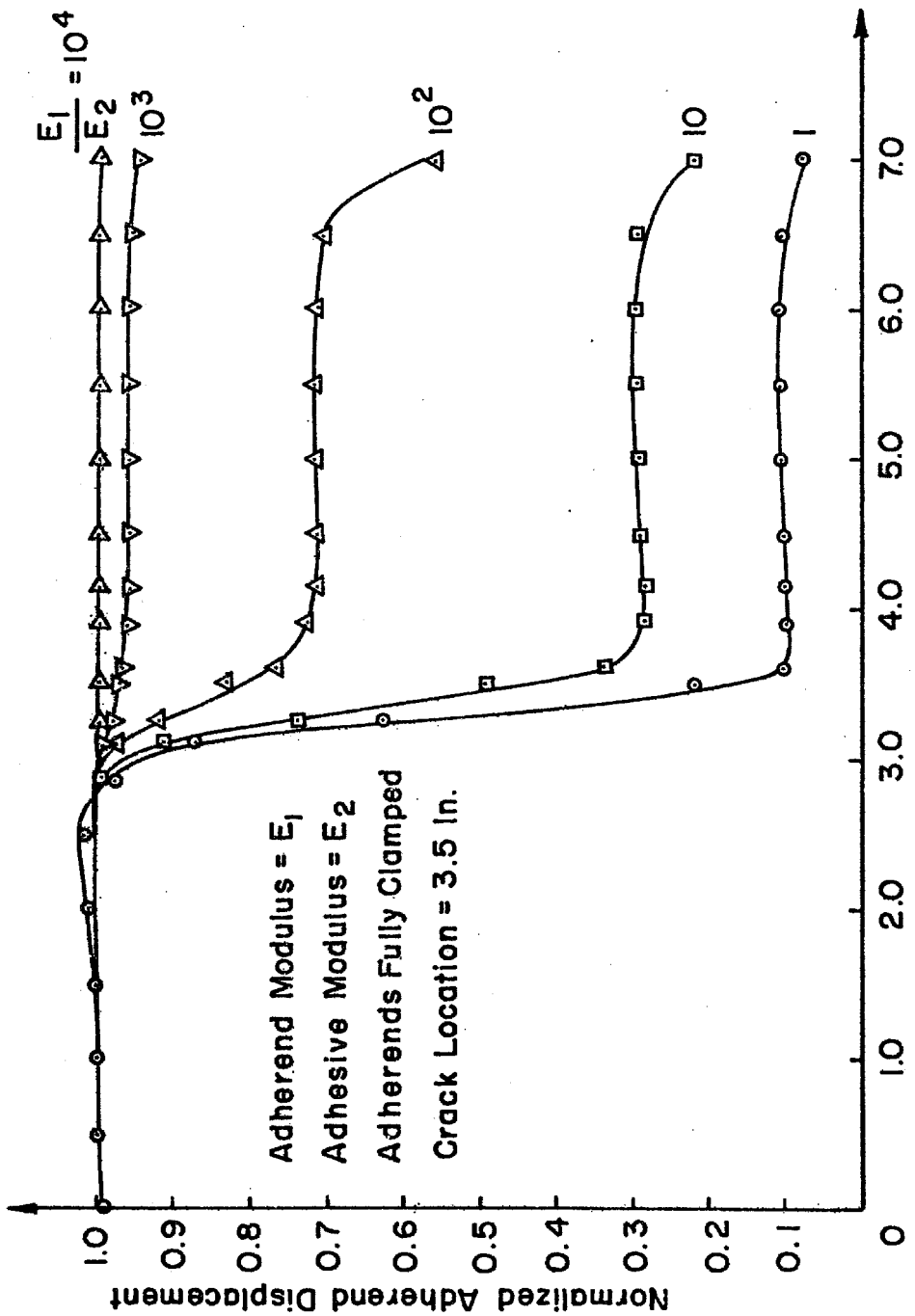

FIG. 7 EFFECT OF THE RATIO OF ADHEREND TO ADHESIVE MODULI ON THE ADHEREND DEFORMATION 0.1 INCHES FROM THE BONDLINE

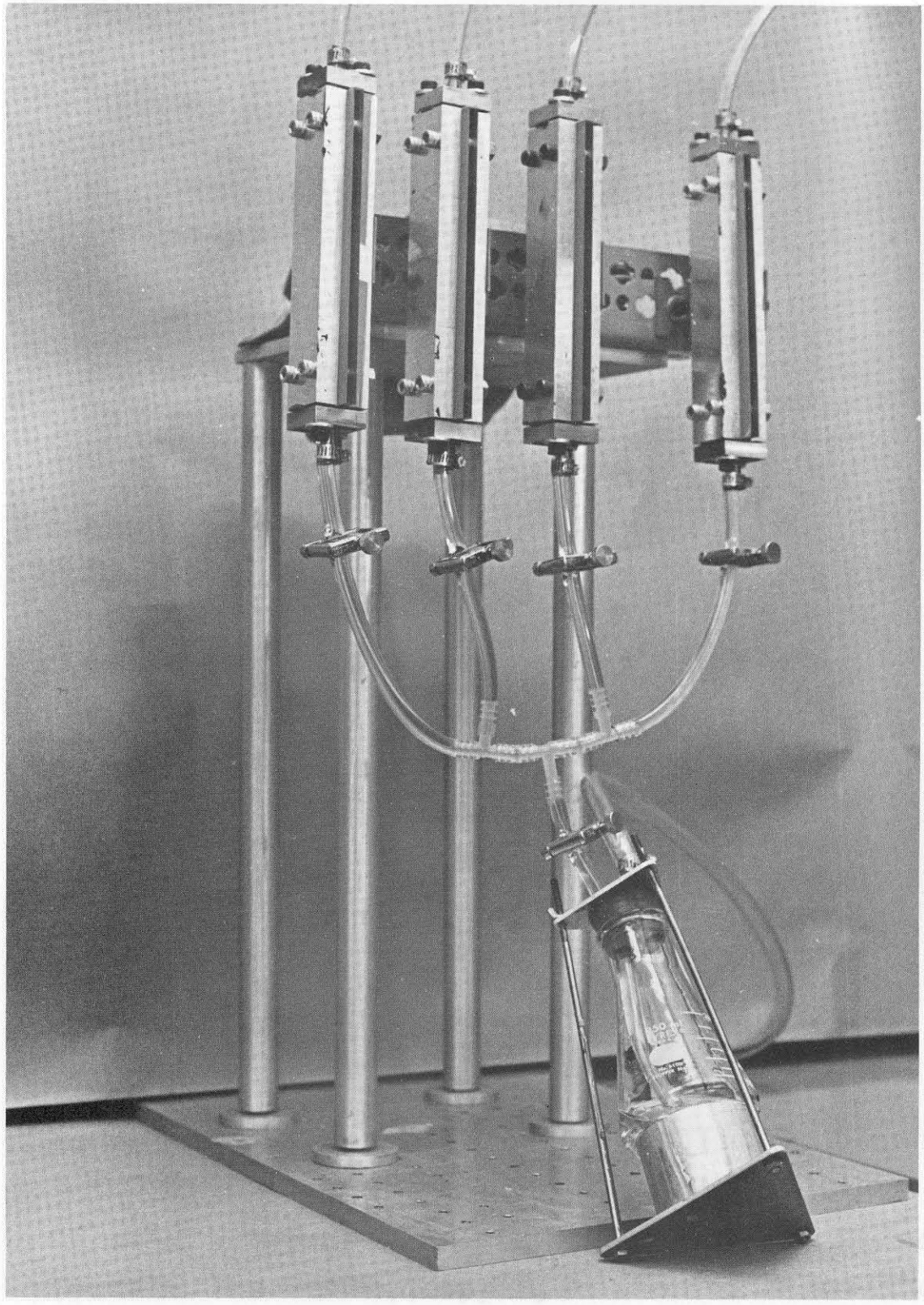

FIG. 8. SPECIMEN CASTING SYSTEM

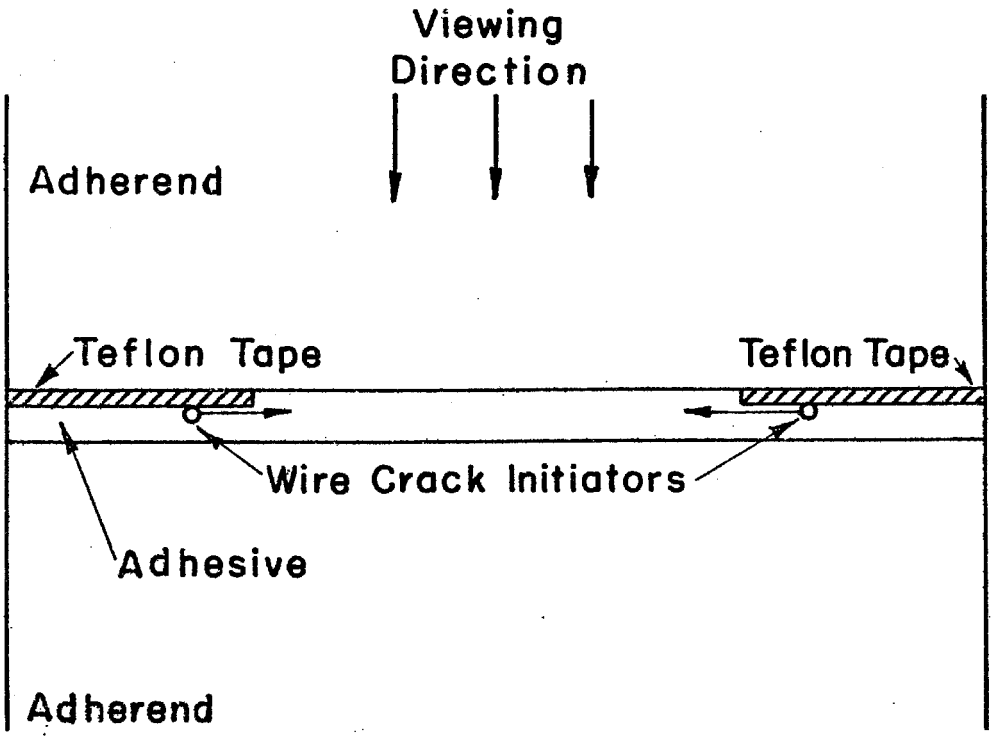

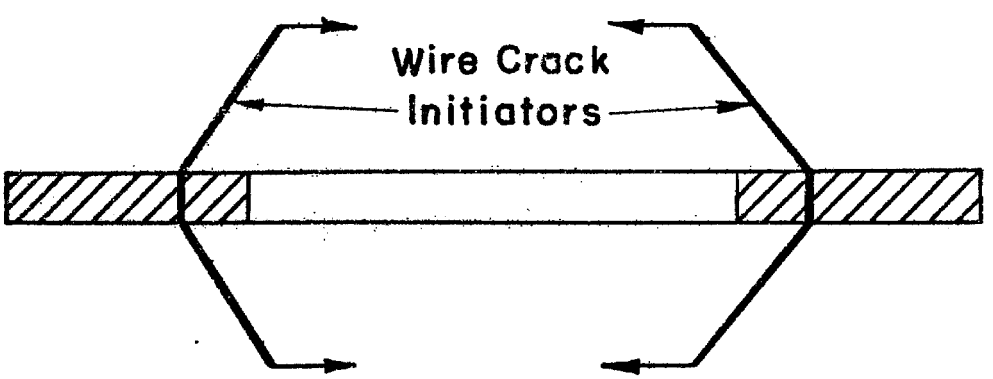

To Initiate A Crack From Each Edge Of The Specimen, A 0.003" Diameter Wire Is Inserted At The Teflon Adhesive Interface At The Specimen Edge And Pulled Towards The Centre, Stopping At The End Of The Teflon.

FIG.9 CRACK INITIATION PROCEDURE

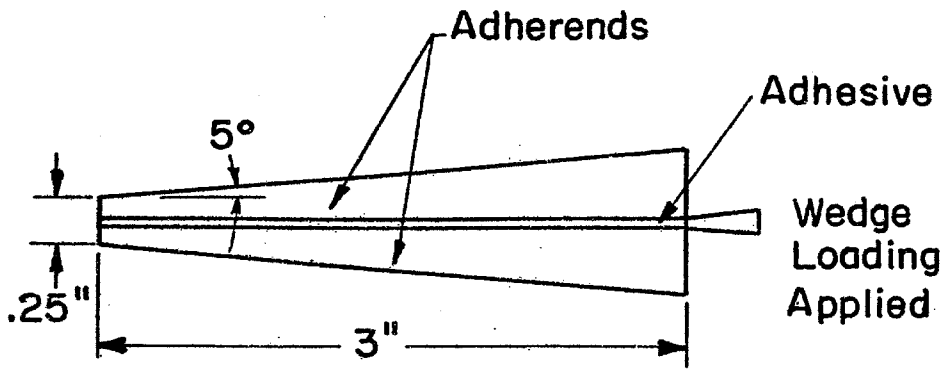

(a)

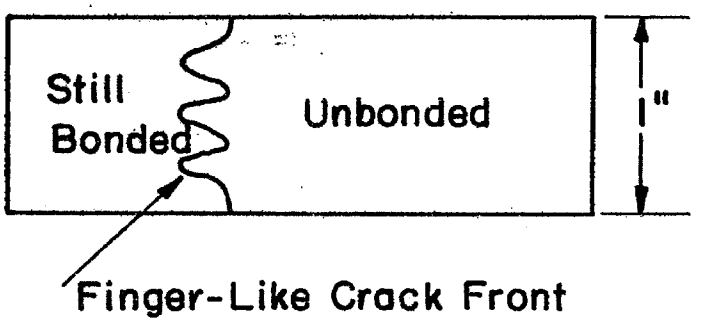

(b)

FIG. 10 PROTOTYPE SPECIMEN

Optical Components

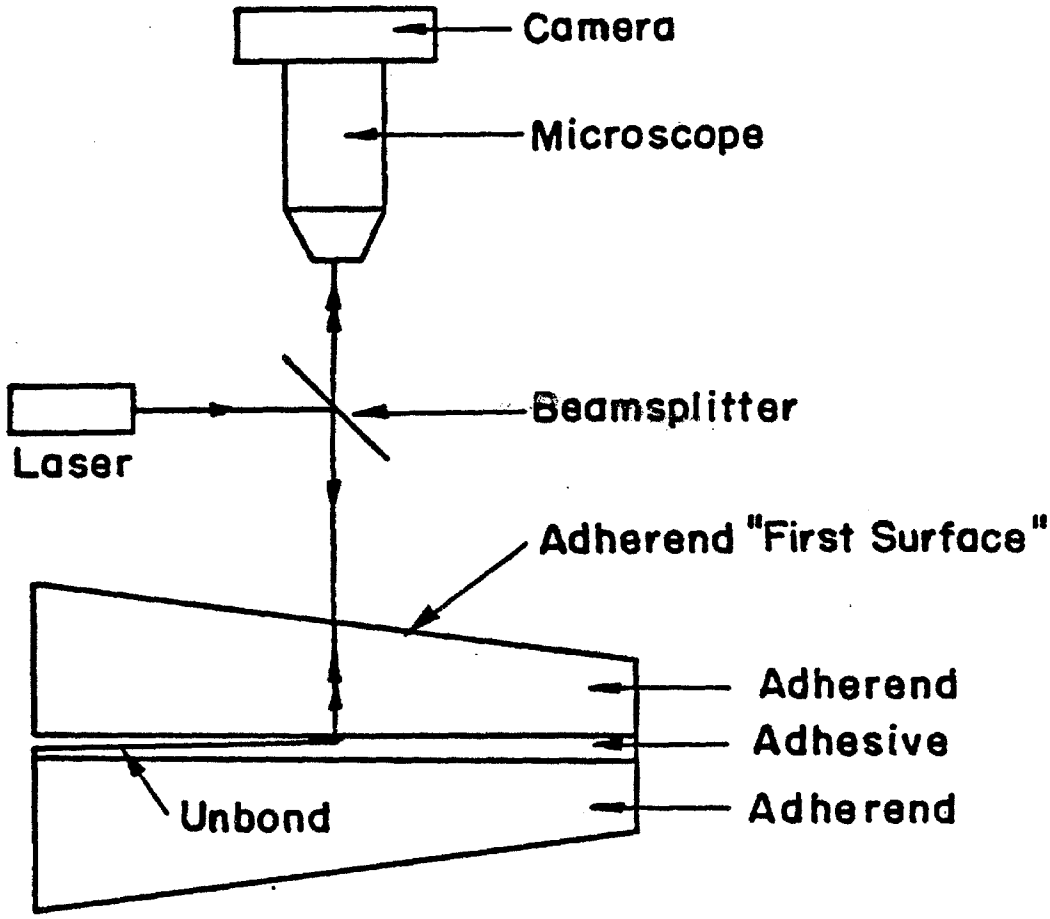

Crack Face Separation

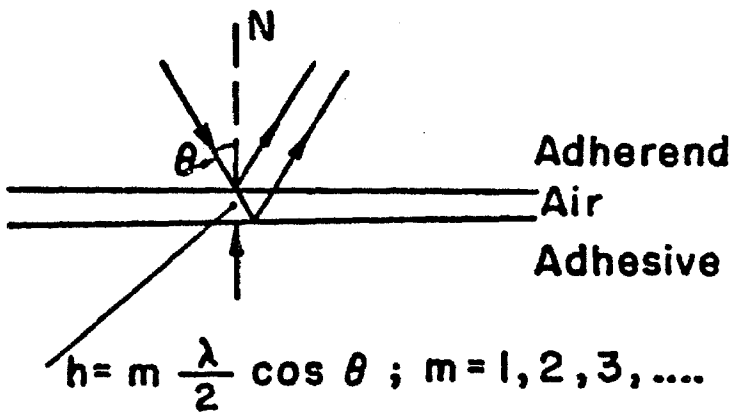

$$h = m \frac{\lambda}{2} \cos\theta \; ; \; m = 1, 2, 3, \ldots$$

FIG. 11 CRACK OPENING INTERFERENCE METHOD

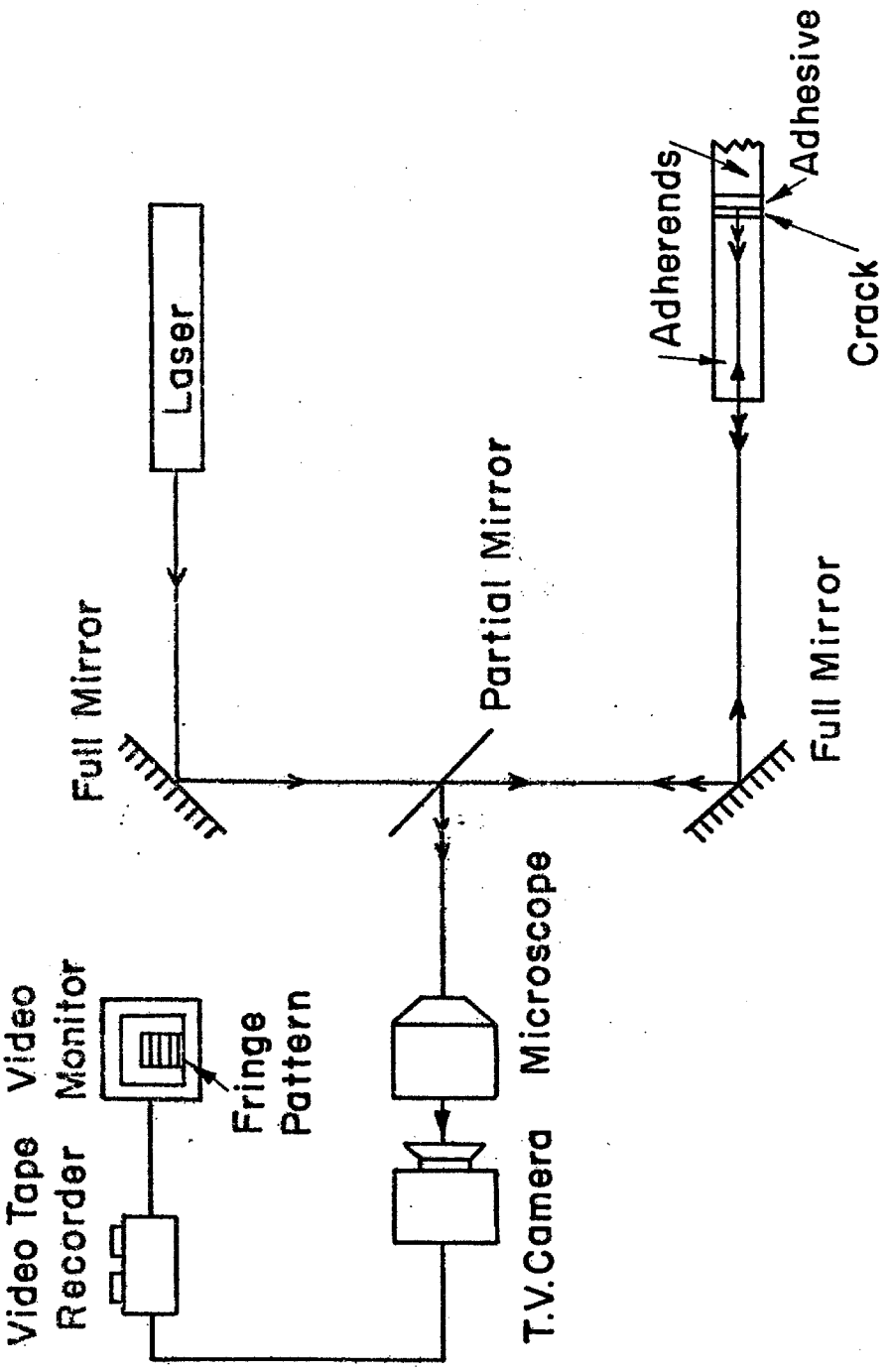

FIG. 12 CRACK PROFILE MEASUREMENT SYSTEM

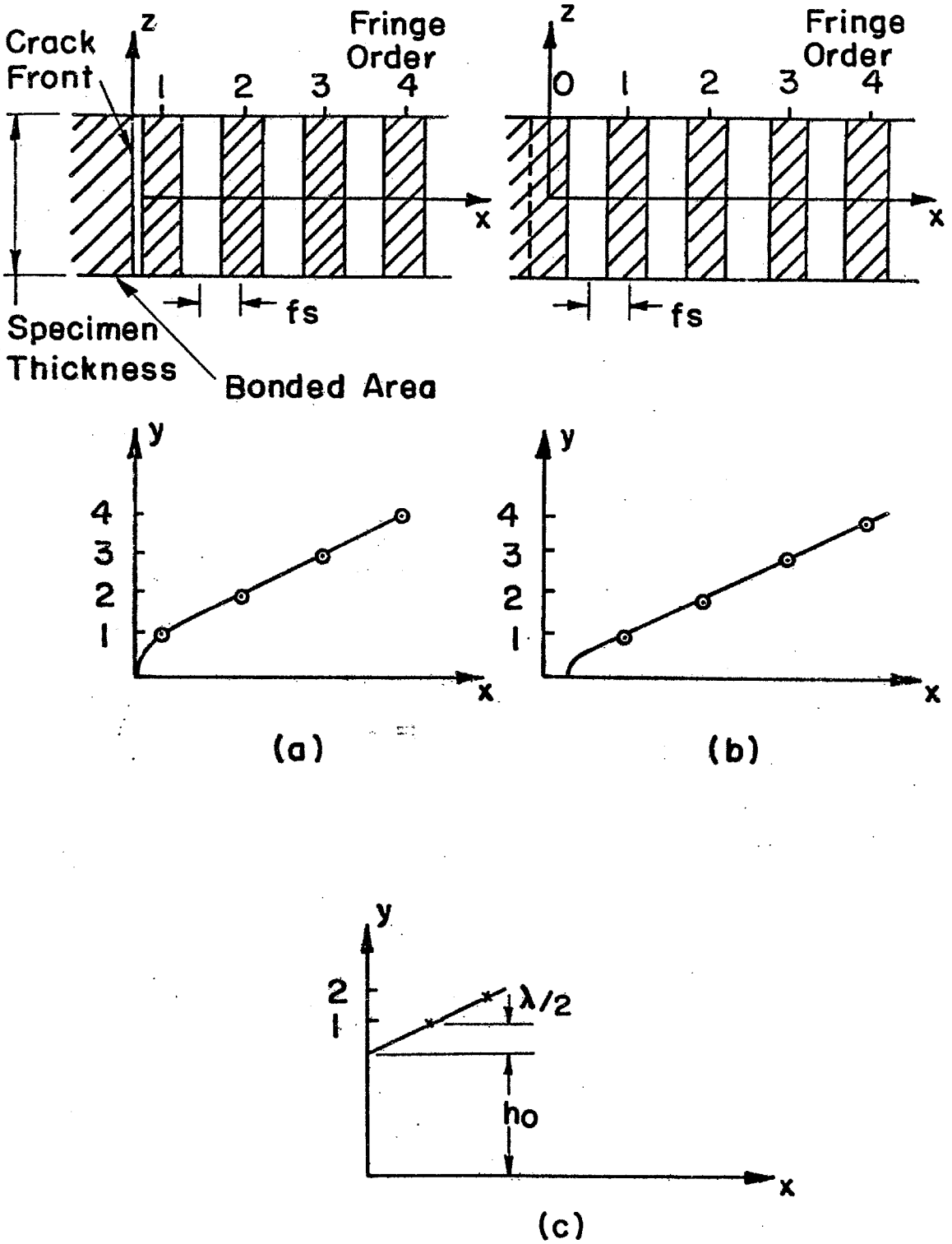

FIG. 13 CRACK FRONT LOCATION

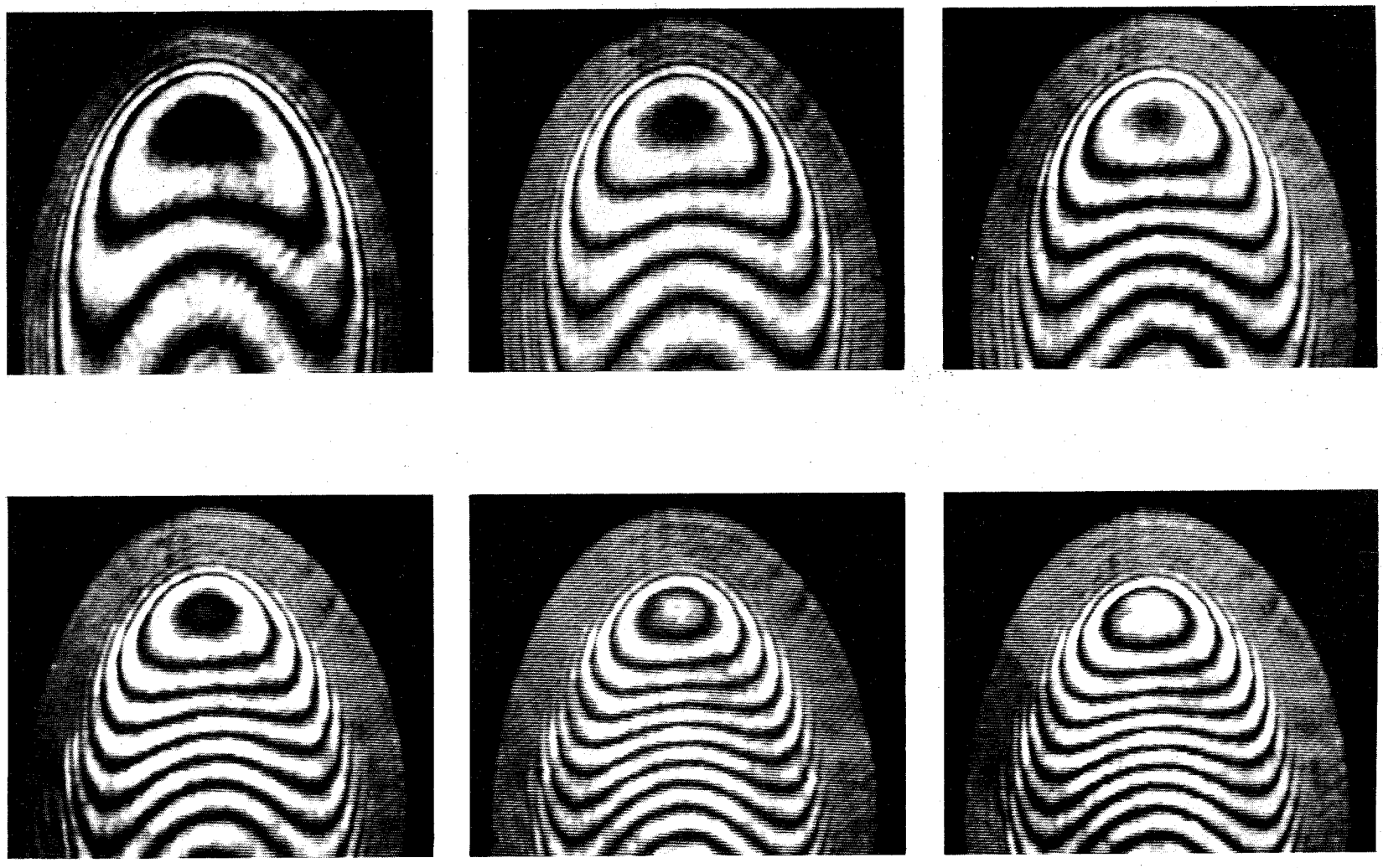

FIG. 14. INTERFERENCE FRINGE PATTERNS OF AN INTERFACE CRACK AT SUCCESSIVE NORMAL LOAD LEVELS.

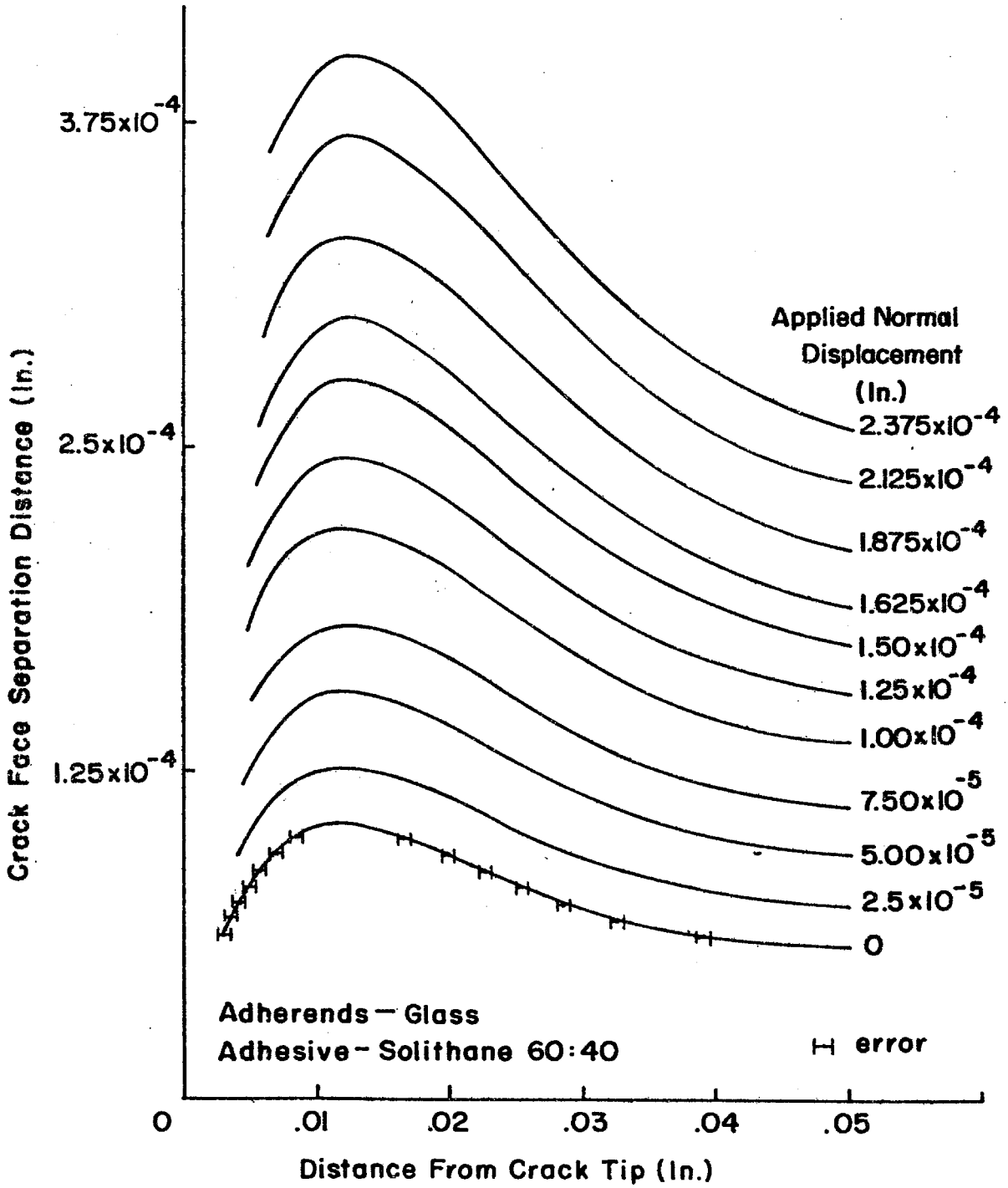

FIG. 15 CRACK PROFILES FOR DIFFERENT APPLIED NORMAL DISPLACEMENT

REFERENCES

1. Bikerman, J. J.: Experiments in Peeling, J. Appl. Poly. Sci., 2 (1959) pp. 216-224.

2. Kaelble, D. H.: Peel Adhesion, Adhesives Age, May 1960,pp. 37-42

3. Kobatake, Y. and Inoue, Y: Mechanics of Adhesive Joints, Part IV: Peeling Test, Applied Scientific Research (A), 8 (1959) pp. 321-338.

4. Ripling, E. J.; Mostovoy, S. and Patrick, R. L. : Measuring Fracture Toughness of Adhesive Joints, Material Research and Standards, March 1964, pp. 129-134.

5. Williams, M. L.: The Continuum Interpretation for Fracture and Adhesion, J. Appl. Poly. Sci., 13 (1969) pp. 29-40.

6. Jemain, W. A. and Ventrice, M. B.: The Fracture Toughness of Adhesive-Bonded Joints, J. Adhesion, 2 (1970) p. 106.

7. Ripling, E. J.; Corten and Mostovoy, S.: Fracture Mechanics: A Tool for Evaluating Structural Adhesives, J. Adhesion, 3 (1971) pp. 107-123.

8. Mostovoy, S., Bersch, C. R. and Ripling, E. J.: Fracture Toughness of Adhesive Joints, J. Adhesion, 3 (1971) pp. 125-144.

9. Stone, S. E.; Westmann, R. A. and Fourney, M. E.: Analytical and Experimental Studies in Adhesive Mechanics, UCLA-ENG-7556 (1975), Univ. of Calif., Los Angeles.

10. Romanko, J.: Behavior of Adhesively Bonded Joints under Cyclic Loading, AGARD-LS-102 - Bonded Joints and Preparation for Bonding 4-1 (1979).

11. Sykes, J. L.; Greene, G. W. and Chow, C. L.: Experimental Techniques and the Mixed-Mode Fracture of Adhesive Joints, VDI Berichte, 313 (1978) pp. 503-509.

12. Knauss, W. G.: On the Steady Propagation of a Crack in a Viscoelastic Sheet: Experiments and Analysis, in Deformation and Fracture of High Polymers, ed. Kausch, Hassel and Jaffee, Plenum Press (1973).

13. Dunham, R. S. and Becker, E. B.: TEXGAP, The Texas Grain Analysis Program, TICOM Report 73-1 (1973), The University of Texas at Austin.

14. Hong, C-C. and Stern, M.: The Computation of Stress Intensity Factors in Dissimilar Materials, J. of Elasticity, 8 (1978) pp. 21-34.

15. Lindsey, G. H., Schapery, R. A., Williams, M. L. and Zak, A. R.: The Triaxial Tension Failure of Viscoelastic Materials, ARL 63-152 (1963), Aerospace Research Laboratories.

16. Sommer, E.: An Optical Method for Determining the Crack Tip Stress Intensity Factor, Engng. Fract. Mech., 1 (1970) p. 705.

17. Crosley, P. B., Mostovoy, S. and Ripling, E.J.: An Optical Interference Method for Experimental Stress Analysis of Cracked Structures, Engng. Fract. Mech., 3 (1971) pp. 421-433.

18. Packman, P. F.: The Role of Interferometry in Fracture Studies, in Experimental Techniques in Fracture Mechanics 2, ed. Kobayashi, SESA Monograph Series (1975).

19. Hung, Y. Y. and Durelli, A. J.: Simultaneous Measurement of Three Displacement Derivatives Using a Multiple Image-Shearing Interferometric Camera, J. of Strain Analysis, 14 (1979) pp. 81-88.

PART 2

An Experimental Investigation of the Deformation and Propagation of an Interfacial Crack

ABSTRACT

The tools developed in Section 1 provide direct observations and measurement of the unbond profiles in a cracked butt joint under precisely controlled applied displacements normal to and tangential to the bondline (.16 μm resolution). These tools are now used in two situations.

In the first experiment, carried out with stationary cracks, the linearity of the relationship between the crack flank displacements and the applied displacements is examined. Information is thus provided on the limits to which current linear stress analyses are valid and/or useful.

In the second experiment the effects of loading normal to or tangential to the bondline on the crack profile and associated unbonding rates are determined for steadily propagating cracks. The measurements allow an examination of both global and local fracture criteria. In a global criterion, the applied displacements are related through an energy conservation argument to the fracture (surface) energy. The crack profile measurements are then also used to formulate a critical crack profile gradient criterion, a critical crack normal crack opening displacement criterion and a critical vectorial crack opening displacement criterion as local fracture criteria. The vectorial crack opening displacement criterion, which is the vectorial addition of crack opening displacements

both normal and tangential to the bondline, was found to provide the most consistant results.

TABLE OF CONTENTS

LIST OF FIGURES

2.1 INTRODUCTION

Section 1 provided the general motivation for this study on adhesive joint failure and also described the development and capabilities of the necessary experimental tools. To summarize, we developed the capability to independently apply displacements normal to and tangential to the bondline and, at the same time, measure the changes in the profile of an interfacial unbond in a cracked butt joint. The local fracture processes can thus be observed directly through displacement measurements of 1/4 μm accuracy. Such detailed observations may then be exploited to examine failure models for adhesive joints based on fracture mechanics principles.

We are interested primarily in the crack growth history of an unbond. The adhesives used to manufacture structural joints are polymeric and potentially viscoelastic or time dependent. In the fracture of monolithic materials it has been found that failure of a structural element having viscoelastic or rate sensitive material properties need not be due to a catastrophic increase in crack length of an existing flaw under a critical loading (as is usually the case for rate insensitive materials such as most metals). Rather, the element may fail after a long period of time due to very slow crack growth rates which are direct consequences of the viscoelastic material properties. We expect the time dependent material properties of the adhesive layer in an

adhesive joint to produce similar effects in the interfacial unbond growth history.

The constraint applied by relatively stiff adherends on the adhesive will also affect the crack growth history, particularly through different combinations of displacements of the adherends normal to and tangential to the bondline. The joint failure models to date have used linear stress analysis theory which predicts infinite stresses near the unbond front. While we do not expect infinite stresses on a physical basis, the local stresses may be high enough to induce a nonlinear kinematic and material response. Large local deformations would violate the linearized kinematic response assumed. Such nonlinearities may be confined to relatively small domains giving little or no measurable perturbation to a gross linear response.

These considerations have motivated two initial experiments in what is expected to be a continuing study. The first, for stationary cracks, determines the linearity of the response of the crack profile in the region of the crack front resulting from adherend displacements applied normal and tangential to the bondline. In the second experiment the effects of loading direction on crack propagation rate and the crack profile are then determined for steadily propagating cracks. A discussion of these experiments and their results are presented next in Sections 2.2 and 2.3 respectively.

2.2 LINEARITY ANALYSIS - STATIONARY CRACKS

Current designs and analyses that are prevalent today average out the effect of the adhesive layer. This procedure results from ignoring the details of the fracture processes in the region of the crack front and assuming the effect of the adhesive layer to be negligible. Fracture mechanics parameters are made functions of bond thickness and the joint is then considered to be a monolithic body. The consequences of these simplifying assumptions were discussed earlier in the introduction to Part 1 where peel and thickness-averaged fracture mechanics approaches were discussed.

The neglect of the local fracture processes has not, in general, been confined to analysis but also to experimental approaches, where it is much easier to measure global effects. Experiments making the same a priori assumptions as theoretical analysis are therefore conducted which may not expose deficiencies in the modelling. However, deficiencies have been exposed in service environments where factors such as temperature and humidity variations (which affect the local fracture processes) produce an apparent randomness to joint failure, when failure is characterized only in terms of global parameters.

If the response of the region local to the crack front is a linear function of the globally applied loading, then a thickness averaging, linear approach is exact. We are

able to precisely measure and control the globally applied loading as well as measure the change in crack surface normal displacements very close to the crack front. We are therefore in a position to determine the extent of linearity of the relationship between the crack flank displacements normal to the bondline in the crack front region and the applied displacements. Note that this experiment makes no a priori theoretical assumptions inasmuch as only measured quantities are involved.

The crack flank normal displacements were determined for two cases. In the first, displacements were applied normal to the bondline, holding the tangential displacements to zero. Secondly, displacements were applied tangential to the bondline, while keeping the normal displacements equal to zero.

The case of the crack flank displacements normal to the bondline produced by an applied tangential displacement requires some explanation. The question arises as to whether a linearity analysis based on the measurement of the crack flank normal displacements is reasonable because the crack flank tangential displacements themselves may affect that measurement. This would be the case if the displacement gradients were high. However, the measurements are made only in the region where fringes are fully resolved. The fringes can only be resolved for profile gradients less than 33 minutes. The crack flank displacements do not therefore produce an error in the measurement of the crack flank normal displacements.

Before presenting the results for these two cases, we discuss the general crack profile and shapes obtained in the glass-Solithane joints used in this study. Figure 1 shows a sequence of video pictures of an interface crack taken under increasing applied displacement levels. The field of view covered in these pictures corresponds to approximately 0.6 mm. The pictures are centered on the specimen midthickness. We see that the crack does not extend all the way through the specimen thickness but has a finger-like shape. The separation of the crack faces is given by the order and location of the fringes in the interference pattern contained within the outline of the crack. This finger

phenomenon or tunnelling mode of fracture always developed from the through-the-thickness initial crack generated as described in Section 1.3.3. The width of this finger was found to vary with the type of loading. For displacements applied normal to the bondline it is approximately 0.45 mm (0.018 inches) wide whereas a tangential loading produces widths on the order of 2 mm (0.078 inches). However the crack front still retains considerable curvature in this case.

To explain this finger fracture we draw on studies of the "poker chip" analysis by Gent and Lindley [1] and Lindsey et al [2]. The butt joint used in this study closely satisfies the assumptions made in the analysis of the poker chip problem because the glass adherends are rigid compared to the thin layer of the flexible Solithane adhesive. The details of the analysis are provided in Appendix 1. Figure 2 shows the distribution of the stresses normal to the bondline across the specimen thickness. Solithane is nearly incompressible. In this non-fractured virgin geometry, the stresses are therefore very high in the region of the specimen midthickness. The expected concentration along the edges does not appear because the assumed displacement field does not account for edge effects. Lindsey et al [2] did account for edge effects but found that, for nearly incompressible materials ($\nu > .49$), the stresses along the specimen midthickness were much higher than those along the specimen edges. It appears clear then

why cracks propagated so consistently through the specimen in the finger or tunnelling mode.

In characterizing the crack profiles for these studies we confined ourselves consistently to one scan along the center of the crack. The full three dimensional shape of the crack would be generated by a series of scans spanning the full crack width. The data acquisition and reduction task involved in generating the full crack shape is considerable and was temporally not feasible within the present study. Later work plans incorporate a video digitizer in the video system and automate this part of the data reduction.

A sequence of profiles for increasing normal applied displacements is shown in figure 3. The "zero load" profile indicates the presence of cure shrinkage stresses. The specimens were cured at room temperature to avoid the introduction of thermal residual stresses. However, even when a specimen was left in a dry atmosphere, at room temperature and under zero applied load, a crack propagated, again in a finger mode. The only remaining cause of residual stresses was cure shrinkage. The extent of residual cure stresses was therefore determined by assuming a displacement field similar to that used in Appendix 1 but also including shrinkage. The details of the analysis are presented in Appendix 2. Figure 4 shows the distribution of stresses normal to the bondline. They are again concentrated along the specimen

midthickness and even become compressive towards the specimen edges. The cure shrinkage and volumetric coefficient of thermal expansion for Solithane were experimentally determined to be $\frac{\Delta v}{v} = 1.34 \times 10^{-2}$ and $\alpha_v = 5.36 \times 10^{-3}$ cm^3/cm^3 ^oC, respectively [6]. Thus the cure shrinkage corresponds to a thermal cool down of 25^oC. This sizeable cure shrinkage makes its neglect rather questionable for this material and also explains why there is a separation of the crack faces in figure 3, even under a zero applied load.

Another noticeable feature of the crack profiles in figure 3 is the fact that the crack face separation reaches a maximum. This maximum becomes more pronounced as the normal applied displacement increases. From linear fracture mechanics considerations, one expects the profile to be parabolic out to a distance of the order of the bond thickness and then remain constant at a value of the applied normal displacement, u_N say. However, even when the zero profile is subtracted out the maximum separation reaches a value of 1.24 u_N dropping 0.84 u_N at about two bond thicknesses from the crack front. This "sucking in" of the material is due to the incompressibility of the Solithane and the constraint applied by the stiff adherends.

The high deformations produced by the incompressibility in the crack front region cannot be fully resolved all the way to the crack front by the present method. Improvements are proposed for any subsequent work in Section 1.4.3

(page 35). This explains why the profiles shown in figure 3 are incomplete near the crack front, although the crack front location itself is well identified (see Section 1.4.2, page 31). Nonetheless, in the regions where the profile can be resolved, the resolution and consistency is extremely good. The error bars on the profiles correspond to the spatial resolution of the microscope which is 2.56×10^{-4} inches. That is, the location of the crack front and fringes can be determined to within 6.5 μm (2.56×10^{-4} inches). We are therefore able to make definitive statements on the linearity of the response in the crack front region due to the globally applied loading.

2.2.1 Crack Profile Response Due to Displacements Applied Normal to the Bondline

The incremental response at various locations behind the crack front due to the applied displacements is obtained by determining the change in crack face separation from the zero load profile. We call this change in the crack face separation the crack flank normal displacements and plot them against the applied normal displacements in figures 5 and 6. These "response curves" are shown for various locations behind the crack front. Figure 5 shows the response curves for locations as far behind the crack front as the location of the profile maximum, figure 5 for locations

beyond that. The separation by these figures is made to avoid confusion in overlapping response curves.

For normal applied displacements up to about .5 μm (2×10^{-5} inches, 0.1% strain), the response is nearly the same for all locations and fairly linear. At higher levels of applied displacement we see that the response is no longer the same for all locations, nor is it linear.

2.2.2 Crack Profile Response to Displacements Applied Tangentially to the Bondline

The insert in figure 7 identifies the directions of the sequence of tangentially applied loading required to produce the series of crack profiles. In this case, the crack develops a finite length. Applied tangential displacements do indeed produce local opening mode deformations in the crack faces. The crack front from which propagation would occur were the magnitude of applied displacements sufficiently high is called the "leading crack front." The crack face separation only reaches a maximum close to this leading crack front, decreasing with much smaller profile gradients towards the "lagging crack front." As the tangentially applied displacements are increased, the profile gradients near the leading crack front increase. At the lagging crack front the gradients remain much the same but there is crack closure. In fact, the profile could be fully resolved to within a half wavelength separation from the adherend sur-

face at the lagging crack front. The steepening of the profile and maximum at the leading crack front as well as the smooth crack closure at the lagging crack front has been predicted theoretically by Comninou and Schmueser [3] for an interface crack at a bimaterial interface of two semi-infinite linearly elastic bodies. Although we are dealing here with an adhesive joint geometry of finite thickness, the qualitative behavior should be the same.

The crack flank normal displacements under a series of tangentially applied displacements is shown in figure 8. In contrast to the previous case of normally applied displacements, we see a highly nonlinear response, even for small applied tangential displacements (less than 0.001 strain). The tangentially applied displacements required to produce the same crack flank displacement as that due to a normal applied displacement are approximately twenty times greater.

Figure 9 shows the effect on the crack profile of reversing the direction of the applied tangential displacements. The maximum in the crack profile at what was the leading crack front moves to the other end of the crack as the magnitude of the reversed displacement is increased. If the magnitude were increased sufficiently, the crack would then propagate (as a bubble) in the opposite direction to that in which it was propagating under the previous

load.

The fracturing at the leading crack front and rehealing at the lagging crack front under a sliding motion of the adherends has been predicted by Broberg [7]. The rehealing has repercussions when a fatigue loading is considered. The bond between the adhesive and adherend is weaker in rehealed regions than in the as yet uncracked or virgin regions. Nonetheless, while each load reversal might open up one end of the crack, the other end would be rehealed. As a result, the crack location would change but its length would remain constant. Thus a crack could never reach a critical length for failure under a purely tangentially applied relative cyclic displacement of the adherends.

2.2.3 Linearity Analysis - Conclusion

We have been able to consistently and precisely characterize the response of the region close to the crack front due to the globally applied loading. Ultimately, it is the local crack tip response which determines the onset of fracture. Measures of the local response have hitherto been unavailable and analyses have therefore characterized joint failure in terms of global parameters under assumptions of a linearized theory. The results show that for normal displacements the linearity assumptions are indeed valid (for strains less than 0.1%), at least to engineering accuracy. However, in the case of displacements applied

tangential to the bondline, the local response is highly nonlinear. Linear modelling in this case must therefore be suspect. Since even small amounts of tangentially applied displacements produce a nonlinear response, this suspicion must also be extended to cases of combined loading. Most joints will experience combined loads and any realistic modelling and analysis of failure should incorporate measurements of the local failure processes.

2.3 STEADY CRACK PROPAGATION STUDIES

We expect the failure of adhesive joints using polymeric adhesives to occur in a gradual way and, in general, under initially very small crack propagation rates. Only in the final stages of failure will fracture occur catastrophically as in rate insensitive and brittle materials. Thus it becomes necessary to examine the relation between critical fracture parameters and the rate of unbonding. The life of the joint can then be estimated from a knowledge of the load history to which it is to be subjected and the resultant crack propagation rates. The number of fracture parameters to be related to the unbonding rate will depend on how the fracture process is to be modelled. In engineering applications, simplicity of modelling has obvious attractions. The optimum model is that which uses the minimum of parameters to capture the essentials of the process. The modelling can again be based on the local fracture processes or by averaging out local effects and considering only global parameters. Our experimental tools allow us to measure directly the local crack profile at a particular crack propagation rate as well as the globally applied loading which produced them. We are therefore in a position to compare local and global crack propagation criteria.

Even in highly nonlinear situations, the local profile should reflect the applied loading. For a local fracture

criterion, we wish to characterize the local profile in a simple yet complete manner. For example, critical crack openings have been used to predict the onset of fracture. Another measure might involve the profile gradient. Since this effectively involves the derivative of the crack opening displacement it should be more sensitive in reflecting change than the crack opening displacement itself. Furthermore, the local crack profile gradient can be shown to be proportional to the stress intensity factor (based on linear viscoelasticity). Since any local mode I and mode II deformations should contribute to the local profile gradient and also remembering its association with the stress intensity factor (albeit through linearized theory), the local profile gradient might be viewed as an effective stress intensity factor. It should account for any combination of local deformations normal to and tangential to the bondline. We might therefore postulate that a critical profile gradient governs the onset and subsequent propagation of a crack.

Two crack opening displacement criteria are also considered as local fracture criteria. In the first, the onset of fracture is characterized by the normal (mode I) crack opening displacement reaching a critical value. The total interface separation is considered in the second case where the crack opening displacements normal to and tangential to the bondline are added vectorially to produce the vectorial crack opening displacement.

Alternately, one might consider a global criterion which essentially draws on the first law of thermodynamics by considering the strain energy released and equating it to a fracture energy which depends on the rate of crack propagation. The strain energy calculations are based on the displacement field assumed in the poker chip specimen analysis.

Some remarks on the adhesive material Solithane are presented by way of introduction in Section 2.3.1. The considerations and results for the local criteria of critical profile gradient and critical crack opening displacements are presented in Sections 2.3.2 and 2.3.3 respectively. Finally, the global criterion is discussed in Section 2.3.4.

2.3.1 Solithane Material Properties

Solithane 113 is a polyurethane elastomer sold by the Thiokol Chemical Corporation. It is obtained by mixing a liquid prepolymer with a catalyst. The ratio of the two components can be varied to provide a considerable range of material properties. In the present study a mixture of 60% prepolymer to 40% by weight catalyst was used. Reasons for using Solithane as the adhesive material were discussed in Section 1.3.1 (page 23).

We further note here that it fractures under relatively small strains (0.01), making comparison with fracture models

based on small deformation theory more valid. The fracture surface is featureless even at low crack propagation rates, indicating a brittle type of fracture. Analysis is thus simplified by not having to account for plasticity effects. The master creep curve for Solithane, obtained in [4], is shown in figure 10. Solithane is thermorheologically simple and its time temperature shift curve is also shown in figure 10. Time temperature shifting can therefore be used to extend the range of experimentally acceptable time scales.

2.3.2 The Critical Crack Profile Gradient Criterion

The crack opening interference method allows us to measure the profile of a crack, close to the crack front. If the profile could be determined sufficiently close to the crack front, the profile gradient, which is to be used as the fracture parameter, can then be determined by differentiation. Unfortunately, the high deformation gradients close to the crack front could not be resolved by the present, unmodified crack opening interface method. Our original intention was to measure the crack profile as close as 2.54 μm (1×10^{-4}) inches from the crack front. However, the first resolvable fringes were usually on the order of 0.254 mm (0.01 inches) from the crack front. We therefore wished to fit any available data to an analytically obtained curve so as to determine the profile gradients

closer to the crack front than 0.254 mm.

The choice of profiles to which to fit the data is rather limited. There are no nonlinear analyses of the full three dimensional cracked adhesive joint geometry. The best alternative is provided by the findings of Knowles and Sternberg [5] in the nonlinear analysis of crack face deformations in two dimensional monolithic solids. They found that the crack profile near the crack tip followed a combination linear and power law of the form

$$y = ax^{\frac{1}{2}} + bx \quad , \tag{1}$$

where y is the crack face separation and x the distance from the crack tip.

The locations of the crack tip and the first two resolvable fringes were used in the curve fit to determine the coefficients a and b. This allowed the profile gradient to be determined much closer to the crack tip (2.54 μm was chosen). In view of the tenuousness of this estimate, another measure of the gradient was taken to be the height of the maximum of the profile divided by its distance from the crack tip. The two measures differed by a factor of ten but gave otherwise very consistent results. In the following discussion only the first measure will be used.

The crack propagation rates that could be measured ranged from 10^{-6} to 10^{-3} in/sec. The lower limit was dictated by the length of time necessary to achieve a

crack front displacement such that the relative error in crack front displacement measurement was less than 20%. The upper limit was determined by the field of view in the microscope and relative error in time measurement. The crack velocities obtainable at room temperature were increased by heating the specimens to 60°C. These velocities can be compared with tests at other temperatures using the appropriate time-temperature shift factor for Solithane.

The loading history in the crack propagation tests is illustrated in figure 11a. The applied displacements were applied to the joints in a sequence of discrete increments (ΔV) each of which was held constant for 500 seconds. The crack front velocity was monitored continuously once these load levels were reached. The measurement of the crack profile for each load level was made when the crack propagation rate (the average of at least three measurements) was constant. The limitation to constant crack propagation rates is made for simplicity. Before presenting the results, we note some interesting phenomena.

Cracks were intiated from both edges of the specimen. Under applied normal displacements, both initial cracks grew to meet eventually at the center of the specimen. However, they did not join in a sudden, catastrophic manner. Instead, they stopped, leaving an as yet bonded region on the order of the bond thickness between them. The plan form width of the finger shaped cracks then increased until

crack front displacement such that the relative error in crack front displacement measurement was less than 20%. The upper limit was determined by the field of view in the microscope and relative error in time measurement. The crack velocities obtainable at room temperature were increased by heating the specimens to 60°C. These velocities can be compared with tests at other temperatures using the appropriate time-temperature shift factor for Solithane.

The loading history in the crack propagation tests is illustrated in figure 11a. The applied displacements were applied to the joints in a sequence of discrete increments (ΔV) each of which was held constant for 500 seconds. The crack front velocity was monitored continuously once these load levels were reached. The measurement of the crack profile for each load level was made when the crack propagation rate (the average of at least three measurements) was constant. The limitation to constant crack propagation rates is made for simplicity. Before presenting the results, we note some interesting phenomena.

Cracks were intiated from both edges of the specimen. Under applied normal displacements, both initial cracks grew to meet eventually at the center of the specimen. However, they did not join in a sudden, catastrophic manner. Instead, they stopped, leaving an as yet bonded region on the order of the bond thickness between them. The plan form width of the finger shaped cracks then increased until

the crack fronts extended completely through the thickness. This observation confirms that of Schmueser and Comminou [8] who analyzed the interactions of cracks at bimaterial interfaces. They found that, as the distance between interacting cracks decreased, so the stress intensity factor descreased, indicating that such cracks do not have a tendency to join and form larger cracks. In our experiments such interaction effects could only be observed for displacements applied normal to the bondline. Under applied tangential displacements only one of the initial cracks could grow (due to the asymmetry of this type of loading).

Another phenomenon to be noted here is that the crack opening displacement (and therefore the profile gradient) did not remain constant during the time that the applied normal displacements were held constant. They decreased by a rather consistent amount (Δv_N, figure 11b). The data for the applied normal displacement tests were obtained from three separate experiments. The applied displacement increments (ΔV, figure 11a) were different in each case. As a result, the consistent decrease (Δv_N, figure 11b) in crack opening displacement, which occurred while the applied displacement was held constant, was different in each test.

Finally, under applied tangential displacements, the crack opening displacements were found to increase during the time that the applied displacements were held constant (figure 11c). In contrast to the applied normal displace-

ment tests, the increments in applied tangential displacements ΔV were the same in all the tests. The increase in crack opening displacements (Δv_T, figure 11c) was therefore the same in all tests.

The time dependence of these local crack opening displacements during the periods of constant applied loading imply a viscoelastic response in the bulk material and not just in the local crack front region. While these effects are only noted here, they do indicate the value of measuring the local crack profile. They would not have been noticed in an experiment measuring only global parameters such as the applied load. In the results which follow, it will be seen that the crack profile measurements, which better reflect localized effects than global measurements, have less scatter.

The results for the crack profile measurements are now shown in figure 12 where the dependence of the velocity on the profile gradient is plotted for the two separate cases of displacements applied purely normal to or purely tangential to the bondline. The two curves are closely parallel. Note that the gradient for a given velocity is greater for the normal loading case. The cracks grown under normal loading maintained their finger-shaped plan form, the width of the finger remaining constant for all load levels and crack velocities (figure 11b). However, under a tangential loading, the crack front remained stationary while the

finger progressively widened from the original initiation shape. Propagation of the crack front occurred once the widening reached the crack front area (figure 11c). Thus there was growth of the crack, but in a lateral manner at crack front gradients lower than those shown for the tangential loading in figure 12. The difference in plan form of the cracks grown under the two loading conditions complicates comparison on two counts. First, there is less new surface created when a crack propagates under an applied normal loading. Secondly, the critical crack profile gradient may be influenced by the plan form shape.

Comparison is further complicated by the fact that the profile cannot be fully resolved all the way to the crack front. Although the gradient in the resolvable region is less in the tangential loading case (as is the crack opening), the gradient in the unresolvable region may not follow the assumed combination power and linear law. It could become just as steep right at the crack front as for the normal case. Nonetheless, some comments and comparisons with crack growth in monolithic viscoelastic fracture [4] are in order.

In [4], Knauss developed a model describing the growth of a crack in a viscoelastic material. The results were compared with experimental data for the growth of a semi-infinite crack in an infinite strip displaced uniformly at its boundaries. The physically unrealistic phenomenon of

infinite stresses produced by linear singularity analyses is avoided by postulating a region ahead of the crack front in which the material is disintegrating. There are cohesive forces acting in this region which decay to zero at the crack front. The size of this cohesive zone is determined by a finiteness condition where the combination of stress intensity factors due to the loading and the cohesive forces is required to be zero. A comparison of the crack propagation rates predicted by the model with the experimental results indicated good agreement for both a constant crack opening displacement criterion and an energy criterion, provided the maximum cohesive stress at the crack tip was velocity independent. By matching the velocity scales from the analysis and experiment, it was possible to estimate the cohesive zone size.

We might postulate that the difference (or shift) in the two curves presented in figure 12 is due to the fact that the cohesive zone sizes are different under applied normal or tangential loading. However, we are unable to estimate the cohesive zone sizes at this time. In order to do so, an analysis, following that of [4], relating the cohesive zone size to the crack profile gradient, the rheological material properties and crack propagation rate would have to be developed. The analysis presented in [4] cannot be used because it was developed for a monolithic body whereas we are dealing with an interface crack. Even to obtain the

ratio of the two cohesive zone sizes requires an analytical development.

In proposing a critical crack profile gradient as a possible fracture criterion, it was hoped that, since the gradient could be thought of as an effective stress intensity factor incorporating any kind of loading, it would provide a unified fracture criterion. The results of figure 12, where the profile gradients lie on separate curves for applied displacements purely normal to or tangential to the bondline, indicate that our measure of the gradient, by itself, does not provide such a unifying criterion. Or, alternatively, there is a different critical gradient for every possible combination of loading cases.

2.3.3 Critical Crack Opening Displacement Criteria

We now propose two crack opening displacement criteria. Even under, say, an applied displacement normal to the bondline, we expect the local crack front displacements to have components of displacements both normal (mode I) and tangential (mode II) to the bondline. The presence of both displacement components is due to the material mismatch at the boundary and also the finite deformations at the crack front. In contrast to critical crack opening criteria used as fracture parameters in the fracture of monolithic materials, where only the displacement component normal to the

plane of the crack is considered, the displacement criterion for cracks at bimaterial interfaces should therefore involve the total interface separation, both normal to and tangential to the bondline. The total interface separation, $\underset{\sim}{S}$ (figure 13), is obtained by vectorial addition of the displacement components normal to and tangential to the bondline (u and v, respectively in figure 13).

To emphasize the need for this vectorial measure, let us first consider a crack opening displacement criterion where only the displacement normal to the bondline is used. This mode I crack opening displacement was obtained at a distance of 2.54 μm from the crack front by fitting the crack profile data to equation (1). In figure 14 we plot the mode I displacements versus the crack propagation rate for displacements applied either normal to or tangential to the bondline. We see that, once again, the critical fracture parameter is different for the two loading cases; the critical mode I displacement being consistently higher under the normal loading. Considering only the mode I component of displacement in a critical crack opening displacement criterion does not furnish a unifying criterion. Note that the critical profile gradient considered earlier reflects only the mode I opening displacement.

We now consider a critical vectorial crack opening displacement criterion and postulate that crack propagation occurs when the magnitude of the vector sum of the compo-

nents of the crack opening displacements normal to and tangential to the bondline reaches a critical value. We expect the (velocity dependent) critical vectorial crack opening to be the same regardless of the loading direction. Under a normal loading the major contribution to the magnitude of the critical vectorial crack opening displacement comes from crack face displacements normal to the bondline (figure 13a), whereas under a tangential loading the major contribution comes from the crack face displacements tangential to the bondline (figure 13b). Based on a vectorial crack opening displacement criterion, we can therefore see that the critical mode I displacements considered earlier would be higher under a normal loading.

In order to support this postulate further, we now make an estimate of the local mode I and mode II displacements to be added vectorially to obtain the vectorial crack opening displacement. To achieve this experimentally, the mode II displacements would have to be measured, possibly using speckle holography, in addition to the present measurements of the mode I displacements. The mode II measurements were beyond the scope of the present investigation and we now consider the following two methods for estimating the vectorial crack opening displacements:

a) Estimation of the angle of the vectorial crack displacement.

We obtain an estimate of the angle of the vectorial

crack opening of an interface crack in an infinite bimaterial body. This angle is determined for uniformly applied loadings normal and also tangential to the interface. We then assume that the angle is the same for the adhesive joint geometry under similar loading conditions. The vectorial crack opening is then obtained as a projection of the measure mode I crack opening displacement using these calculated angles.

We use the results of Stern and Hong [9] and Smelser [10]. There it was found that the magnitude of the vectorial crack opening near the front of a crack at a bimaterial interface (figure 13) was given by

$$|\underset{\sim}{s}| = \frac{1}{4\sqrt{2}} \left(\Lambda_s + \Lambda_G\right) \frac{k_o}{\lambda_o} \sqrt{r} \tag{2}$$

and the angle of the vectorial opening

$$\phi = \varepsilon \ln r - \beta - \delta + \pi/2 \tag{3}$$

where

$k = k_o e^{i\beta} = k_I + i\, k_{II}$ is the complex stress intensity factor,

$\lambda = \lambda_o e^{i\delta}$ is the eigenvalue used in the complex potential,

$\lambda_o = \sqrt{1/4 + \varepsilon^2}$, $\delta = \tan^{-1} 2\varepsilon$,

$\Lambda_\alpha = \frac{4}{\mu_\alpha} (1 - \nu_\alpha)$ —— plane strain,

$\varepsilon = \frac{1}{2\pi} \ln \gamma$, $\gamma = \frac{\mu_s + \mu_G \kappa_s}{\mu_G + \mu_s \kappa_G}$, is the bimaterial constant,

and $\kappa_\alpha = 3 - 4\nu_\alpha$ —— plane strain.

In order to obtain the angle of the vectorial crack opening in equation (3), we must first determine the angle of the complex stress intensity factor β. The components, k_I and k_{II}, of the complex stress intensity factor are measures of the local stress intensification normal to and tangential to the interface, respectively. The ratio of k_I and k_{II} gives the tangent of the angle of the complex stress intensity factor. In [11], Rice and Shih determined k_I and k_{II} at the tip of a crack at the interface of two joined semi-infinite bodies. A combination of loading, applied uniformly at infinity, normal to and tangential to the bimaterial interface was considered.

Let us first consider the case of an applied normal loading. In this case, the ratio of the components of the complex stress intensity factor is given by [11] as the tangent of the complex stress intensity factor angle

$$\tan \beta_N = \left| \frac{-(\sin \xi - 2\varepsilon \cos \xi)}{\cos \xi + 2\varepsilon \sin \xi} \right| \tag{4}$$

where $\xi = 2 \log a$, and the subscript N denotes the normal loading. Combining (3) and (4) gives the corresponding angle of the vectorial crack opening, ϕ_N

$$\phi_N = \varepsilon \ln r + \tan^{-1} \left| \frac{\sin \xi - 2\varepsilon \cos \xi}{\cos \xi + 2\varepsilon \sin \xi} \right| - \tan^{-1} 2\varepsilon + \frac{\pi}{2} \tag{5}$$

Similarly, under a tangential loading, one obtains

$$\beta_T = \tan^{-1} \left| \frac{\cos \xi + 2\varepsilon \sin \xi}{\sin \xi - 2\varepsilon \cos \xi} \right| \tag{6}$$

and

$$\phi_T = \varepsilon \ln r - \tan^{-1} \left| \frac{\cos \xi + 2\varepsilon \sin \xi}{\sin \xi - 2\varepsilon \cos \xi} \right| - \tan^{-1} 2\varepsilon + \frac{\pi}{2} \tag{7}$$

For our particular choice of materials, the bimaterial constant is given by $\varepsilon = 6.64 \times 10^{-6}$, a very small quantity. Thus

$$\phi_N \simeq \pi/2 \text{ and } \phi_T \simeq 0 \tag{8}$$

The results of equation (8) imply that mode II displacements induced under an applied displacement normal to the bondline and the mode I displacements due to an applied displacement tangential to the bondline are neglible for this particular choice of materials in an infinite bimaterial body. In the case of an adhesive joint, we do observe and can measure mode I displacements induced under an applied tangential displacement. The assumption, made earlier, that the angle of the vectorial crack opening displacement is the same for an interface crack in both an infinite bimaterial body and an adhesive joint is therefore invalid. Thus we cannot estimate the vectorial crack opening displacement using this assumption.

b) Estimation of mode II crack opening displacements due to a shear loading.

We now estimate the local mode II displacements of an interface crack in an infinite bimaterial body loaded

uniformly in shear parallel to the interface. These mode II displacements are assumed to be of the same order as those produced in an adhesive joint under applied displacements tangential to the bondline. They are added vectorially to the mode I opening displacements obtained from the crack profile data for a joint under tangential loading to obtain the magnitude of the vectorial crack opening displacement.

Once again, using the analytical results presented in [11] for a bimaterial body containing an interfacial crack length, a, subjected to a uniform shear loading parallel to the interface, we obtain the magnitude of the complex stress intensity factor.

$$k_o = \tau \sqrt{a} \sqrt{1+4\varepsilon^2} \qquad (9)$$

where τ is the uniform shear loading.

As a first estimate, the loading is particularized to the case of an adhesive joint whose adherends are displaced tangentially to one another by an amount u_T. Thus

$$\tau = \frac{\mu_s}{2h} u_T$$

where 2h is the bond thickness. Furthermore, we replace the crack length, a, in (9) by the bond half-thickess, h, as the characteristic length in the problem. Note that this is consistent with the findings in [12] where the stress intensity factor for a semi-infinite crack in an infinite

strip was shown to be proportional to the square root of the strip half-width. Equation (9) then becomes

$$k_o = \frac{\mu_s}{2\sqrt{b}} \sqrt{1+\varepsilon^2}\, u_T \tag{10}$$

substituting (10) in (2) we obtain the mode II crack opening displacement

$$u = |\underset{\sim}{s}| = \frac{1}{4\sqrt{2}} (\Lambda_s + \Lambda_G)\, \mu_s \sqrt{\frac{r}{b}}\, u_T \tag{11}$$

or $u = C\, u_T$.

For our choice of materials and geometry

$$C = 3.16 \times 10^{-2} \quad . \tag{12}$$

The vectorial addition of the measured mode I displacements, v, due to an applied tangential displacement and the calculated mode II displacements gives the magnitude of the vectorial crack opening displacement as

$$|\underset{\sim}{s}| = \sqrt{u^2 + v^2} = \sqrt{C^2 u_T^2 + v^2} \tag{13}$$

We now plot the vectorial crack opening due to an applied tangential loading in figure 14 as a function of the crack propagation rate. In the normal loading case, we have assumed that the induced mode II displacements are small, and plot the measured mode I crack opening displacements as the vectorial crack opening displacements without any further corrections. We see that the critical vectorial crack opening displacements for the two loading cases are very

nearly the same. There is certainly an improvement over the mode I crack opening criterion. Thus a critical vectorial crack opening displacement criterion which accounts for both mode I and mode II crack opening displacements provides a more unified fracture parameter than when only the mode I crack opening displacement or the profile gradients are used.

2.3.4 A Global Fracture Criterion

In formulating a global fracture criterion, we wish to relate the applied displacements to the crack propagation rate. One convenient method is through the strain energy release rate, defined as the rate of change of strain energy with respect to the change in crack length. Crack propagation occurs when the strain energy release rate is greater than or equal to the fracture (surface) energy.

The evaluation of the strain energy release rate requires the knowledge of the stresses and strains in the adhesive layer. The stresses and strains in the adhesive layer due to a displacement normal to the bondline have been calculated in Appendix 1 and presented in figure 2. An apparent modulus, E_A, reflecting the constraint of the stiff adherends can be determined on the basis of the thickness-averaged normal stress. The details of this calculation are presented in Appendix 3. It is the apparent modulus, rather than simply Young's Modulus, E, that is

used to calculate the thickness-averaged strain energy due to a displacement applied normal to the bondline. The calculation of the strain energy due to a displacement applied tangential to the bondline is straightforward.

The displacements applied normal to the bondline were such that the normal strains in the bulk of the adhesive layer were less than 0.001. The shear strain in the bulk of the adhesive layer due to the displacements applied tangential to the bondline was less than 0.01. These low strains justify the use of linearized viscoelasticity. The change in strain energy density is considered in regions well away from the crack front. Further simplification to the use of linearized elasticity is therefore allowed by the fact that the strain rates were low enough to preclude any viscoelastic response in the bulk material far removed from the crack front region. Note that a viscoelastic response in the material in the crack front region is expected due to the high strain rates induced by the propagation of the crack. This is reflected in a velocity dependent fracture surface energy.

With reference to figure 15 for definition of nomenclature and crack geometry, we now proceed with the calculations.

Under a given normal displacement u_N, the strain energy density ahead of the crack is given by

$$\Delta U_{o_1} = \frac{1}{2} E_{A_1} \left(\frac{u_N}{2h}\right)^2 \quad , \tag{14}$$

while far behind the crack front it is

$$\Delta U_{o_2} = \frac{1}{2} E_{A_2} \left(\frac{u_N}{2h}\right)^2 \tag{15}$$

in each of the remaining "legs" (figure 15) of the rubber.

E_A is the apparent modulus due to the constraint on the adhesive layer in a poker chip effect and is determined in Appendix 3. The loss in energy due to a unit crack advance is therefore

$$\Delta U_N = \Delta U_{o_1} \cdot 2t_s \cdot 2h - 2 \cdot \Delta U_{o_2} \cdot 2t_N \cdot 2h \quad . \tag{16}$$

Substituting equations (2) and (3) and equation (A3.2) for the apparent modulus from Appendix 3 into equation (16) we obtain

$$\Delta U_N = \frac{E_\infty}{3} \left[a_s(a_s^2 + 2) - 2a_N(a_N^2 + 2)\right] u_N^2 \tag{17}$$

where

E_∞ is the rubbery modulus of Solithane,

$a_s = t_s/h$ is the aspect ratio of the bonded region ahead of the crack front,

$a_N = t_N/h$ is the aspect ratio of the remaining "legs" behind the crack front;

and, with reference to figure 15,

$2t_s$ = specimen thickness,

$2t_N$ = "leg" thickness under normal loading,

$2h$ = the bond thickness.

Notice here that we have been able to make a small improvement on most global approaches in that we have accounted for the differing crack surface areas in the different loading cases.

Similarly, under a given tangential displacement u_T, the loss in strain energy due to a unit crack advance is

$$\Delta U_T = \frac{1}{2}\mu_\infty \left(\frac{u_T}{2h}\right)^2 \cdot 2t_s \cdot 2h - 2 \cdot \frac{1}{2}\mu_\infty \left(\frac{u_T}{2h}\right)^2 2t_T \cdot 2h \quad (18)$$

where

μ_∞ = rubbery shear modulus of Solithane and

t_T = "leg" thickness under a tangential loading.

Assuming Solithane to be incompressible ($\nu = 1/2$) and further simplifying (18) leads to

$$\Delta U_T = \frac{E_\infty}{6} (a_s - a_T)\, u_T^2 \quad (19)$$

For crack propagation to occur, the fracture surface energy S must be equal to or exceed the rate of change of strain energy. Since the crack length can be considered infinite with respect to the bond thickness and the displacements are applied uniformly we assume that the change in strain energy per unit crack advance is the same as an incremental change in strain energy for an infinitely small crack advance. We also note that S is the rate dependent

fracture surface energy comprising the constant, intrinsic fracture energy (Γ in Ref. [4]) and the rheological response of the material around the crack front.

Thus $S(\dot{c}) = \Delta U_N + \Delta U_T$.

From (17) and (19) we obtain (20)

$$S(\dot{c}) = \frac{E_\infty}{6}\left[\left\{2a_s(a_s^2+2) - 4a_N(a_N^2+2)\right\}u_N^2 + (a_s-a_T)\,u_T^2\right].$$

For our particular geometry,

$2t_s = 0.235"$, $2t_N = 0.109"$, $2t_T = 0.087"$ and $2h = 0.025"$.

Thus

$$S(\dot{c}) = \frac{E_\infty}{6}\left[1332\,u_N^2 + 5.92\,u_T^2\right] \quad . \tag{21}$$

Note that for the present experiments, either u_N or u_T are zero so that we have either

$$S(\dot{c}) \simeq 222\,E_\infty\,u_N^2 \tag{22a}$$

or

$$S(\dot{c}) \simeq E_\infty\,u_T^2 \tag{22b}$$

Let us therefore plot the square root of $S(\dot{c})$ versus the crack velocity in figure 16 by determining the applied displacements which caused the crack to run at that particular rate. The square root is chosen in order to make comparison with the gradient measurements later. Three different load histories were used in the three tests providing the data for the normal loading case. This fact, coupled with the bulk viscoelastic response noted earlier

(page 83), produces the scatter in the normal loading data. Although there was also a bulk viscoelastic response in the tangential loading tests, the load histories were the same in each test, resulting in a masking of the scatter in the tangential loading data.

In spite of the scatter and the relatively small velocity range considered, we see that the fracture energy is consistently greater, for a given velocity, for the normal loading case. We recall that a similar difference was observed in the gradient measurements. In that case a difference in cohesive zone sizes due to applied displacements normal to or tangential to the bondline was postulated in order to account for the difference. The postulate was inconclusive because the necessary analytical development required to estimate cohesive zone sizes was not available.

For the present case of a global criterion we again propose that the difference between the two curves presented in figure 16 is due to a difference in cohesive zone sizes for the two loading cases. This time the postulate can be examined in detail because the fracture (surface) energy can be related to the cohesive zone size. In [4] a finiteness condition, enforcing finite stresses in the crack front region, rather than the infinite stresses predicted by linearized theory, was used to relate the cohesive zone size to the loading conditions and geometry (characterized by the stress intensity factor K) and the cohesive forces acting

in the cohesive zone. We now relate the fracture energy to the stress intensity factor and therefore to the cohesive zone size.

The stress intensity factor, K, is related to the fracture energy through

$$K^2 = ES \tag{23}$$

under a displacement applied normal to the bondline, equations (23) and (22a) render

$$K_N^2 = 222\ E_\infty^2\ u_N^2 \quad . \tag{24}$$

Similarly, using equations (23) and (22b), we find that

$$K_T^2 = E_\infty^2\ u_T^2 \tag{25}$$

under a displacement applied tangential to the bondline. For the case of a velocity independent cohesive stress, σ_o, the cohesive zone size, α, is related [4] to the stress intensity factor, K, through

$$\alpha = \frac{\pi}{8} \frac{K^2}{\sigma_o 2} \quad . \tag{26}$$

The cohesive zone size due to a displacement applied normal to the bondline, α_N, is obtained by combining (24) and (26)

$$\alpha_N = \frac{\pi}{8} \cdot \frac{222\ E_\infty^2\ u_N^2}{\sigma_{o_N}^2} \tag{27}$$

Equations (25) and (26) supply the tangential cohesive zone size, α_T.

$$\alpha_T = \frac{\pi}{8} \cdot \frac{E_\infty^2 \, u_T^2}{\sigma_{o_T}^2} \quad . \tag{28}$$

The cohesive stresses σ_{o_N} and σ_{o_T} can be viewed as yield stresses. From a Tresca yielding consideration we expect that

$$\sigma_{o_T} = \frac{1}{2} \sigma_{o_N} \quad . \tag{29}$$

Furthermore, a plot (figure 17) of the applied displacements versus crack velocity shows that, for any given velocity, the ratio between the normal and tangential applied displacements is the same and is given by

$$u_N = 0.16 \, u_T \quad . \tag{30}$$

With a view to using equations (29) and (30), we now form the ratio of the cohesive zone sizes from (27) and (28)

$$\frac{\alpha_N}{\alpha_T} = 222 \, \frac{\sigma_{o_T}^2}{\sigma_{o_N}^2} \cdot \frac{u_N^2}{u_T^2} \quad . \tag{31}$$

Combining equations (29), (30) and (31) yields

$$\alpha_N = 1.57 \, \alpha_T \quad . \tag{32}$$

Thus, based on strain energy considerations of the adhesive layer, the cohesive zone size under displacements applied either normal to or tangential to the bondline are

of the same order; the normal cohesive zone size being slightly larger. The difference is not enough to produce the shift between the fracture energy curves for normal and tangential loading in figure 16. The rheological response of the material surrounding the crack front region must be different for the two loading cases.

To illustrate this further, let us consider the fracture (surface) energy S, which is dependent on the crack velocity. In [4], Knauss showed that this fracture energy S could be viewed as the product of a rate dependent function, θ say, and a constant, intrinsic fracture energy Γ. The constant, intrinsic fracture energy is a basic material property, probably of molecular origin, reflecting the energy required to break the individual molecular bonds. It is therefore independent of the direction of application of any macroscopic loading. Thus any differences in S due to the applied loading direction must be due to differences in the rate dependent function θ. The function θ embodies the rheology of the material surrounding the crack front. A difference in the rheological response could therefore account for the shift in fracture energy curves. A global criterion is not able to account for such local differences and therefore does not provide a unifying criterion.

2.4 STEADY CRACK PROPAGATION STUDIES - CONCLUSION

Four possible fracture criteria governing the time dependent propagation of an interfacial crack in an adhesive joint have been considered. In three of the criteria considered, namely: critical profile gradient, critical normal opening displacement and a global fracture energy criterion, the critical parameter was consistently and considerably greater when the loading direction was normal to the bondline. However, the time dependence of the critical parameters was the same over the somewhat limited range of crack propagation rates considered. On a closer examination of the fracture energy criterion, it was found that the cohesive zone sizes due to normal and tangential loadings were of the same order of magnitude, suggesting the use of a critical zone size as a possible fracture criterion.

The fourth criterion postulated that the vectorial crack opening displacement reach a critical value for crack propagation to occur. It was the only criterion accounting for crack opening displacements both normal to and tangential to the bondline. However, the vectorial displacement could not be completely determined experimentally as measurements of mode II crack opening displacement were beyond the scope of this study. An estimate based on linearized theory was therefore used to obtain the mode II crack opening displacements. The results nonetheless indicate that the vectorial crack opening displacement criterion provided the

most unified fracture parameter of the four criteria considered. Furthermore, the close agreement in the two cohesive zone sizes due to displacements applied normal and tangential to the bondline as well as the vectorial crack opening displacement emphasize the need to consider local, rather than global, unbonding processes in the time dependent unbonding of an adhesive joint.

APPENDIX 1

THE STRESSES IN THE ADHESIVE LAYER DUE TO LOADING NORMAL TO THE BONDLINE

We consider the stresses in the (uncracked) adhesive layer of an adhesive joint whose adherends have suffered a relative displacement normal to the bondline. The adhesive layer is taken to be incompressible ($\nu = 1/2$). Following the poker chip analysis in [1], [2], the displacement field in the adhesive layer is assumed to be

$$v(y,z) = \varepsilon_o \, y \, , \qquad \varepsilon_o = \frac{u_N}{2h}$$

$$w(y,z) = f(z) \, (1 - y^2/h^2)$$

where v and w are the displacements in the y and z directions, respectively. (See figure 15b.) The strains are therefore given by

$$\varepsilon_y = \varepsilon_o$$

$$\varepsilon_z = f_{,z} \, (1 - y^2/h^2) \qquad \text{(A1.1)}$$

$$\varepsilon_{yz} = - \, y/h^2 \, f(z)$$

where

$$f_{,z} \equiv \frac{df(z)}{dz} \quad .$$

The incompressibility of the adhesive layer implies that there is no volume change in the adhesive layer due to the applied load. Thus

$$\frac{1}{2h}\int_{-h}^{h} (\varepsilon_z + \varepsilon_y)\, dy = 0 \quad . \tag{A1.2}$$

We use equations (A1.1) and A1.2) and symmetry arguments $\left(\text{i.e. } w(y,0) = 0\right)$ to obtain

$$f(z) = \frac{3}{2}\,\varepsilon_o\, z \quad . \tag{A1.3}$$

Thus

$$\begin{aligned} \varepsilon_y &= \varepsilon_o \\ \varepsilon_z &= -\frac{3}{2}\,\varepsilon_o\,(1 - y^2/h^2) \\ \varepsilon_{yz} &= \frac{3yz}{2h^2}\,\varepsilon_o \quad . \end{aligned} \tag{A1.4}$$

The stresses are related to the strains through the constitutive relations

$$\begin{aligned} \sigma_y &= p + 2\mu\varepsilon_y \\ \sigma_z &= p + 2\mu\varepsilon_y \\ \sigma_{yz} &= 2\mu\varepsilon_{yz} \end{aligned} \tag{A1.5}$$

where

p is the hydrostatic pressure

and μ is the shear modulus of the adhesive. Combining equations (A1.4) and A1.5) we obtain

$$\sigma_y = p + 2\mu\varepsilon_o$$

$$\sigma_z = p - 3\mu\varepsilon_o (1 - y^2/h^2) \qquad \text{(A1.6)}$$

$$\sigma_{zy} = 3\mu\varepsilon_o \frac{yz}{h^2} \quad .$$

Satisfaction of the full three dimensional equilibrium equations reduces to satisfying

$$\sigma_{z,z} + \sigma_{yz,y} = 0 \quad . \qquad \text{(A1.7)}$$

Thus equations (A1.6) and (A1.7) imply that

$$p_{,z} + 6\mu\varepsilon_o \frac{z}{h^2} = 0$$

and integration with respect to z therefore yields

$$p = - 3\mu \frac{z^2}{h^2} \varepsilon_o + C_2 \qquad \text{(A1.8)}$$

C_2 is a constant of integration determined by the boundary condition that the thickness-averaged normal stress at the edge of the specimen be zero,
that is, at z = t

$$\frac{1}{2} \int_{-h}^{h} \sigma_x \, dy = 0 \quad . \qquad \text{(A1.9)}$$

Equations (A1.8) and (A1.9) render

$$C_2 = 3\mu\varepsilon_o \left(\frac{t^2}{h^2} + 2/3 \right) \qquad \text{(A1.10)}$$

The stresses in the adhesive layer are then obtained by combining equations (A1.10) and (A1.8) in (A1.6).

Thus

$$\sigma_y = 3\mu\varepsilon_o \left\{ \frac{t^2}{h^2} \left(1 - \frac{z^2}{t^2}\right) + 4/3 \right\}$$

$$\sigma_z = 3\mu\varepsilon_o \left\{ \frac{t^2}{h^2} \left(1 - \frac{z^2}{t^2}\right) + \frac{y^2}{h^2} - 1/3 \right\} \qquad \text{(A1.11)}$$

$$\sigma_{yz} = 3\mu\varepsilon_o \frac{yz}{h^2}$$

APPENDIX 2

THE STRESSES IN THE ADHESIVE LAYER DUE TO A CURE SHRINKAGE

In estimating the stresses in the adhesive layer due to cure shrinkage, we follow the developments in Appendix 1. However, the assumed displacements now account for cure shrinkage effects.

The following displacement field is assumed

$$v\ (y,z) = (\varepsilon_o - \varepsilon_c)\ y$$

$$w\ (y,z) = f(z)\ \left(1 - \frac{y^2}{h^2}\right) - \varepsilon_c z$$

where ε_c is the cure shrinkage strain and ε_o is the (unknown) strain due to the constraint of the adherends. The incompressibility condition is used to determine f(z) and we find

$$f(z) = -\frac{3}{2}\ (\varepsilon_o - 2\varepsilon_c)\ z\ .$$

The hydrostatic pressure, p, is obtained through the constitutive and equilibrium equations.

$$p = 3\mu\ (2\varepsilon_c - \varepsilon_o)\ \frac{z^2}{h^2} + C_2\ .$$

In this case both ε_o and C_2 are unknown and must therefore be determined by the two thickness-averaged boundary conditions

$$\frac{1}{2h}\int_{-h}^{h} \sigma_z dy = 0 \qquad \text{along } z = t$$

and

$$\frac{1}{2t}\int_{-t}^{t} \sigma_y dz = 0 \qquad \text{along } y = \pm h \ .$$

These yield

$$C_2 = \frac{-4\mu\varepsilon_c}{1+2\ h^2/t^2} \quad \text{and} \quad \varepsilon_o = \frac{2\varepsilon_c\left(\frac{t^2}{h^2}+1\right)}{\left(\frac{t^2}{h^2}+2\right)} \ .$$

The stresses in the adhesive layer due to a cure shrinkage can then be found to be

$$\sigma_y = \frac{2\mu a^2\varepsilon_c}{a^2+2}\left[\frac{3z^2}{t^2} - 1\right]$$

$$\sigma_z = \frac{2\mu a^2\varepsilon_c}{a^2+2}\left[\frac{3z^2}{t^2} - \frac{3y^2}{t^2} + \frac{h^2}{t^2} - 3\right] \qquad \text{(A2.1)}$$

$$\sigma_{yz} = \frac{4\mu\varepsilon_c}{a^2+2}\left[\frac{3yz}{h^2} - a^2\right]$$

where $a = \frac{t}{h}$ is the aspect ratio of the adhesive layer.

APPENDIX 3

THE APPARENT MODULUS OF THE ADHESIVE LAYER

In a standard uniaxial tensile test, the Young's Modulus is given by the ratio of the axial stress and strain. The specimen dimensions and loading are arranged such that the grips do not affect the uniformity of the stresses and strains over the gage length. In the poker chip specimen, the axial stress is no longer uniform due to the proximity of the grips. An apparent modulus, which accounts for the constraint applied by the grips, was defined as the ratio of the average axial stress and the nominal axial strain. We now extend this to the case of an adhesive joint to account for the constraint on the adhesive layer due to the relatively stiff adherends.

We define the apparent modulus, E_A, as the ratio of the average stress to the applied strain, both normal to the bondline, as

$$E_A = \frac{\bar{\sigma}_y}{\varepsilon_o} = \frac{1}{2t\varepsilon_o} \int_{-t}^{t} \sigma_y dz \quad . \tag{A3.1}$$

Note that the normal stress need only be averaged in the z direction since it is independent of y (equation A1.11). Combining equations (A1.11) and (A3.1) we therefore obtain

$$E_A = \frac{2E}{3} (a^2 + 2) \tag{A3.2}$$

where $a = \frac{t}{h}$ is the aspect ratio of the adhesive layer and, since $\nu = 1/2$, $E = 3\mu$ is the Young's Modulus of the adhesive.

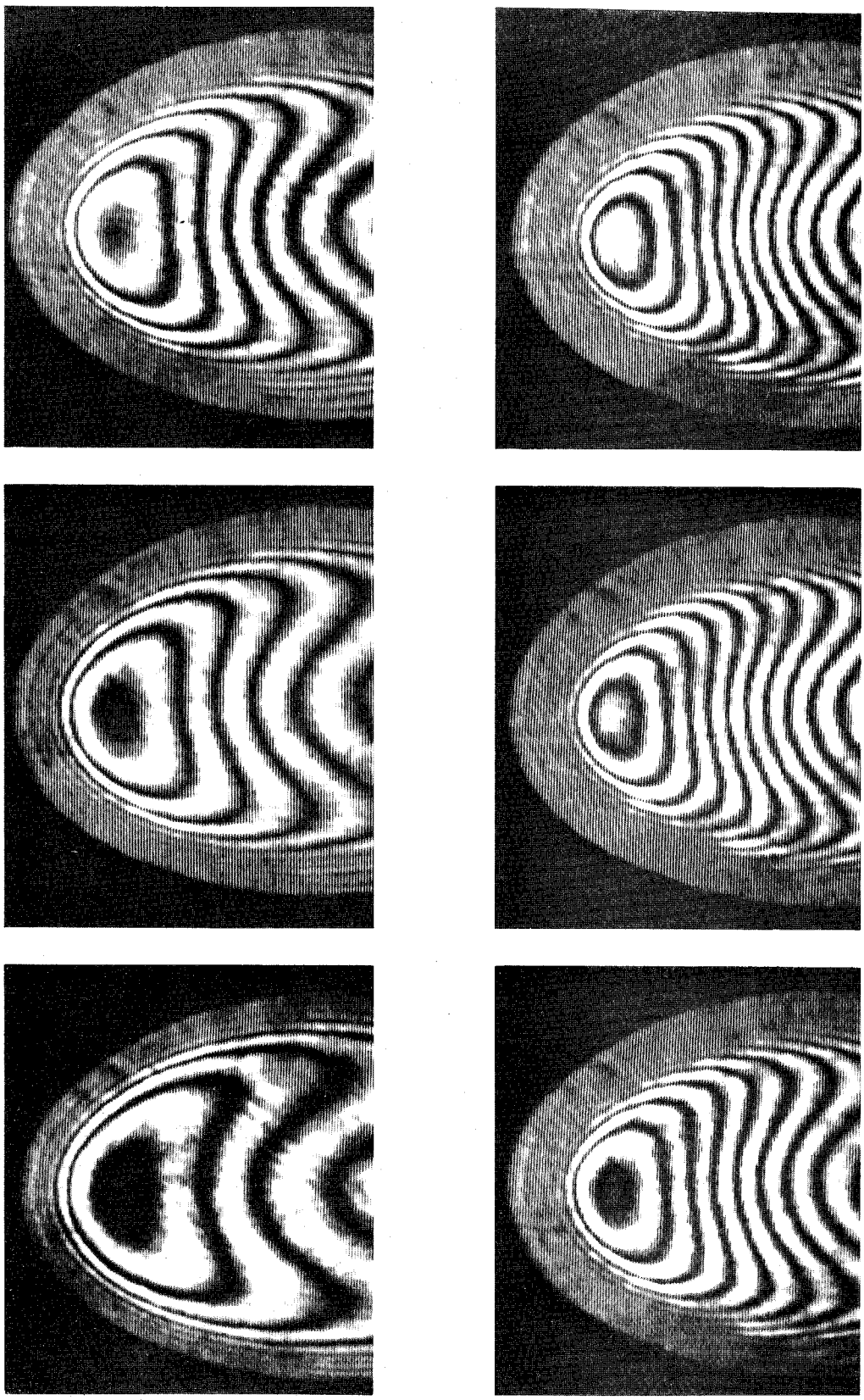

FIG. 1. INTERFERENCE FRINGE PATTERNS OF AN INTERFACE CRACK AT SUCCESSIVE NORMAL LOAD LEVELS

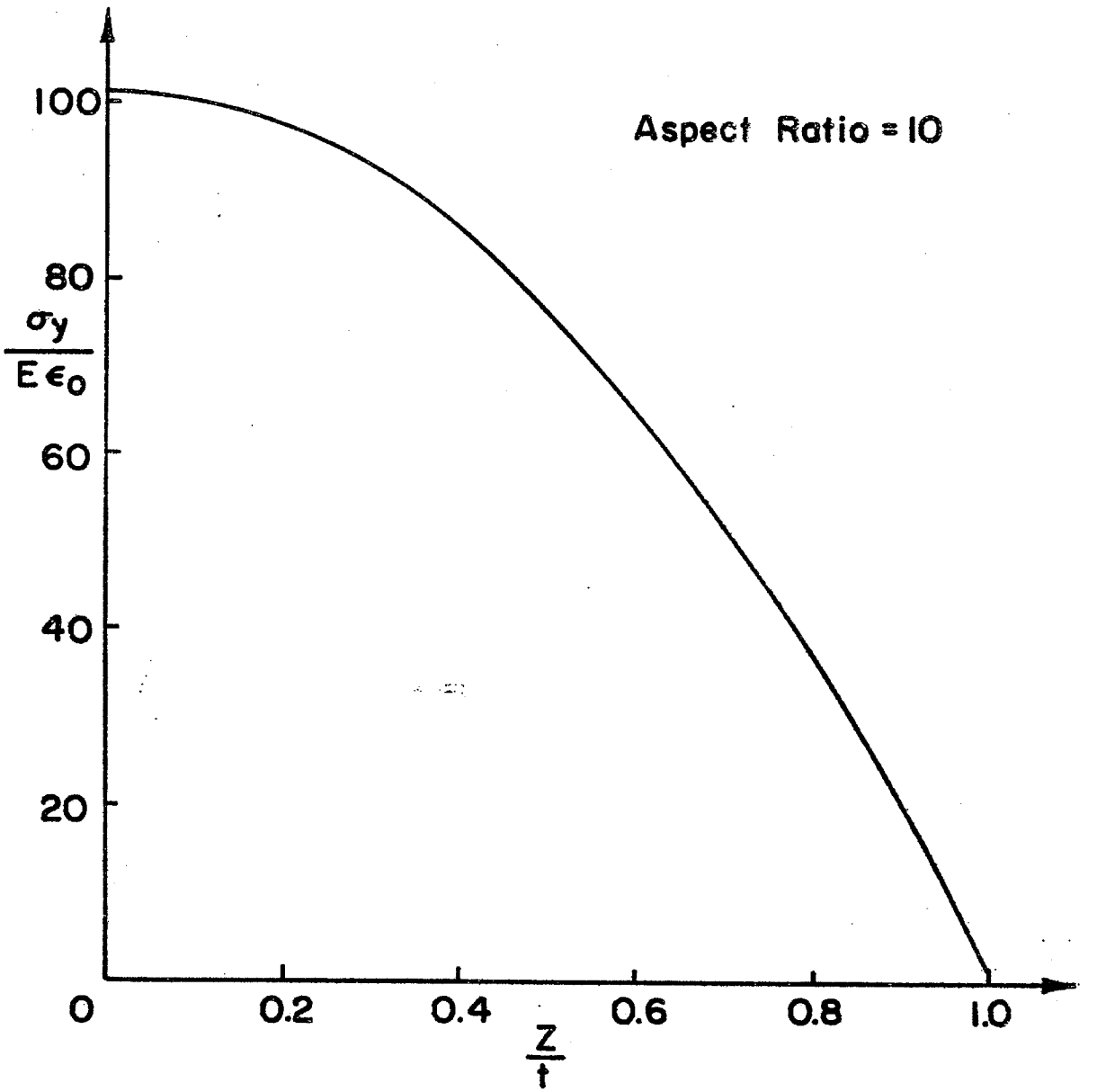

FIG. 2 Y-NORMAL STRESS IN THE ADHESIVE LAYER VS Z/t DUE TO AN APPLIED NORMAL STRAIN ϵ_0

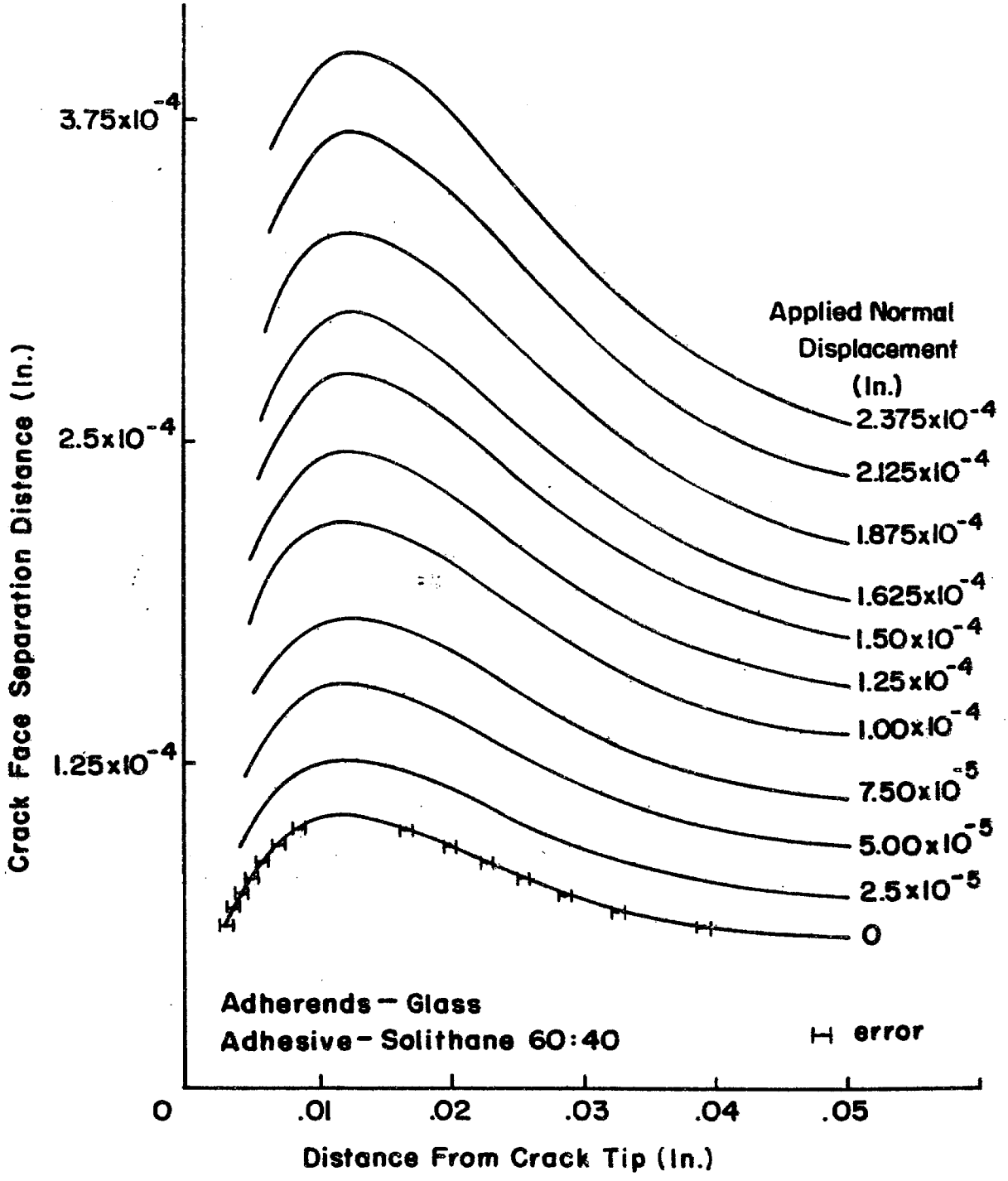

FIG. 3 CRACK PROFILES FOR DIFFERENT APPLIED NORMAL DISPLACEMENT

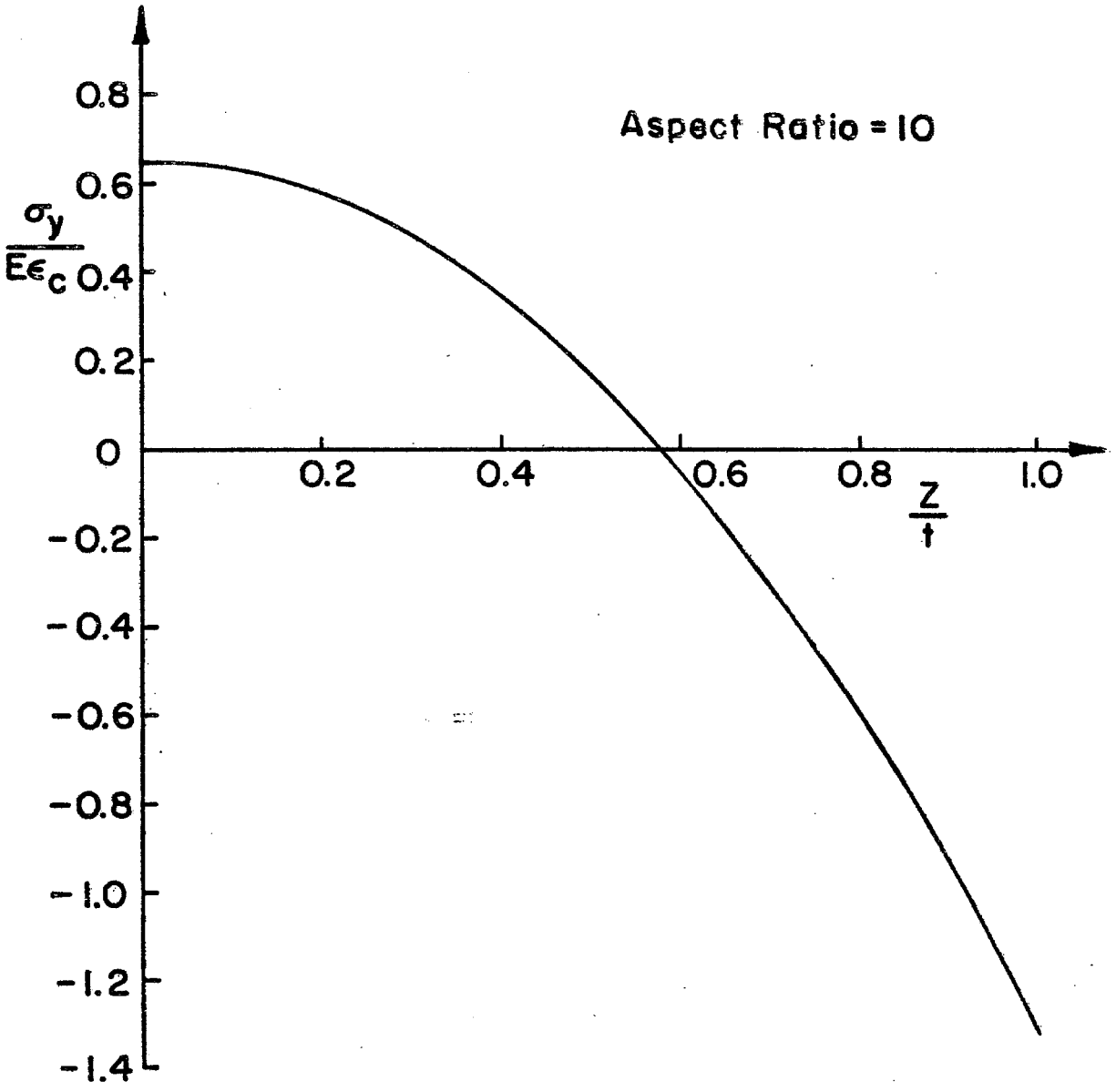

FIG. 4 Y-NORMAL STRESS IN THE ADHESIVE LAYER VS Z/t DUE TO A CURE SHRINKAGE ϵ_c

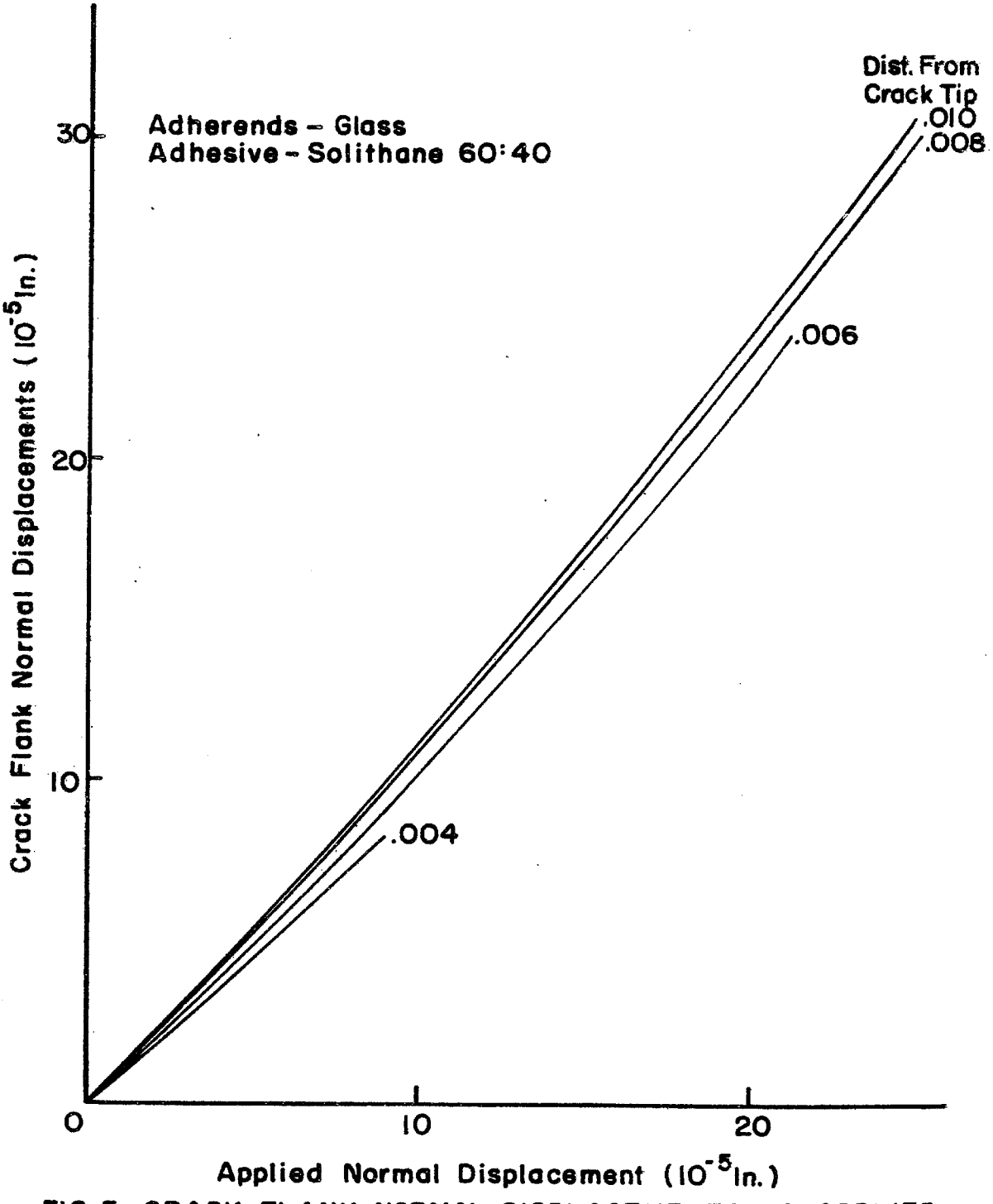

FIG. 5 CRACK FLANK NORMAL DISPLACEMENTS VS. APPLIED NORMAL DISPLACEMENTS

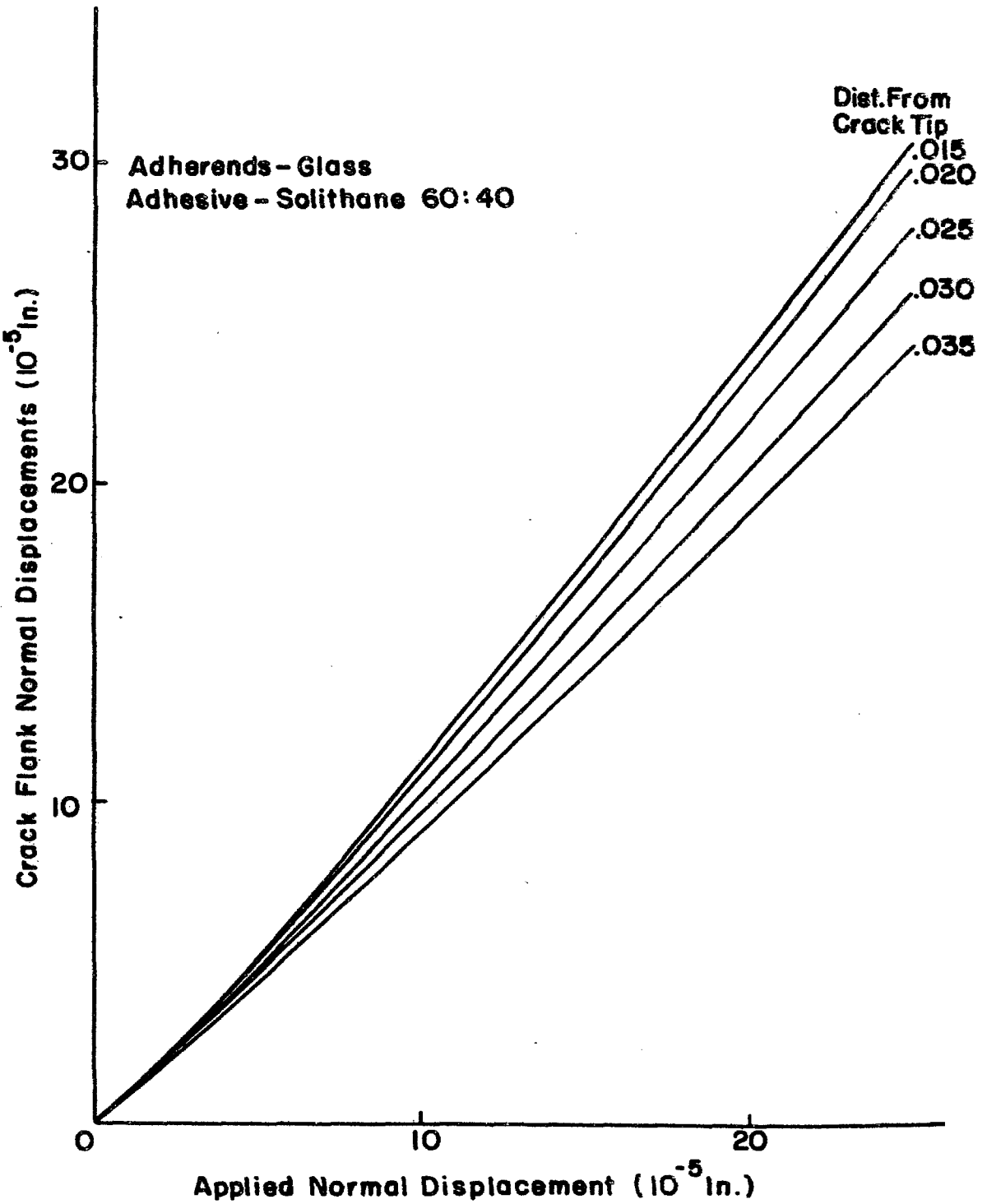

FIG.6 CRACK FLANK NORMAL DISPLACEMENTS VS. APPLIED NORMAL DISPLACEMENT

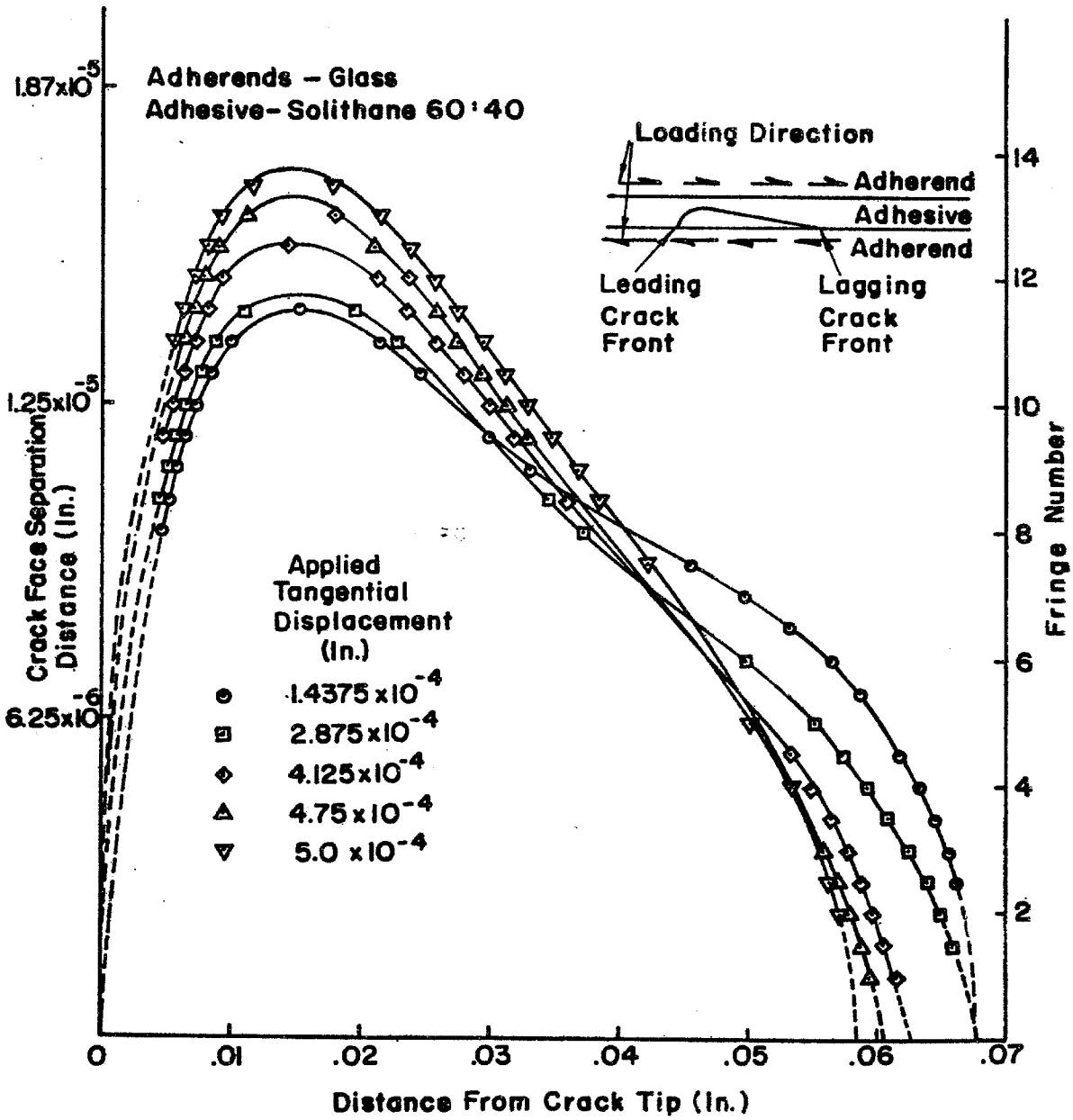

FIG.7 CRACK PROFILE FOR DIFFERENT TANGENTIAL DISPLACEMENTS

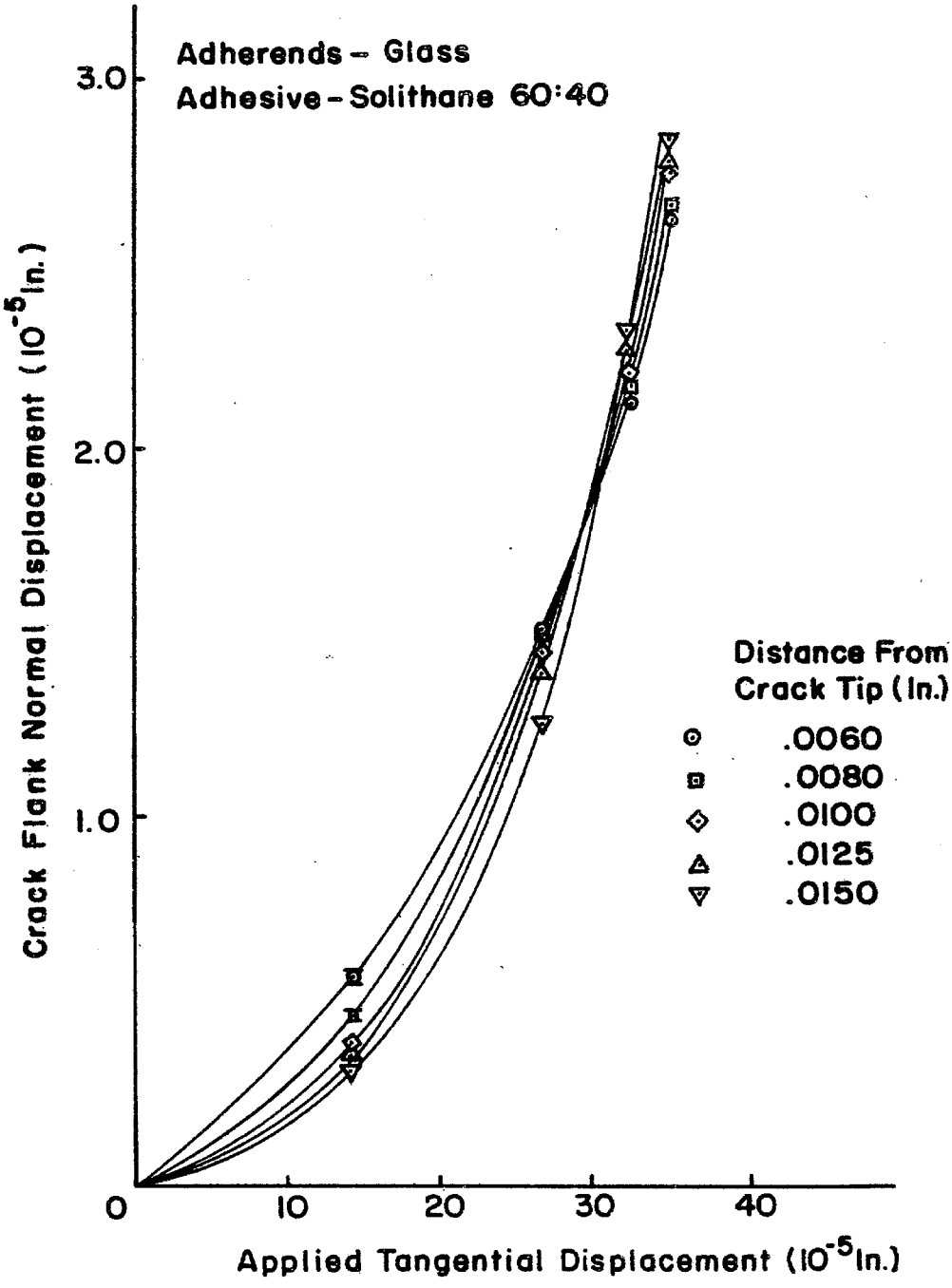

FIG. 8 CRACK FLANK NORMAL DISPLACEMENT VS. APPLIED TANGENTIAL DISPLACEMENT

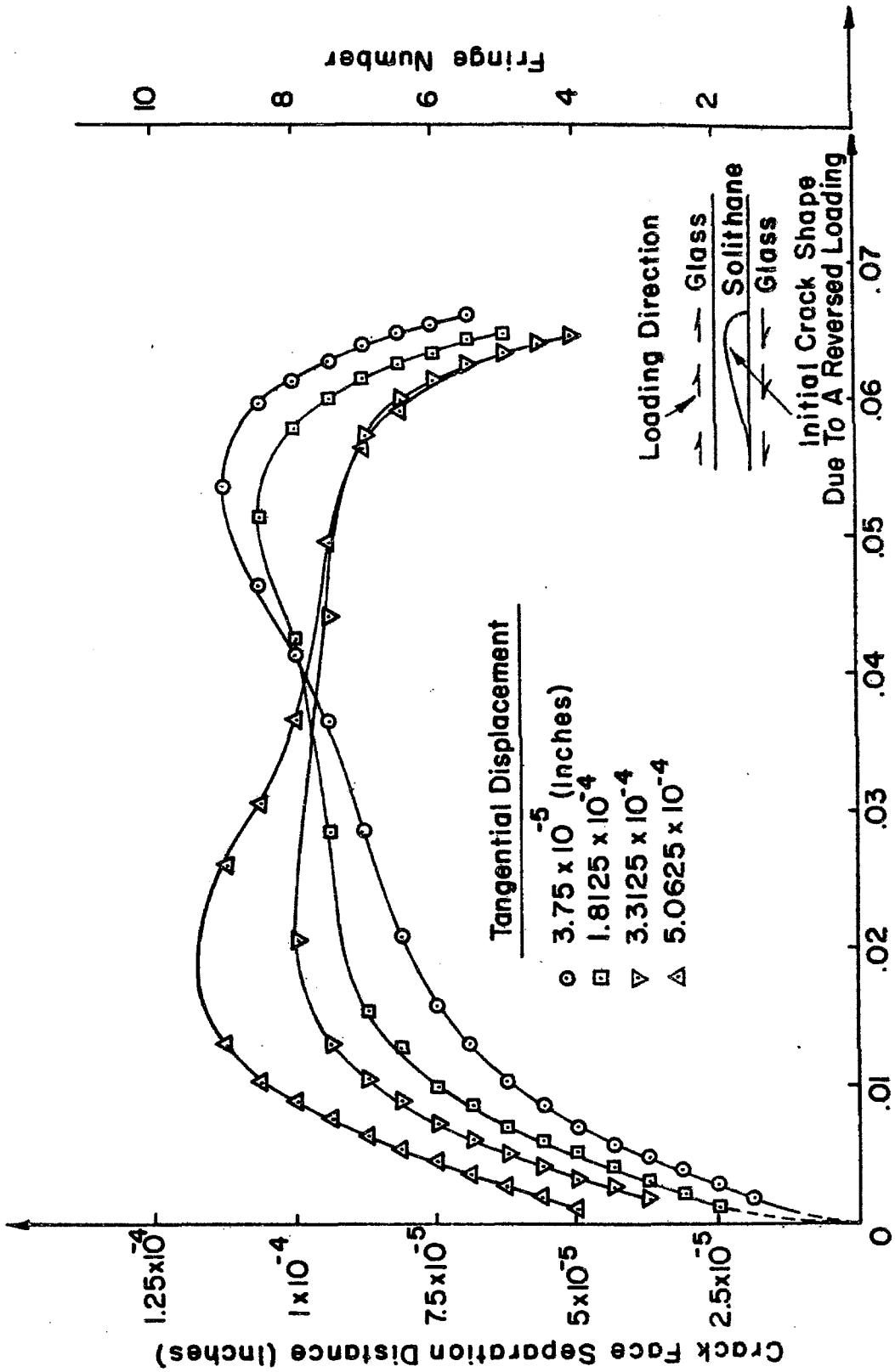

FIG. 9 CRACK PROFILES DUE TO A REVERSED TANGENTIAL LOAD

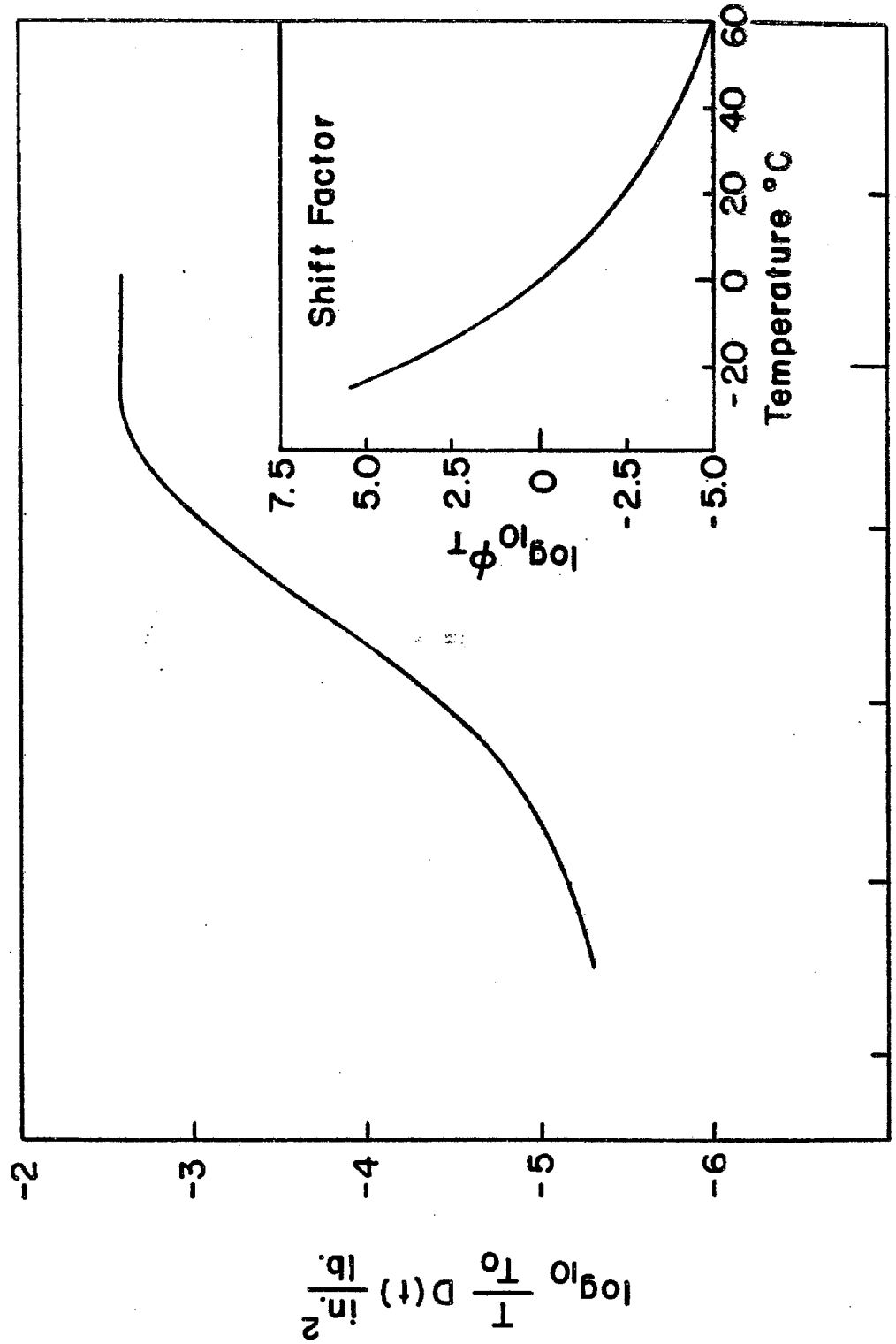

FIG. 10 MASTER CREEP COMPLIANCE AND SHIFT FACTOR CURVES FOR SOLITHANE

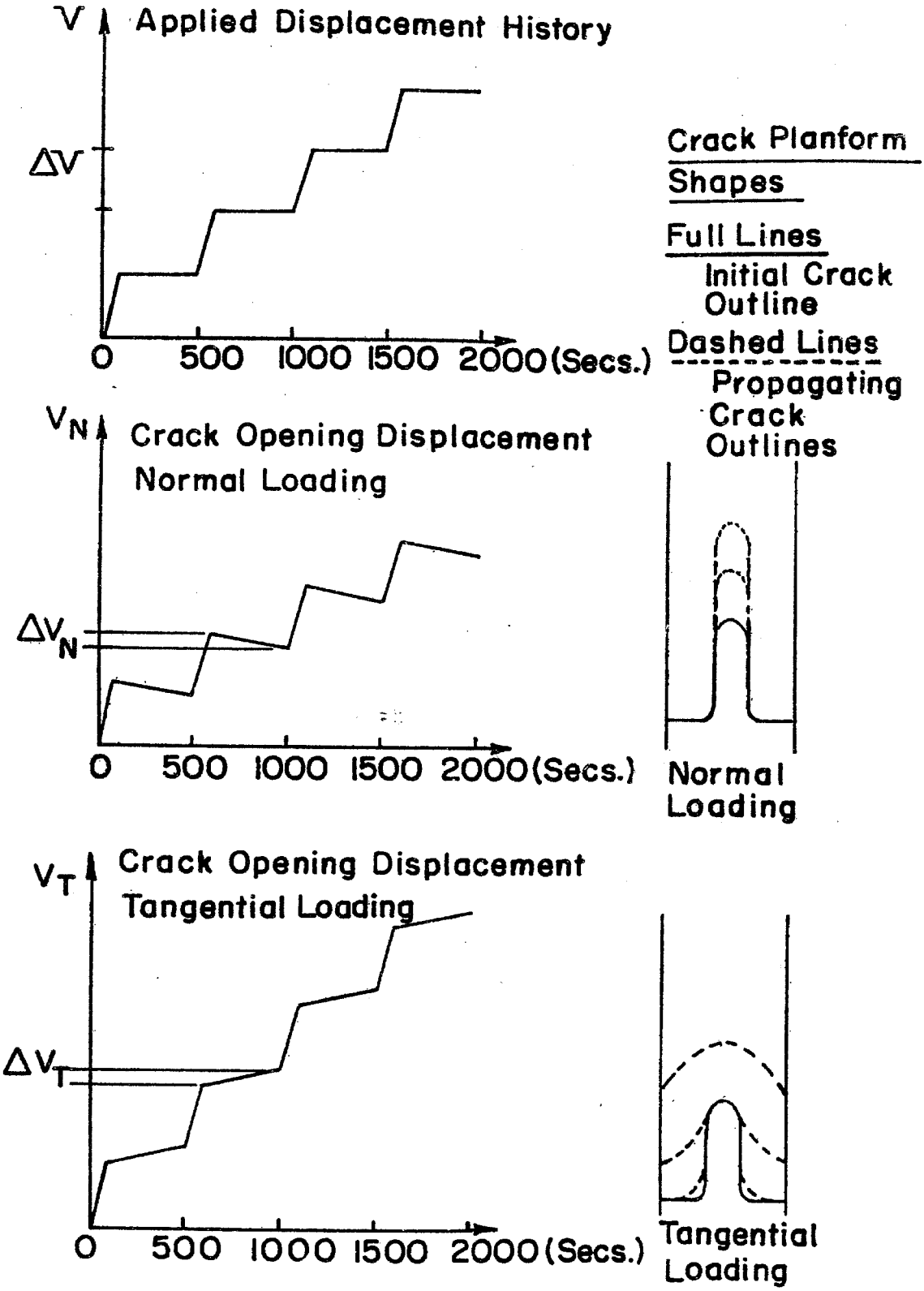

FIG. 11 CRACK PROPAGATION FEATURES FOR NORMAL AND TANGENTIAL LOADING

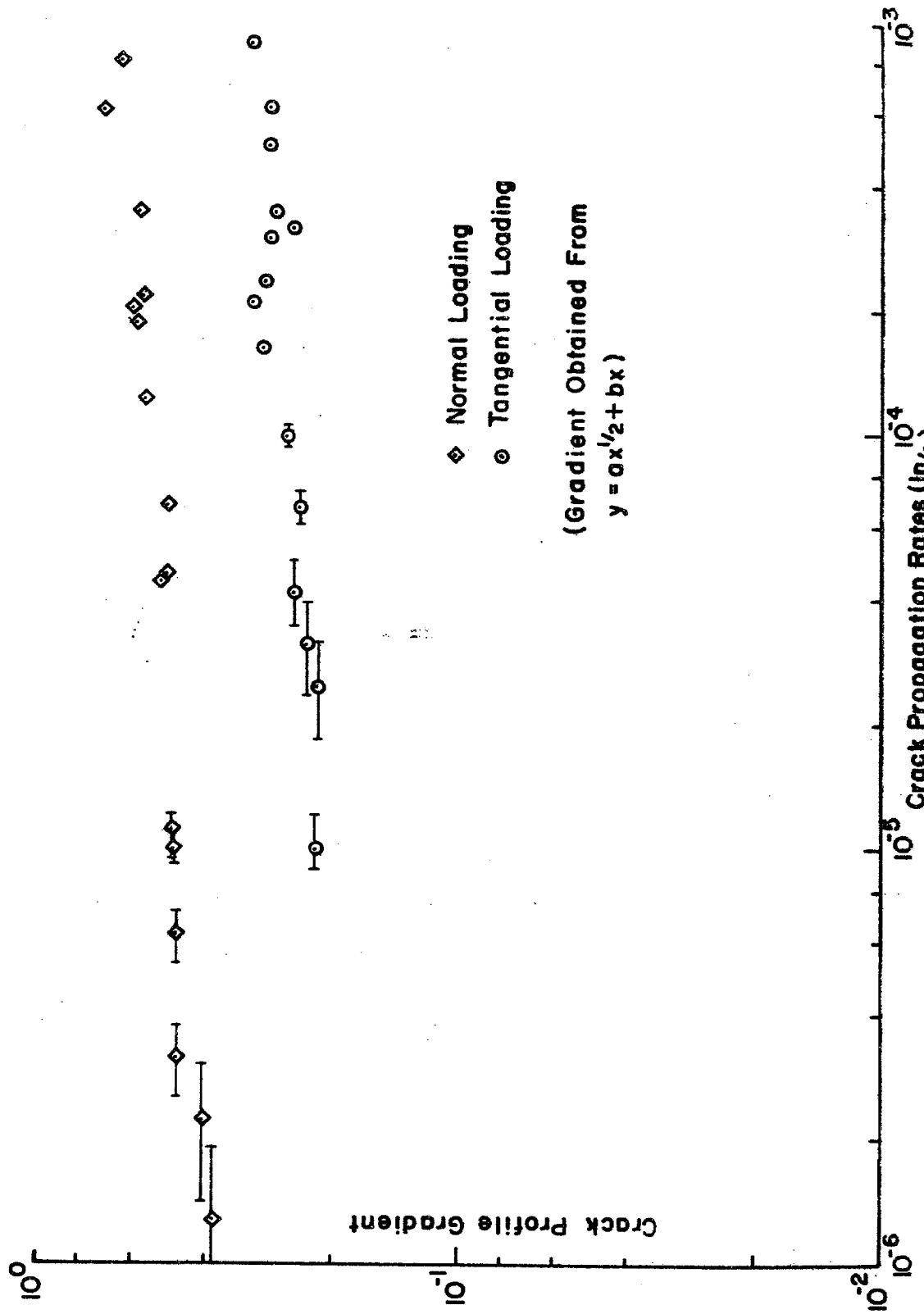

FIG.12 CRACK PROFILE GRADIENT CRITERION

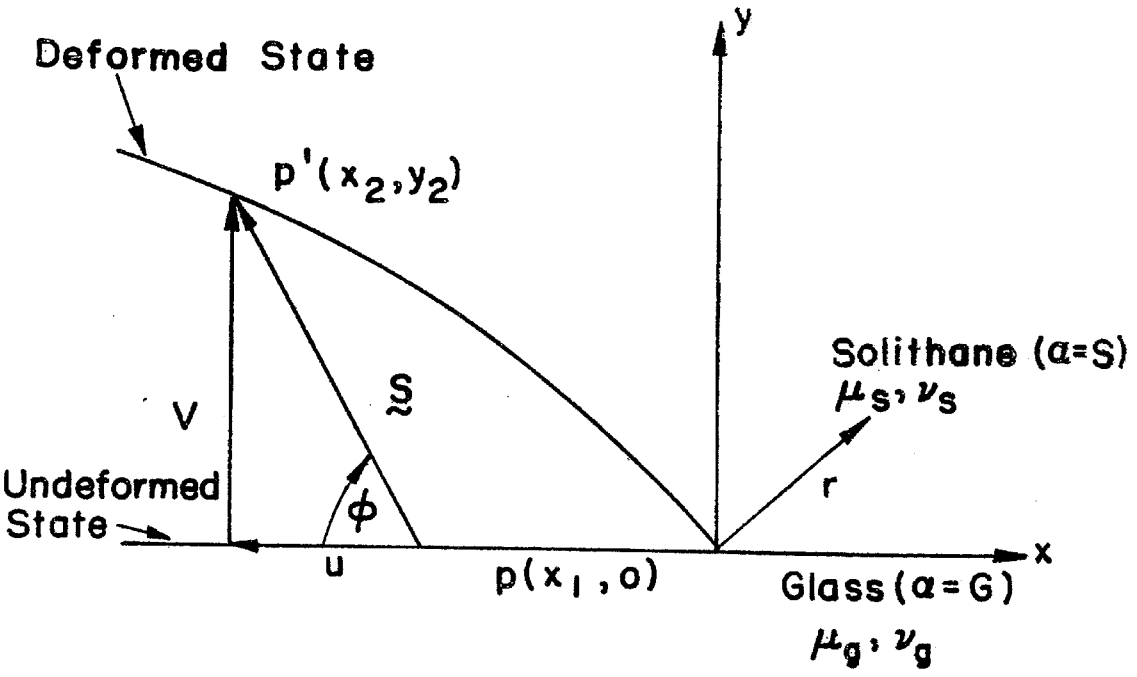

$\underset{\sim}{S}$ Vectorial Crack Opening Displacement

V Mode I Crack Opening Displacement

u Mode II Crack Opening Displacement

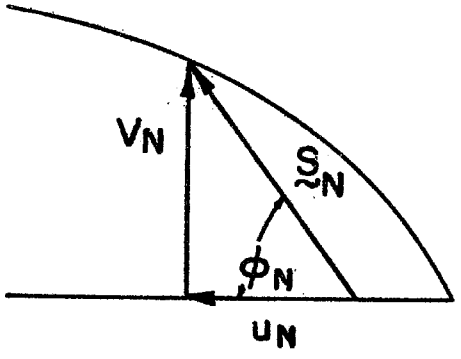

(a) Normal Loading

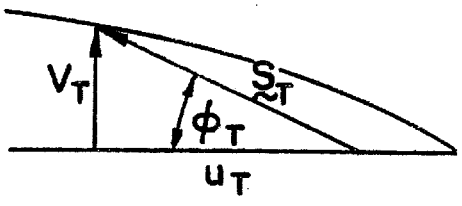

(b) Tangential Loading

For Fracture $|\underset{\sim}{S}_N| = |\underset{\sim}{S}_T| = S_c \Rightarrow V_N > V_T$

FIG. 13 CRACK OPENING DISPLACEMENT CRITERION

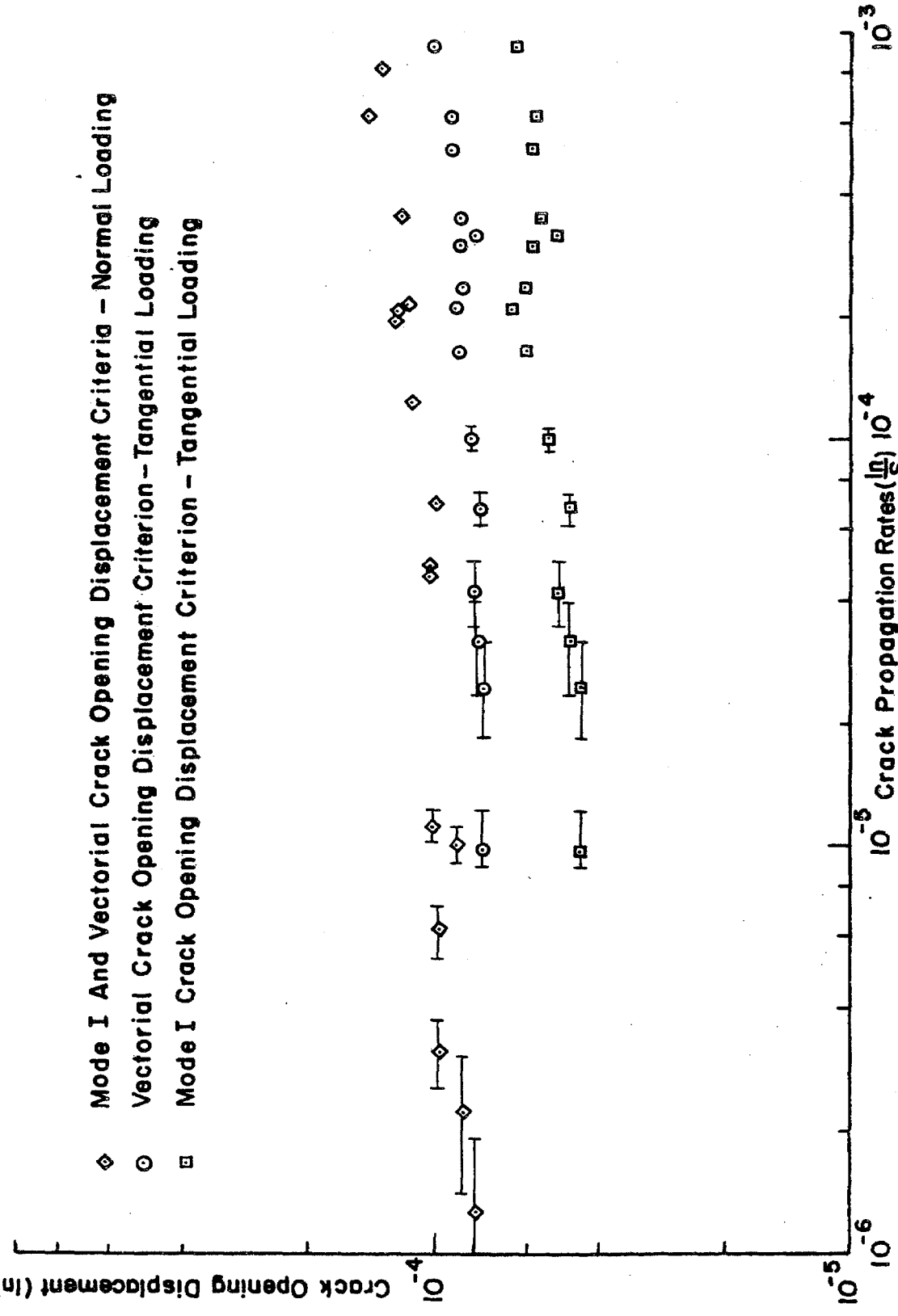

FIG.14 MODE I AND VECTORIAL CRACK OPENING DISPLACEMENT CRITERIA

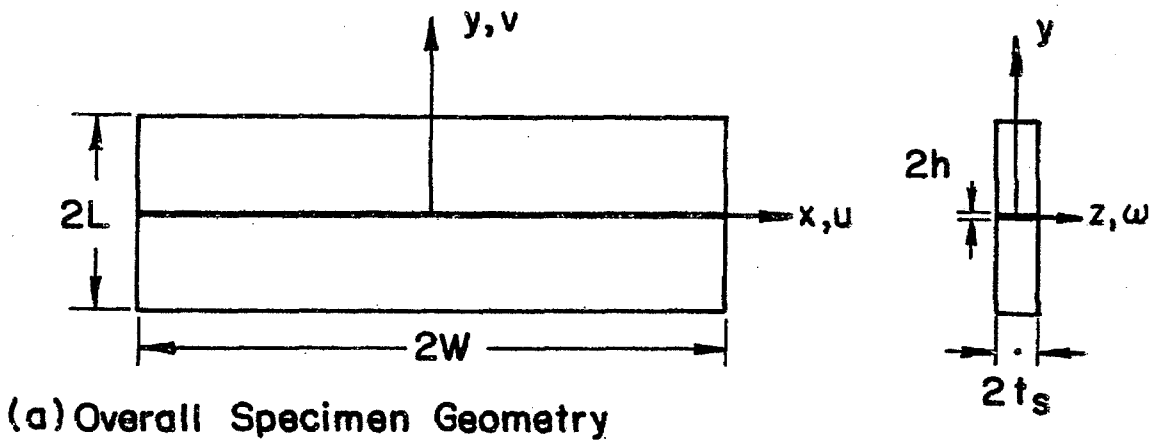

(a) Overall Specimen Geometry

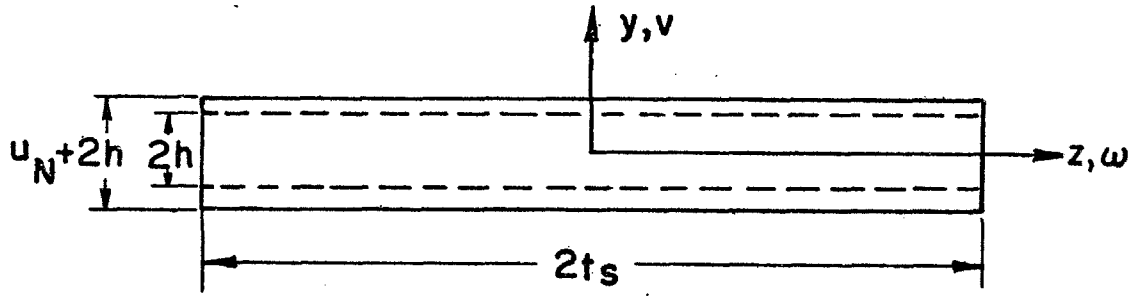

(b) Adhesive Layer Geometry

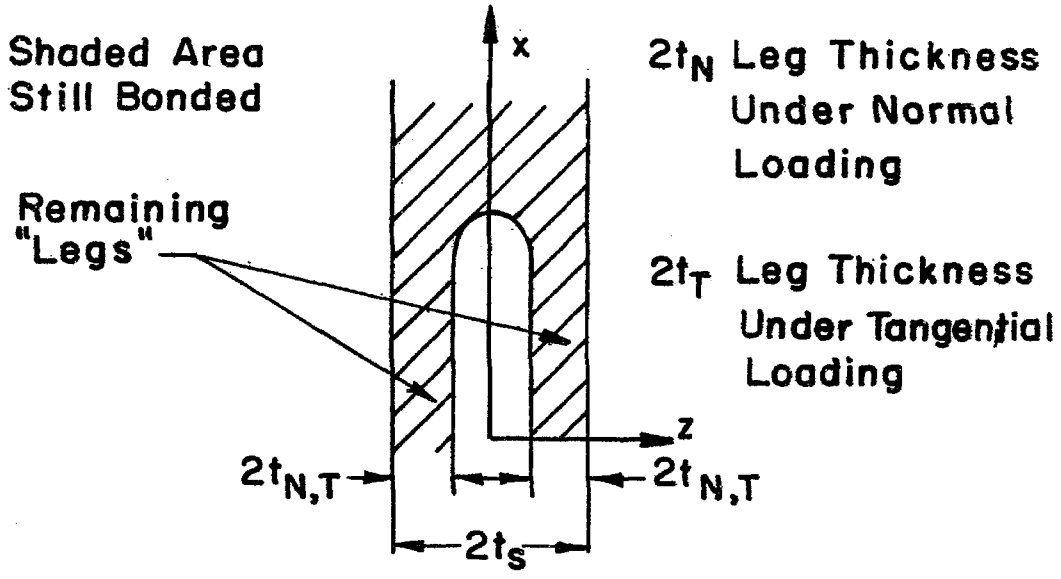

(c) Crack Geometry

FIG. 15 SPECIMEN AND CRACK GEOMETRIES

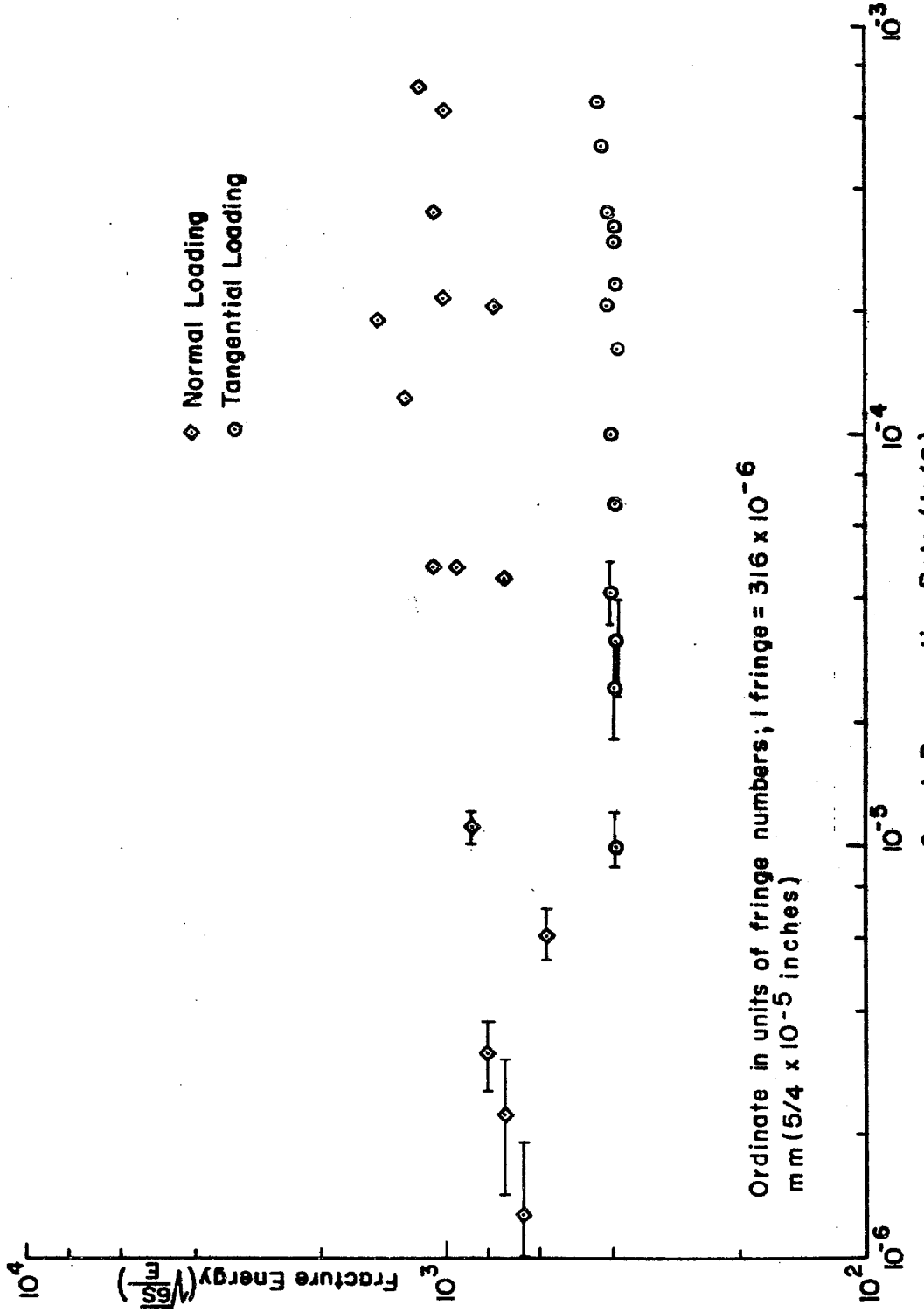

FIG.16 FRACTURE ENERGY CRITERION

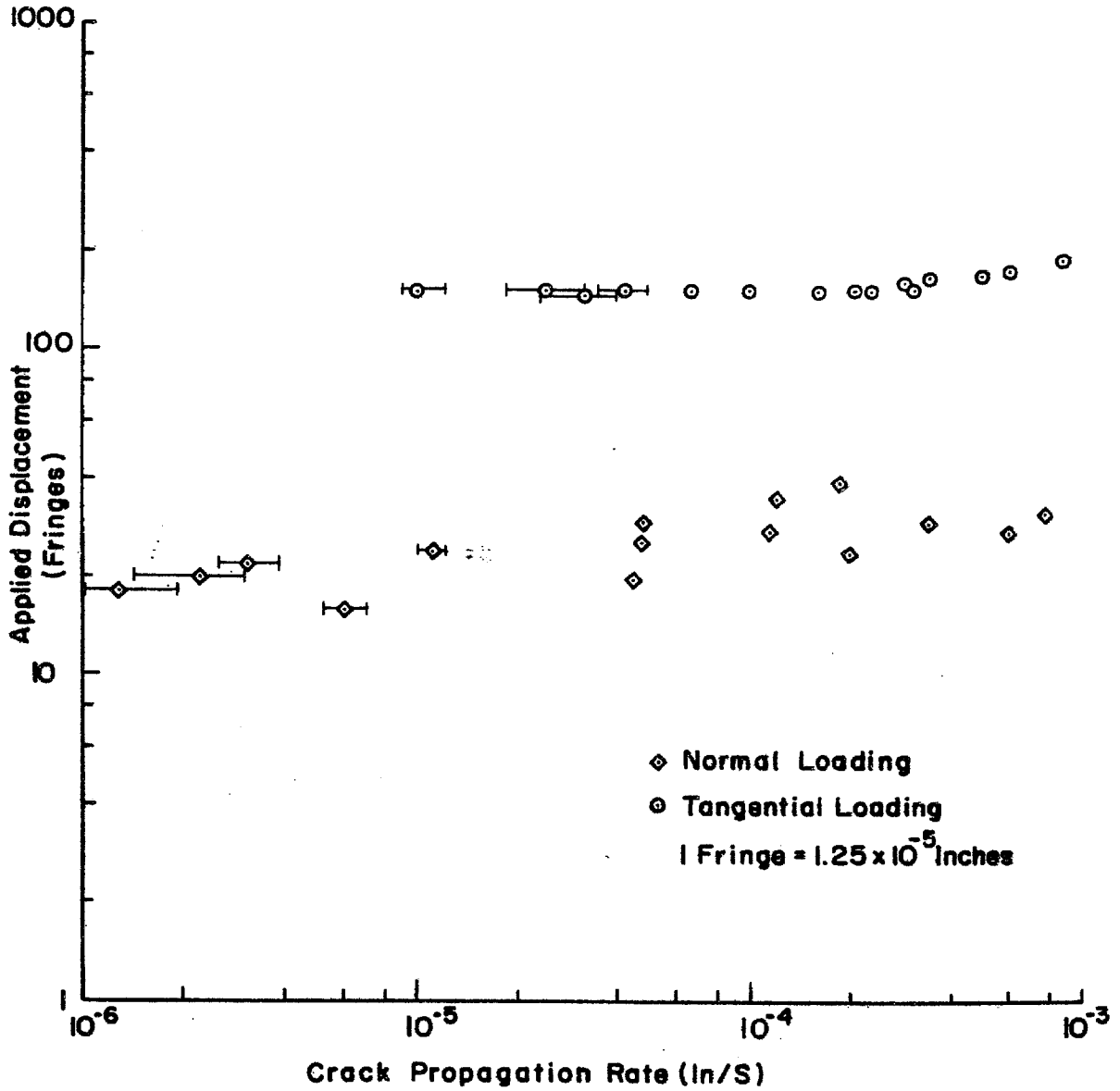

FIG. 17 APPLIED DISPLACEMENT VS. CRACK PROPAGATION RATE

REFERENCES

1. Gent, A. N. and Lindley, P. B.: The Compression of Bonded Rubber Blocks, Publication No. 324, J. of British Rubber Producer's Association, 173 (1959) p. 111.

2. Lindsey, G. H.; Schapery, R. A.; Williams, M. L. and Zak, A. R.: The Triaxial Tension Failure of Viscoelastic Materials, ARL 63-152 (1963), Aerospace Research Laboratories.

3. Comninou, M. and Schmueser, D.: The Interface Crack in a Combined Tension-Compression and Shear Field, J. Appl. Mech., 46 (1979) pp. 345-348.

4. Knauss, W. G.: On the Steady Propagation of a Crack in a Viscoelastic Sheet: Experiments and Analysis, in Deformation and Fracture of High Polymers, ed. Kausch, Hassel and Jaffee, Plenum Press 1973.

5. Knowles, J. K. and Sternberg, E.: On the Singularity Induced by Certain Mixed Boundary Conditions in Linearized and Nonlinear Elastostatics, Int. J. Solids and Structures, 11 (1975) p. 1173.

6. Private Communication, Heymans, L. J., California Institute of Technology.

7. Broberg, B.: On Transient Sliding Motion, GALCIT SM 76-12, California Institute of Technology.

8. Schmueser, D. and Comninou, M.: The Periodic Array of Interface Cracks and Their Interaction, Int. J. of Solids and Structures, 15 (1979) pp. 927-934.

9. Stern, M. and Hong, C-C.: Stress Intensity at a Crack Between Bonded Dissimilar Materials, Advances in Engineering Science, 2 (1976) pp. 699-710. (Proc. 13th Annual Meeting, Soc. Eng. Sci., Hampton, Va., Nov. 1976.)

10. Smelser, R. E.: Evaluation of Stress Intensity Factors For Bimaterial Bodies Using Numerical Crack Flank Displacement Data, Int. J. Fracture, 15 (1979) pp. 135-143.

11. Rice, J. R. and Shih, G. C.: Plane Problems of Cracks in Dissimilar Media, J. Appl. Mech., 32 (1965) pp. 418-423.

12. Knauss, W. G.: Stresses in an Infinite Strip Containing a Semi Infinite Crack, J. Appl. Mech., 33 (1966) p. 356.

PART 3

Proposals for Improvements in Microprofilometry Techniques and Further Experiments

ABSTRACT

A natural continuation of the experiments conducted in part 2 is to extend the range of crack propagation rates and number of loading combinations (normal and shear) considered there. Before this can be done, improvements in the resolution of the crack profile measurement system must be made in addition to determining methods to produce straight crack fronts through the specimen thickness. Changing the adhesive material or using a bimaterial geometry as possible means of producing straight crack fronts are proposed. Improvements in the resolution of the profile measurement were already discussed in part 1. Finally, we outline the incorporation of an automatic frame referencing technique and a digitizer into the video system in order to more effectively use the information contained in the interference patterns.

TABLE OF CONTENTS

LIST OF FIGURES

3.1 INTRODUCTION

The original purpose of this study was to examine the interrelation of unbonding rate, crack surface displacement and applied loading in an adhesive joint. The time spent in resolving development difficulties in the new experimental techniques necessary for the study has restricted the effort available for exhausting the capability of the apparatus. Nonetheless, the tests conducted thus far have demonstrated the feasibility of the experiment, indicated the limits of linear analysis and provided new information on crack propagation in adhesive joints.

The extent of the crack propagation rate range considered in the experiments reported in part 2 need to be extended in order to compare the effects of different loading combinations. Additional loading combinations themselves (normal and shear loads) need to be examined. However, before more in depth comparisons can be made, it is necessary to attend to two aspects of the present set-up. The first is to improve the resolution of the crack profile measurement scheme so as to measure the crack profile close to the crack front. These improvements have been extensively discussed in section 1.4.3. Secondly, a joint or interface configuration must be found which consistently provides unbonds extending through the specimen

thickness and having straight fronts, regardless of loading direction. This two dimensionality not only makes an experimental comparison between different loading conditions more valid, but increases the chances of a comparison with an analytical treatment of the problem.

The finger-like shape of the crack is caused by the near incompressibility of Solithane and the constraint supplied by the relatively stiff adherends on the thin adhesive layer. We expect to be able to produce through the thickness cracks by choosing a different adhesive or by considering a different geometry. These possibilities are discussed in sections 3.2 and 3.3, respectively. Section 3.4 discusses improvements in the data acquisition and processing to make fuller use of the information contained in the interference patterns produced in the crack opening interference scheme.

3.2 CHOICE OF ADHESIVE MATERIAL

The choice of adhesive material is governed by requirements which are not all mutually compatible. The final material choice will therefore represent some kind of optimum choice, balancing the priorities of the various requirements. At this stage of development the primary priority should be that the adhesive allow straight crack fronts across the specimen thickness.

Since the bulk modulus of polymers is roughly the

same, any polymer having a higher compressibility (lower Poisson's ratio) will have a higher modulus. Thus, increasing the adhesive compressibility already threatens the constraint on the relative sizes of the adherend and adhesive moduli. However, the modulus ratio constraint may be relaxed somewhat if one grips the adherends along their entire length instead of only near the ends (figure 1); in addition it may be necessary to treat the interface for a suitable value of interface adhesion in order to prevent adherend (glass) fracture. The viscoelastic response of the more rigid polymers will require crack propagation experiments of longer duration in order to illustrate their viscoelastic response. It would be preferable to find an adhesive exhibiting no or small plasticity effects.

The adhesive Araldite (modulus $E \simeq 2 \times 10^5$ p.s.i.) has already been investigated as an alternative adhesive material. The crack fronts did extend through the specimen thickness in a straight line. Stable crack growth could be obtained but for lower applied displacements and over longer periods than for Solithane. Larger applied displacements resulted in unstable crack growth.

At low crack propagation rates, the crack front would advance unevenly, leading first at one specimen side and then the other in an alternating manner as shown in figure 2. At higher rates, the advance was even but the crack front was then quite curved, the curve being symmetrically

located. Cracks which had remained stationary for some time developed considerable plastic flow at the crack front. This manifested itself in a sharp discontinuity in the fringe pattern (figure 3) once the crack did propagate. The stiffer adhesive layer did result in deformations in the adherend close to the bondline.

The pick up locations for the Michelson interferometers are 2.36 mm (0.093 inches) from the bondline and 15.875 mm (0.625 inches) from each of the specimen edges. A single edge crack was used. The edge containing the crack will, in general, have a greater displacement compared to the other, still intact edge (see figure 6, part 1). The difference increases as the modulus of the adherend decreases relative to the adhesive modulus; i.e., as the modulus ratio approaches unity from above. This difference resulted in a rotation of the Michelson interferometers which was sometimes sufficient to invalidate the results. However, the rotation can be prevented or at least minimized in a more symmetrical arrangement by starting with two edge cracks. Furthermore, the interferometer pickups could be located more centrally to better reflect the deformations in the as yet uncracked region.

Solithane and Araldite represent two distinctly different materials. Time constraints precluded a further, more comprehensive material search. However, such a search should be conducted, considering the variety of adhesives

on the market. Another possibility would be to run crack propagation tests in Solithane at temperatures below room temperature. Poisson's ratio would be reduced to somewhere around $\nu = 0.4$ but the time span of the tests would, of course, have to be greatly increased. Thermal strains would also be introduced.

3.3 CHANGES IN SPECIMEN GEOMETRY

The constraint on the adhesive layer provided by the proximity of the adherends can be decreased by increasing the bond thickness. A limiting case would be to eliminate one adherend and consider a bimaterial specimen consisting of two equally sized bars joined along a common edge. The literature abounds with solutions for bimaterial interfaces containing cracks. Thus, in addition to providing two dimensional cracks, a bimaterial specimen would allow direct comparison with analysis. The comparisons could be extended to time dependent failure in monolithic materials because Solithane could, perhaps, again be used as one phase, glass being the other.

The question might then arise as to why we did not first consider the more analytically tractable bimaterial geometry before proceeding to an adhesive joint geometry. It was felt that modal interactions in the crack front region would be greater and also that kinematic and material nonlinearities were more likely to occur in the

adhesive joint. Furthermore, the adhesive joint is more prevalent in practical use. Thus, given our precise and analytically independent experimental tools, we were in a good position to greatly improve the understanding of a practical problem as well as stimulate further analysis.

The results of part 2 indicate that, for Solithane, strains ranging from one to ten percent are necessary to produce observable crack propagation rates. If the overall dimensions of the bimaterial specimen are kept the same as those of the adhesive joint specimen, strains of one to ten percent across the one inch bar of Solithane result in displacements of 0.254 mm to 2.54 mm (0.01 to 0.1 inches), respectively. For comparison the loading device was designed to provide displacements up to 0.254 mm. Displacements up to 2.54 mm could be provided by using aluminum tubes, extending the portion of the tubes to which heating and cooling is applied and increasing the amount of heating and cooling. Initial checks show that buckling and yielding limits in the tubes and frame would not be exceeded by such displacement increases.

However, a different method of monitoring the applied displacements would need to be used. Edge displacements of 0.254 to 2.54 mm correspond to 800 to 8000 fringes on the Michelson interferometer. The fringe spacing and intensity vary considerably over this range. The fringe spacing would become too small to be resolved by the two photodiodes

providing phase information for the fringe counting. However, the displacements would now be within the resolution of L.V.D.T.'s or photonic sensors although their long term stability might become an issue. A digital encoder system using gratings attached to the specimen might be developed. Such systems are stable and could well be easily incorporated in the microprocessor fringe counting method already developed for the Michelson interferometers.

Although the constraint supplied by the adherends on an interface crack in an adhesive joint causes stronger modal interactions in the local crack front region than for a bimaterial bar, we still expect some interactions to occur at an interface crack in the bimaterial specimen, at least due to the material mismatch. The time dependent behavior would be introduced through the viscoelastic response of the Solithane. Experiments using bimaterial specimens could be compared with analysis and also provide some insight into adhesive joint failure.

3.4 IMPROVEMENTS IN DATA ACQUISITION AND PROCESSING

If it is not possible to obtain two dimensional crack geometries, then greater use will have to be made of the information contained in the crack profile interference patterns. At present, the crack profiles are generated from a single scan of the interference pattern along the crack centerline. The full profile can be generated by a series

of scans spanning the crack width. However, a lot of work is involved, even for a single frame.

The requisite data acquisition can be automated by including a video digitizer in the video system in conjunction with the microprocessor. While the initial outlay of software development work would be high, variations from two dimensional behavior under different loading conditions could be accounted for.

One of the features of the video tape recorder used in this study is the stop action playback feature. This feature allows any frame to be stopped and analyzed. Frames can also be advanced manually for frame by frame inspection. When a recording is made at the standard 7½ inches per second speed, each frame corresponds to a time interval of 1/30 second. The only way to take advantage of this 1/30 second time resolution at present is to manually advance the tape and count the frames. For rapidly occurring events this need not be restrictive, but when time intervals of even 10 minutes are considered, an automatic method of counting and referencing the frames becomes necessary. Counting the frames can be achieved quite easily by triggering a counter with the video synchronization signal. The frame number can then be incorporated in the video signal for display on the monitor. Thus a recorded frame would contain its number in addition to the event which it captured, making subsequent references to that frame simple

and repeatable. The present method, in which we use a stop watch to reference frames over long time intervals does not fully reflect the 1/30 second time resolution of the video system nor can a particular frame be repeatably accessed. Furthermore, frames must be found by playing back in real time over the full time interval. When the frame number is recorded as part of the video signal frames can be found quickly using the fast forward feature, greatly speeding up data reduction. The technology to display the current time alongside the picture already exists even on commercially available television monitors. Thus we do not expect any great difficulties in developing a system to add the frame number to the video signal.

A further consideration in increasing the resolution of the stop action playback feature is that the digitizer proposed earlier need not have any storage capability, thereby greatly reducing its cost. Moreover, requirements on its conversion rates can be relaxed because the frame of interest can be easily and repeatably found and converted with the tape recorder in the steady still mode.

In conclusion, it is clear that the power of the video system will be greatly increased by incorporating the frame referencing technique and a digitizer.

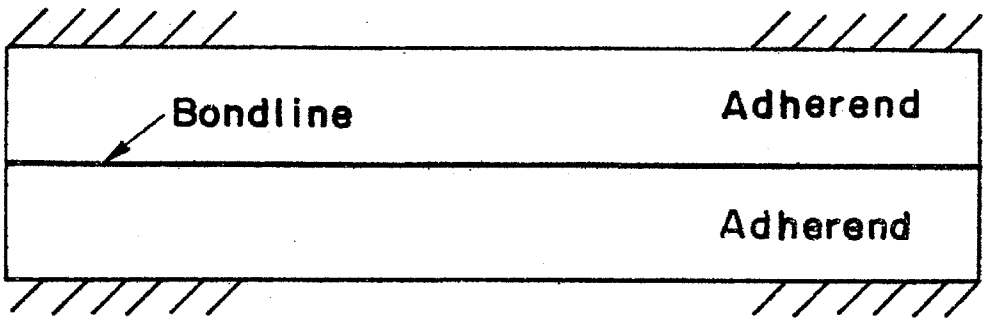

Adherends Partially Gripped

////// Gripping Area

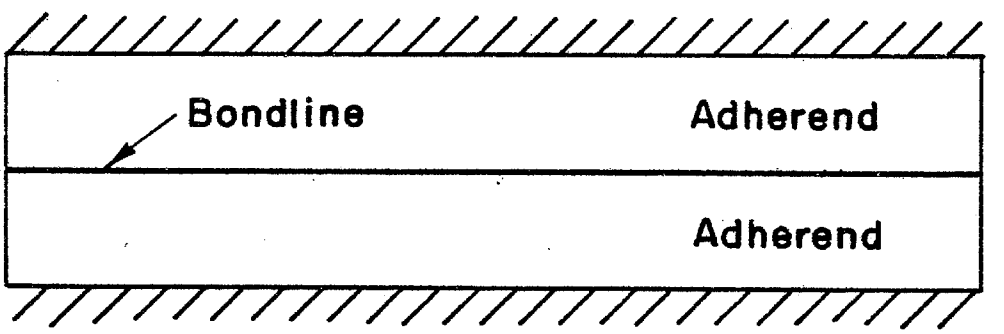

Adherends Fully Gripped

FIG. I SPECIMEN GRIPPING

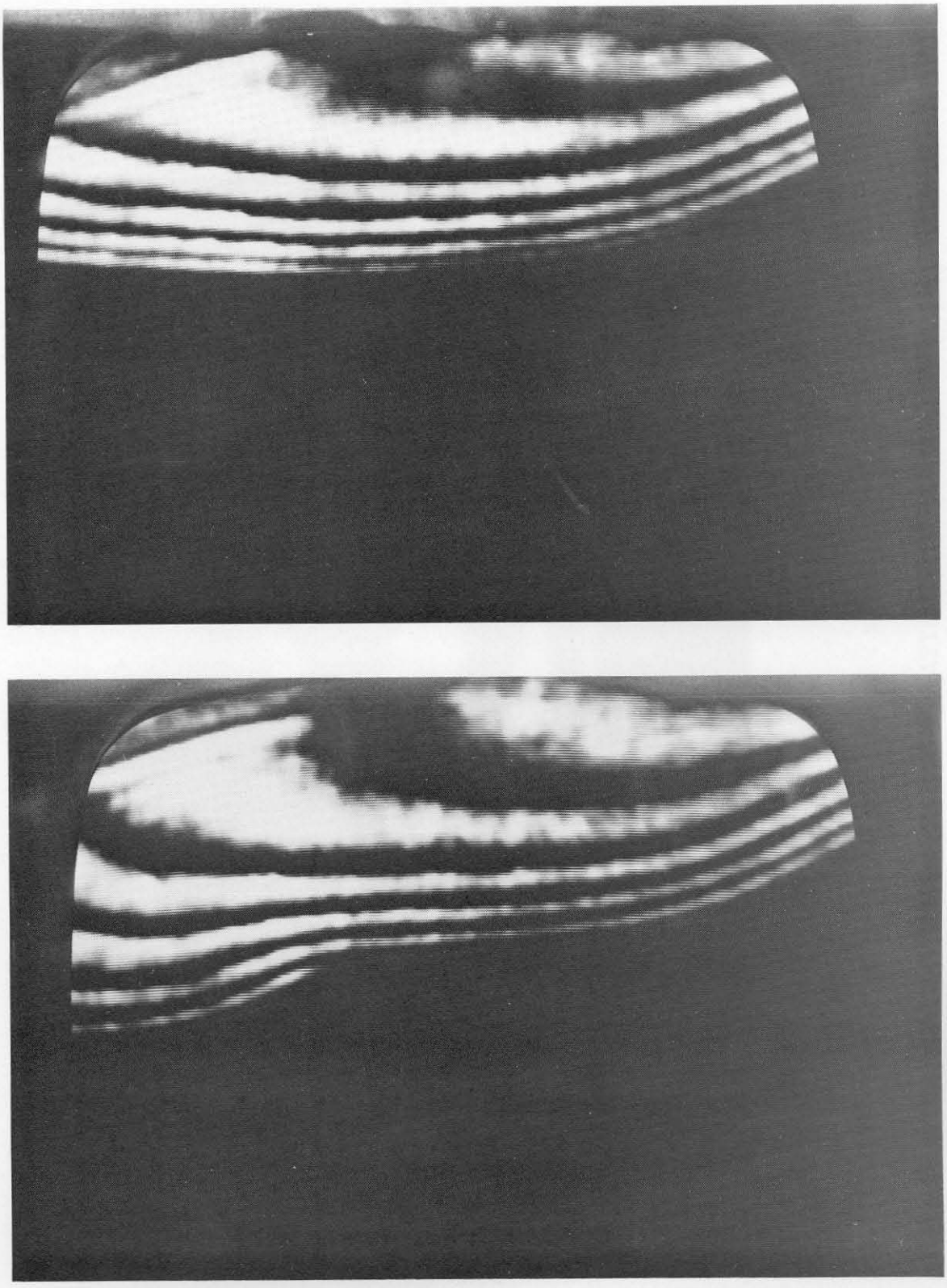

FIG. 2. UNEVEN CRACK ADVANCE. GLASS-ARALDITE JOINT.

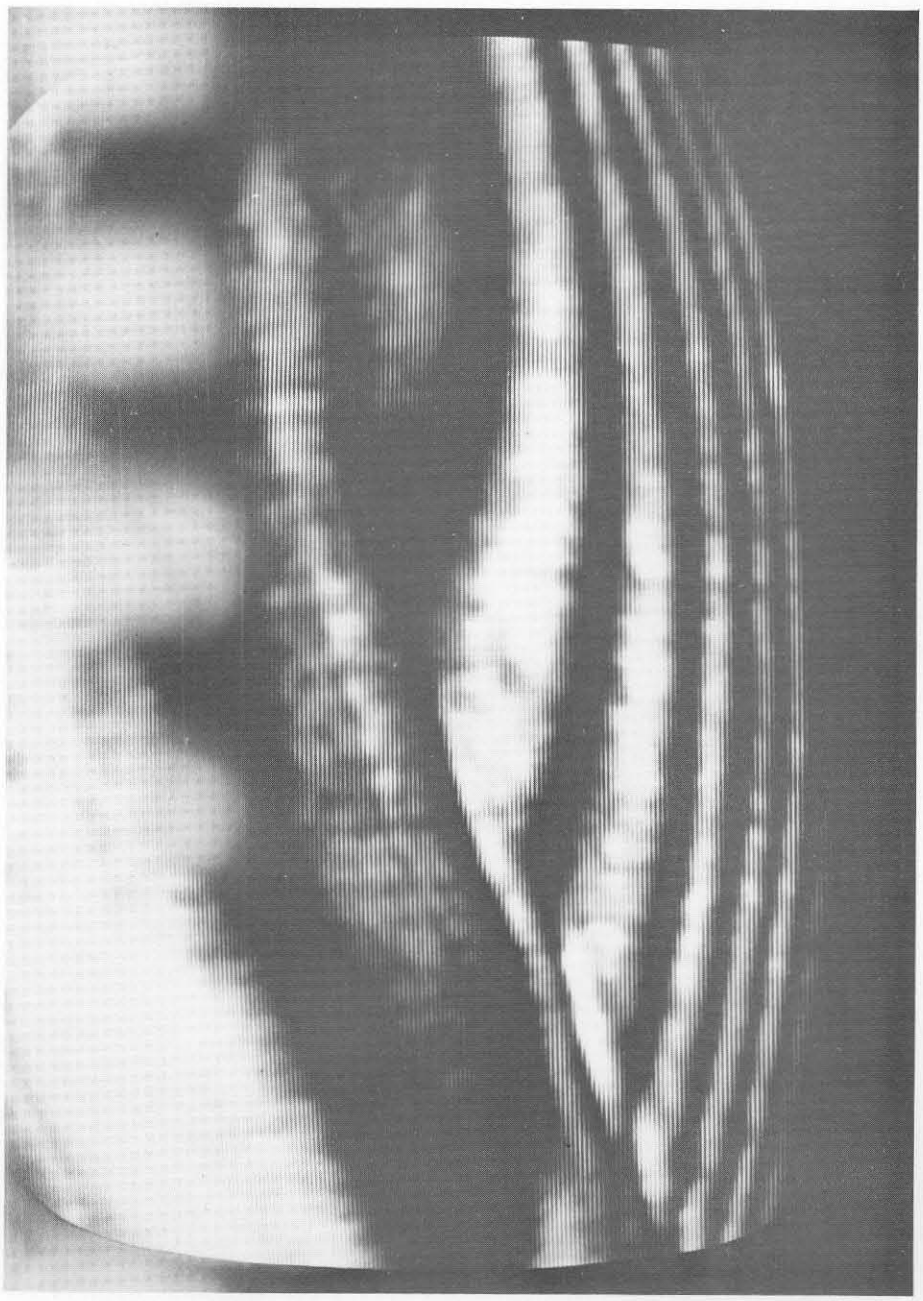

FIG. 3. DISCONTINUITY IN FRINGE PATTERN DUE TO PLASTICITY EFFECTS